Development and application of ion-selective electrode membranes doped with metal oxides nanoparticles for iron cations determination

Paut, Andrea

Doctoral thesis / Disertacija

2022

Degree Grantor / Ustanova koja je dodijelila akademski / stručni stupanj: **University of Zagreb, Faculty of Chemical Engineering and Technology / Sveučilište u Zagrebu, Fakultet kemijskog inženjerstva i tehnologije**

Permanent link / Trajna poveznica: https://urn.nsk.hr/urn:nbn:hr:149:540959

Rights / Prava: In copyright/Zaštićeno autorskim pravom.

Download date / Datum preuzimanja: **2024-05-03**

University of Zagreb

FACULTY OF CHEMICAL ENGINEERING AND TECHNOLOGY

Andrea Paut

DEVELOPMENT AND APPLICATION OF ION-SELECTIVE ELECTRODE MEMBRANES DOPED WITH METAL OXIDES NANOPARTICLES FOR IRON CATIONS DETERMINATION

DOCTORAL THESIS

Zagreb, 2022.

SVEUČILIŠTE U ZAGREBU
FAKULTET KEMIJSKOG INŽENJERSTVA I TEHNOLOGIJE

Kandidatkinja   **Andrea Paut**

predala je dana: 21. ožujka 2022. doktorski rad izrađen pod mentorstvom doc. dr. sc. Petra Kassala, Sveučilište u Zagrebu, Fakultet kemijskog inženjerstva i tehnologije – mentor I i izv. prof. dr. sc. Ante Prkića, Sveučilište u Splitu, Kemijsko-tehnološki fakultet u Splitu.

Povjerenstvo za ocjenu doktorskog rada u sastavu:
    Izv. prof. dr. sc. Šime Ukić, Fakultet kemijskog inženjerstva i
          tehnologije Sveučilišta u Zagrebu
    Izv. prof. dr. sc. Marijana Kraljić Roković, Fakultet kemijskog
          tehnologije Sveučilišta u Zagrebu
    Prof. dr. sc. Josipa Giljanović, Kemijsko-tehnološki fakultet
          Sveučilišta u Splitu
pozitivno je ocijenilo doktorski rad doktorandice Andree Paut, a Fakultetsko vijeće Fakulteta kemijskog inženjerstva i tehnologije Sveučilišta u Zagrebu na sjednici održanoj dana 25. travnja 2022. prihvatilo je ocjenu i odobrilo obranu doktorskog rada pred povjerenstvom u istom sastavu.

Obrana doktorskog rada održana je dana   10. lipnja 2022.

           D e k a n
           Prof. dr. sc. Ante Jukić

Andrea Paut

RAZVOJ I PRIMJENA MEMBRANA OBOGAĆENIH NANOČESTICAMA METALNIH OKSIDA ZA IONSKO-SELEKTIVNE ELEKTRODE ZA ODREĐIVANJE ŽELJEZOVIH KATIONA

DOKTORSKI RAD

Zagreb, 2022.

Sveučilište u Zagrebu

FAKULTET KEMIJSKOG INŽENJERSTVA I TEHNOLOGIJE

Andrea Paut

RAZVOJ I PRIMJENA MEMBRANA OBOGAĆENIH NANOČESTICAMA METALNIH OKSIDA ZA IONSKO-SELEKTIVNE ELEKTRODE ZA ODREĐIVANJE ŽELJEZOVIH KATIONA

DOKTORSKI RAD

Mentori: doc. dr. sc. Petar Kassal i
izv. prof. dr. sc. Ante Prkić

Zagreb, 2022.

University of Zagreb

FACULTY OF CHEMICAL ENGINEERING AND TECHNOLOGY

Andrea Paut

DEVELOPMENT AND APPLICATION OF ION-SELECTIVE ELECTRODE MEMBRANES DOPED WITH METAL OXIDES NANOPARTICLES FOR IRON CATIONS DETERMINATION

DOCTORAL THESIS

Supervisors: Assistant Professor Petar Kassal and Associate Professor Ante Prkić

Zagreb, 2022.

The topic of the doctoral thesis was accepted at the 246th session of the Faculty Council of the Faculty of Chemical Engineering and Technology in Zagreb, held on May 24, 2021, and approved at the session of the Senate of the University of Zagreb held on September 21, 2021.

Tema rada prihvaćena je na 246. sjednici Fakultetskog vijeća Fakulteta kemijskog inženjerstva i tehnologije u Zagrebu, održanoj dana 24. svibnja 2021. te odobrena na sjednici Senata Sveučilišta u Zagrebu održanoj 21. rujna 2021.

Supervisor information

Dr. Ante Prkić ████████████████████ He graduated in 2005 and shortly after was employed (2006) at the Faculty of Chemistry and Technology. He enrolled in a PhD course at Faculty of Chemical Engineering and Technology, University of Zagreb, in 2008. and finished in 2013. In 2014 he became Assistant Professor and Associate Professor at the Department for Analytical Chemistry in 2019. He has been assigned as lecturer for course of Analytical Chemistry (undergraduate study of Chemistry, Chemical Technology and Food Technology), Analysis of Real Samples (undergraduate study of Chemistry) and Physical Methods of Analysis and Chemometrics (Graduate study of Chemistry). His main research topics are development of quality and health properties of food products (e.g., teas and olive oils) as well as development of new potentiometric and spectrophotometric methods for pharmaceuticals' determination. He is leader of Installation Research project Development of new membranes for ion-selective electrodes enriched with nanoparticles of metals and metal oxides – NANOISEM (2018.-2023.) and leader of a workpackage of Horizon2020 project Next generation test bed for upscaling of microfluidic devices based on nano-enabled surfaces and membranes (2020.-2024.) at University of Split. He is author of 30 papers in peer-reviewed international journals.

Summary

Electrochemical sensors, including potentiometric ones, have the ability to transform the effect of electrochemical interaction between analyte and electrode into a useful signal. Potentiometric sensors were first used as an analytical technique in the early twentieth century and experienced rapid development in the 1970s. Today, they are used in many technical and scientific fields. Many of them are used in environmental, clinical and drug analysis. Ion-selective electrodes, as an important member of the electrochemical sensor family, have been in the center of electrochemical research for nearly a century. Their continuous development and combination with other scientific and technological improvements have ensured them a wide range of applications. Properties of ion-selective electrodes such as non-destructive and simple method, low cost, small-sized, short-time for doing a measurement and reliable have made them valuable competitors among other, more sophisticated methods for the analysis of real-samples.

Nanotechnology is a scientific field dealing with the fabrication of nanometer-sized products and has received great attention and development over time, especially during last decade. Since the nano-sized structures have completely different and unique physical, chemical and biological properties than the same matter on a larger size scale, they have found applications in many scientific fields and this phenomenon is mainly related to their large surface-to-volume ratio.

The combination of these two aforementioned fields of science in the form of the development of new nanoparticle-modified ion-selective electrodes led to the improvement of many properties of ion-selective electrodes, especially the sensitivity, linear range, and detection limit of the analyte. This is the main topic of this research and thus, presented in a dissertation. In this work, a new ion-selective membrane incorporated into a newly designed electrode body and modified with various nanoparticles is presented, as well as the synthesis and characterization of all used modificators.

An ion-selective membrane based on ferric phosphate with addition of silver sulphide and polytetrafluoroethylene as matrix was successfully used for the determination of ferric cations with a slope of -20.53 mV dec^{-1} and detection limit of $2.41 \cdot 10^{-5}$ mol L^{-1}. After establishing of ideal composite ratio for the above mentioned three components, a new electrode body design was introduced to ensure miniaturisation and better conductivity. The improved electrode body design enabled greater repeatability of results, thus making the proposed sensor suitable for the determination of ferric cations in pharmaceutical samples. The addition of nanoparticles improved some of the key ion-selective electrode properties. However, not only the application, but also the synthesis and characterization processes, as well as the influence of various synthesis parameters and surfactant addition on the composition of the obtained products, are studied and explained in detail in this doctoral thesis. Special attention is set on microwave-assisted hydrothermal synthesis of iron oxide nanoparticles, which are perspective candidates for the electrochemical sensing field as efficient charge transfers. In addition to iron oxides, alumina and boehmite were also used for electrode modification, and it was found that pure phase hematite had the most attractive effect on ion-selective electrode properties. Ion-selective electrode modified with 0.25% of hematite showed Nernstian response with a slope of -19.75 mV dec^{-1} in the linear range from $1.2 \cdot 10^{-6}$ mol L^{-1} to 10^{-2} mol L^{-1} and a detection limit of $1.01 \cdot 10^{-6}$ mol L^{-1} for the determination of ferric cations.

Since iron is one of the most abundant elements in the world, and also found in many aspects of human life, whether inside or outside the human body. Although iron is necessary for the normal development and functioning of the human body, a deviation of its concentration from

the reference values in the body, whether an excess or a deficiency, affects the development of many disorders and consequently diseases. Therefore, the development of new analytical tools for accurate, selective and rapid measurement of iron concentrations would be of great help both as a diagnostic tool for disorders of human metabolism and as a tool for research and better understanding of iron metabolism in human body.

Prošireni sažetak

Elektrokemijski senzori, uključujući i potenciometrijske, imaju sposobnost pretvorbe učinka elektrokemijske reakcije koja se odvija između analita i elektrode, u analitički koristan signal. Potenciometrijski senzori su kao osjetila u analitičkim metodama, prvi put su korišteni još početkom dvadesetog stoljeća, a njihov ubrzani razvoj počeo je u 1970-tim godinama. Danas se koriste u mnogim tehničkim i znanstvenim područjima uključujući analize okoliša, kliničke analize te analize lijekova.

Ionsko-selektivne elektrode, kao važan član obitelji elektrokemijskih senzora, u središtu su brojnih istraživanja već gotovo cijelo stoljeće. Njihov stalni razvoj te kombinacija s razvojem drugih znanstvenih i tehnoloških područja osigurali su im širok spektar primjene. Svojstva ionsko-selektivnih elektroda kao što su jednostavnost metode, niska cijena, mala veličina, kratko vrijeme očitavanja signala i pouzdanost učinila su ih vrijednim konkurentima među brojnim sofisticiranijim metodama za određivanje koncentracije analita u širokom spektru različitih relnih uzoraka.

Nanotehnologija je znanstveno područje koje se bavi izradom materijala u dimenzijama između jednog i sto nanometara. S obzirom da brojni materijali u nanometarskoj dimenziji imaju potpuno drugačija svojstva od istog materijala većih veličina, ovo područje znanosti se razvija brzo i predmet je brojnih znanstvenih istraživanja. Razlika u kemijskim, fizikalnim i biološkim svojstvima materijala u nano i mikro dimenziji izravna je posljedica velikog omjera između aktivne površine i volumena koje nano materijali posjeduju.

Kombinacija ova dva prethodno spomenuta znanstvena područja u obliku razvoja novih ionsko-selektivnih elektroda modificiranih nanočesticama dovela je do poboljšanja mnogih svojstava ionsko selektivnih elektroda što se posebno odnosi na osjetljivost, linearno dinamičko područje te granicu dokazivanja prisutnosti analita. Upravo je na spomenutom težište ovog doktorskog rada gdje je predstavljena izrada novih ionsko selektivnih elektroda obogaćenih nanočesticama metalnih oksida u svrhu izrade senzora za određivanje željezovih(III) kationa.

Ionsko-selektivna elektroda koja u svom sastavu sadrži željezov(III) fosfat kao aktivni centar, srebrov sulfid kao prijenosnik naboja te politetrafluoroetilen kao nosač, uspješno je korištena za određivanje koncentracije željezovih(III) kationa u dva različita lijeka. Nakon utvrđivanja idealnog omjera prethodno navedenih komponenata, u ovom radu predstavljen je i novi način izrade tijela elektrode u svrhu ravnomjernijeg prijenosa naboja te bolje ponovljivosti rezultata izmjerenih potencijala. Rezultati koji se ističu prilikom testiranja jest nagib od -20.53 mV po dekadi uz granicu detekcije od $2.41 \cdot 10^{-5}$ mol L^{-1}. Spomenuti rezultati dobiveni su za membranu koja je u svom sastavu sadržavala željezov(III) fosfat, srebrov sulfid te politetrafluoroetilen u omjeru 1:1:2 redom.

Iako je spomenuti senzor pokazao mogućnost određivanja koncentracije željezovih(III) kationa, u svrhu povećanja osjetljivosti te linearnog dinamičkog područja, isti je obogaćen nanočesticama metalnih oksida.

Sinteza spomenutih nanočestica provedena je hidrotermalnom metodom potpomognutom mikrovalovima te su procesi sinteze kao i karakterizacija svih dobivenih produkata uključujući njihov sastav, kristalnu strukturu te izgled i veličinu čestice, detaljno prikazani u ovom doktorskom radu. Metalni oksidi koji su sintetizirani, okarakterizirani te korišteni za modifikaciju ionsko selektivnih elektroda su: aluminijev oksid, boemit, hematit i magnetit. Prilikom sinteze nanočestica hematita detaljno je praćen utjecaj promjene temperature te dodatka surfaktanta cetiltrimetilamonijevog bromida (CTAB-a) te je utjecaj spomenutih

efekata praćen različitim metodama karakterizacije. Tako je prilikom proučavanja utjecaja promjene temperature i dodatka surfaktanta uočeno kako je pri nižim temperaturama sintetizirana smjesa hematita i getita, a pri višim temperaturama su uzorci sadržavali samo čisti hematit. Utjecaj dodatka surfaktanta očitovao se u usporavanju procesa transformacije iz faze getita u hematit s obzirom da je primijećeno kako veće koncentracije CTAB-a uzrokuju manji udio formiranja faze hematita u konačnom uzorku.

Membrana koja je u sastavu sadržavala 25% željezovog(III) fosfata, 25% srebrovog sulfida te 50% politetrafluoroetilena modificirana je spomenutim vrstama nanočestica i to u količini od 0.25% do 1% uzimajući u obzir ukupnu masu ionsko-selektivne membrane.

Utjecaj dodatka nanočestica hematita uzrokovao je najznačajnije povećanje osjetljivosti te povećanje linearnog dinamičkog područja elektrode u odnosu na elektrodu bez dodatka nanočestica kao i u usporedbi s membranama koje su modificirane drugim vrstama nanočestica. Rezultat koji je dobiven testiranjem membrane s dodanih 0.25% nanočestica hematita jest nagib od -19.75 mV po dekadi uz granicu detekcije od $1.01 \cdot 10^{-6}$ mol L^{-1} željezovih(III) kationa.

Željezo je jedan od najzastupljenijih elemenata na svijetu te je prisutan u brojnim područjima ljudskog života, uključujući procese unutar i izvan ljudskog tijela. Posebno je važan njegov utjecaj na procese prijenosa kisika, rast i diobu stanica te mnoge druge biološke procese nužne za razvoj i održavanje imunološkog sustava te proizvodnju energije. Iako je željezo neophodno za normalan razvoj i očuvanje ljudskog organizma, odstupanje njegove koncentracije od referentnih vrijednosti u tijelu, u obliku viška ili manjka, utječe na razvoj mnogih poremećaja, a posljedično i bolesti.

Stoga bi razvoj novih analitičkih alata za točno, selektivno i brzo mjerenje koncentracije željeza bio od velike pomoći i kao dijagnostički alat za poremećaje ljudskog metabolizma i kao alat za istraživanje i bolje razumijevanje metabolizma željeza.

Ključne riječi: ionsko selektivne elektrode; željezovi(III) kationi; nanočestice; potenciometrija;

CONTENTS

1. INTRODUCTION

Iron is one of the few elements most abundant in the world. It is used in many aspects of human life. First of all, it is important to mention its indispensability in the human organism. Namely, it is an integral part of all cells in the body. Its influence on oxygen transport processes, cell growth and division, and many other biological processes necessary for the functioning of the immune system and energy production is particularly important. Although iron is necessary for the normal development and functioning of the human body, a deviation of its concentration from the reference values in the body, whether an excess or a deficiency, affects the development of numerous disorders and consequently diseases. Iron is widely distributed not only in the human body, but also in the human environment. Due to the wide range of iron cations present, the development of new analytical tools for accurate, selective and rapid measurement of iron concentrations would be of great help both as a diagnostic tool for disorders of human metabolism and as a tool for research and better understanding of iron metabolism in the human body.

Electrochemical sensors, including potentiometric ones, have the ability to convert the effect of the electrochemical interaction between the analyte and the electrode into a useful signal. The main principle of potentiometric measurements is thus the correlation between the composition of the sample and the magnitude of the electrical potential formed between two electrodes, the reference and the indicator electrode one. Important members of the group of indicator electrodes are ion-selective electrodes (ISEs), which consist of an ion-selective membrane and an electrode body and have the ability to selectively determine the target ion regardless of the presence of interfering species in the sample. The intensity of the development of potentiometric sensors corresponds to the need for fast, cost-effective and accurate analyses. Due to their wide range of applications, low detection limits, low price and simplicity of method, ion-selective electrodes have been continuously developed for almost a century.

During this long period of development, many improvements have been made in the field of potentiometry and ion-selective electrodes. Combined with innovations and advances in other technological and scientific fields, electrochemical sensors experienced enviable improvements. Electrode modification is mainly used to extend the linear range of electrode response to the analyte ion, lower the detection limit, increase sensitivity, selectivity and durability of the sensor. One of the innovations in the field of ion-selective electrodes is their modification with different types of nanoparticles.

The development of nanotechnology, including the synthesis and characterisation methods of particles with a size of 1 to 100 nm, made it possible to modify the electrodes with specific and defined types and sizes of nanoparticles. Many different methods are used in the synthesis of nanoparticles, but one of the most attractive for metal oxide nanoparticles is microwave-assisted hydrothermal synthesis. Microwave heating has many advantages over conventional methods. The most attractive are the reduction of reaction time, energy savings, good dispersion of particles, high phase purity, high homogeneity in stoichiometry and small particle size. Also important is the high controllability of the individual synthesis steps, which ensures a high reproducibility of the products obtained.

In addition to modifying electrodes by changing their membrane composition through the addition of nanoparticles, some of the recent research has focused on the miniaturisation of ion-selective electrodes and new fabrication technologies, with a particular emphasis on solid-state contact and flexible designs. Although internal liquid contact sensors are commercially available and used in routine laboratory analyses, these electrodes have some limitations that prevent their development. The inner solution is sensitive to changes in temperature and pressure in the sample and in the environment, which can lead to its evaporation. Since the ionic strength of the inner solution and the sample solution are different, volume changes can occur due to osmotic pressure, which can lead to delamination of the ion-selective membrane. The use of this type of ISE in flow-through systems is also limited due to the pressure problems. Their miniaturisation, although possible, is very limited, making it very difficult, for example, to reduce the liquid contact to less than one millilitre. All solid state ion selective electrodes (solid contact ISEs) have been developed to overcome some of the limitations of liquid contact ISEs by replacing the internal liquid electrolyte with a solid contact transducer, making them more convenient for storage and miniaturisation while maintaining the efficiency of analyte determination. This type of electrode requires an ion-to-electron transfer transducing layer, an ion-selective membrane and an electronic conductor. They thus consist of a mentioned electronically conducting substrate covered with a transducer layer and a sensing layer (membrane) on top of the transducer layer.

One of the main challenges in developing of solid-state contact ion selective electrodes are establishing ideal ion-selective membrane composition for analyte determination as well as ensuring complete charge transfer between sensing part (membrane) and the conductor.

So, the main hypotheses of this doctoral thesis are:

1. Ion-selective membrane based on sparingly soluble salts, ferric phosphate as active center, silver sulphide as charge carrier and polytetrafluoroethylene as matrix can be used for ferric cations determination.

2. Incorporating an ion-selective membrane in miniaturized electrode body with inner solid state contact will ensure better repeatability of electrode potentials among different measurements.

3. In the process of nanoparticles microwave synthesis, temperature changing and different concentrations of added surfactant will have the influence on final product composite.

4. Ion-selective membrane modified with metal oxide nanoparticles will ensure a wider linear range, better sensitivity and lower detection limit of ferric cations compared to the unmodified ion-selective membranes.

In order to realize the main objective of proposed doctoral research which relates to the development of a ferric cations ion-selective electrode with high sensitivity, wide linear range and low detection limit, a number of individual objectives have been established, the combination of which will enable the aforementioned main objective to be fulfilled:

1. optimisation of the main ion-selective membrane components ferric phosphate, silver sulphide and polytetrafluoroethylene for a sensitive response to the concentration of ferric cations in different samples,

2. designing of the electrode body to ensure high repeatability of the measured potential values in different measurements,

3. optimisation of the conditions for microwave-assisted hydrothermal synthesis to obtain pure phased nanoparticles products of hematite, magnetite, alumina and boehmite and

4. modification of the ion-selective membrane, which consists of three main components, with the aforementioned types of nanoparticles and their incorporation into the newly designed electrode body to develop ferric ion-selective electrodes with improved properties, including a wider linear range, better sensitivity, higher repeatability and lower detection limit.

2. LITERATURE REVIEW

2.1. Potentiometry

Chemical sensor, according to IUPAC 1991 is *a device that transforms chemical information ranging from concentration of a specific sample component to total composition analysis, into an analytically useful signal.* So, two main components of chemical sensor are: receptor, as a recognition system, and transducer, responsible for gaining signal. Accordingly, there are few characteristics of chemical sensors generally accepted: transformation of chemical quantities into signals, rapid response, long lifetime, small size, cheap manufacturing, specificity and high sensitivity. Classification of sensors according to signal transduction includes: optical sensors, electrochemical sensors, electrical sensors, mass sensitive sensors, magnetic sensors thermometric sensors and other [1].

Electrochemical sensors transform the effect of the electrochemical interaction occurred between analyte and electrode, into useful signal. This sensors classification includes: voltammetric sensors, amperometric and potentiometric sensors [1,2].

The main principle of potentiometric measurements is correlation between sample composition and magnitude of the electrical potential formed between two electrodes, reference and indicator one. Among two mentioned electrode types, equipment required for direct potentiometric measurements includes a high impedance potential-measuring device (milivoltmeter) which ensures zero-current conditions measurements [3,4]. Reference electrode is responsible for providing a highly stable potential for an extended time period while indicator electrode shows changeable potential in dependence of the activity of a particular ion species, known as primary or analyte ion [3].

This analytical technique for the first time appeared in the beginning of twentieth century and experiencing rapid development after 1970s [3]. The intensity of potentiometric sensors development meets the need for rapid, inexpensive, and accurate analyses. Potentiometric sensors are nowadays widely used in various aspects of human life such as environmental, clinical [5], and drug analysis [6].

2.2. Ion-selective electrodes

As indispensable members of the electrochemical sensor family and an important topic in analytical chemistry with a wide range of applications, ion-selective electrodes (ISEs) are one of the most rapidly developing detection methods [7]. Ion-selective electrodes, coupled with reference electrode, convert the activity of a target ion into an electrical potential as the measurable signal [8]. Attractive features of potentiometric measurements with ISEs are non-destruction of sample, simplicity of method, low cost, small size, timeliness and reliability [7]. Among the many advantages of this method is the wide range of features of the electrodes themselves, which are also a consequence of their long-term development. The history of electrochemical sensors, i.e. ISEs, dates back to the early years of the 20th century, when the variability of the electrical potential of a thin glass membrane was detected as a function of the pH of the solution [7,9]. Ion-selective electrodes based on silver halide discs are represented in 1937 by Kolthoff and Sanders [10] and served as a starting point for Pungor who developed an AgI-based electrode and, with his collaborators, applied for a patent on heterogeneous selective membranes, which formed the basis for the first commercial solid-state ISEs [11]. After this discovery, several breakthroughs have appeared including crystalline membrane ISEs [12], neutral [13] and charged [14] ionophore-based liquid membrane ISEs, polymeric based membrane ISEs [15,16] and, as one of the most important discoveries in solid contact ISEs development, coated wire electrodes (CWEs) represented by Cattrall et al. in 1971 [17]. Commercialization period of ISEs started in the 1960s with fluoride selective membrane based on LaF_3 lattice [18].

Proof of their usefulness is the fact that they are constantly evolving and have been in use for almost a century. During this long period, many improvements have been made in the field of potentiometry and ion-selective electrodes. Combined with innovations and advances in other technological and scientific fields, electrochemical sensors experienced enviable improvements. Some of the recent development trends in this field are ion-selective microelectrodes, mainly focused on solid contact and flexible designs. Recent research has therefore focused on numerous modifications of ion-selective electrodes, their miniaturization and new manufacturing technologies. Particularly attractive are improvements in form of screen-printed electrodes and wireless wearable electrodes [7].

2.2.1. Ion-selective electrodes, composition and principle

To understand the main principle of ion-selective electrodes and their ability to detect analyte ions, it is important to mention and explain the role of all components in their structure.

Ion-selective electrodes, composition

The ion-selective electrode thus consists of an ion-selective membrane and an electrode body with an internal solid or liquid contact. The internal contact refers to the contact between the ion-selective membrane and the electronic conductor [19].

Liquid-contact ion-selective electrodes, although commercially available and widely used in routine laboratory practise, have some serious shortcomings that limit their future development. The inner solution is sensitive to temperature and pressure changes in the sample and the environment which can cause their evaporization. Since the ionic strength of the inner solution and the sample solution is different, volume changes can occur due to osmotic pressure, which can lead to delamination of the ion-selective membrane. The use of this type of ISE in flow-through systems is also limited due to the pressure issues. Their miniaturization although possible, is very limited, making it very difficult, for example, to reduce the liquid contact to less than one millilitre. [8,20].

All solid-state ion-selective electrodes (solid contact ISEs) were developed to overcome some of the liquid contact ISEs limitations by replacing the inner liquid electrolyte with a solid contact transducer, making them more favourable for storage and miniaturization while maintaining analyte determination efficiency.

This kind of electrode requires an ion to electron transducing layer, ion selective membrane and electronic conductor [21]. They thus consist of a mentioned electronically conductive substrate covered with a transducer layer and a sensor layer (membrane) on top of the transducer layer [22] [21]. When considering new functional materials for solid-state contact layers, certain prerequisites should be studied. Their most important function is to provide a sufficient and fast transition from ionic to electron conduction without side reactions. An ideal solid-state contact layer should have a non-polarisable interface with a large redox/double layer capacitance to protect against the thin current flow applied during potentiometry and the ability to re-establish the equilibrium in the presence of some external perturbations. To ensure reproducibility between electrodes, a well-defined potential is required between the solid contact layer and the sensor membrane. In order to form electrodes with a longer

lifetime, the chemical stability of the functional materials for the solid contact is crucial. The implementation of functional materials should be independent of the composition of the sensor membrane and should not lead to uncontrolled impurities on the backside of the membrane, which affect the electrochemical response. It is also important to ensure the availability of the selected functional material. It should be non-toxic, inexpensive and easy to manufacture [7].

Although all mentioned components are required, the heart and the main part of every ion-selective electrode is the membrane capable of recognition species of interest [23]. The sensing material is also known as active centre of the sensor and there are many different materials used for this purpose. The choice of sensor material depends on the nature of the analyte.

Different materials are reported as sensing materials for ion-selective electrodes such as sparingly soluble salts [22], ionophores [19] or bioreceptors, e.g. enzymes, antibodies, aptameres, peptides or even whole cells [24].

In addition to the mentioned components of ion-selective electrodes, the ion-selective membrane matrix is also worth mentioning. Thus, the most important membrane components together with possible modifiers can be homogenized with a polymeric matrix (poly(viniyl)chloride or another polymer) [25], carbon powder [26], or it can be printed. For crystaline membranes, as a matrix polytetrafluoroethylene (PTFE) can be used [27].

Polymeric, poly(vinyl) chloride (PVC) membranes usually contain ionophores, plasticisers and lipophilic additives in their composition. The polymeric membrane can be inserted into the electrode body with a liquid or solid inner contact. The most important component of the membrane is the ionophore, which is responsible for selective binding to the target ion and acts as an ion carrier for the transfer of ions from the aqueous phase into the polymeric membrane phase. Plasticizer have an important role in optimising the physical properties of the membrane, increasing the mobility of the active species and providing good ionic conductivity [25].

Crystaline membranes (see Chp. 2.2.3. for classification) are made of either polycrystaline or monocrystaline materials [22]. This group of ion-selective membranes includes sparingly soluble inorganic salt as sensing material [20]. There are three types of sensor membranes employing sparingly soluble inorganic salts: single crystal membranes, pressed powder membranes and membranes where the powdered salt is held together by an inert binder, most

commonly, a polymer [28]. Ion-selective electrodes based on silver iodide were introduced in the early 1960s. Since then, a few different embodiments of precipitates in ion-selective electrodes have been produced. One of them, in which precipitates are prepared and incorporated into a suitable support material, and the other, in which sparingly soluble single crystals or pressed crystals are used, form a group of solid-state electrodes [21]. Solid-state electrodes based on silver compounds, most commonly silver sulphide and silver halide, have been successfully used for the determination of halides in the membrane composition [29]. Silver sulphide is used in membranes because it is an solid ionic conductor in which silver ions are the mobile ones [3]. Also, powdered Ag_2S has the ability of being easily pressed into a mechanically stable membrane such as a thin disc [28]. The behaviour of mixed pellets consisting of Ag_2S and AgX (X = Cl, Br, I, SCN) is thus determined by the solubility of products involved. Analogously, mixtures of silver sulphides with metal sulphides showed a response to the metal ion in the membrane composition [3,30-32].

Ion-selective electrodes, principle

The response mechanism of ion-selective electrodes is a complex, time-dependent phenomenon that depends on several factors. It depends on the membrane material and the testing solution, but also on the composition, thermodynamic and kinetic properties of the interface between membrane and solution [33]. Bobacka et al. [33] comprised two possible approaches for ISEs response mechanism explanation. First one, the classical model, explains the basic principles of sensor response and backs them up with simple equations. The other, the advanced model, is provided for fundamental understanding of sensor technology. In the classical models, the electrical potential (E_M) of the ion sensor is a sum of two potentials, the potential at the boundary between the sample and ISE (E_{PB}) and the diffusion potential within the membrane (E_D). This results in the equation (1).

$$E_M = E_{PB} + E_D \tag{1}$$

Classical models are more idealised and thus avoid the mathematical, numerical and computational difficulties inherent in solving non-linear equations that are inherent in advanced models. Two classical models have been proposed: the phase-boundary potential approach and the total membrane-potential approach.

The phase-boundary potential approach is based on following idealising assumptions:

1) the membrane response is determined by the potential at the membrane-sample interface, ignoring the migration effects through the membrane and hence the diffusion potential,

2) electrochemical equilibrium is assumed at the interface between sample and membrane. The difference in chemical potential for each ion that can pass through the interface is balanced by a difference in the internal electrical potentials, E_M (E_M is called the equilibrium potential),

3) electric potentials and the concentrations of the ions in the phases in contact are independent of distance (except for the phase boundaries) and of time,

4) only one ion (the i-ion) can be transferred through the interference,

5) the ion transfer is fast and reversible,

6) the phases in contact have significantly different chemical properties,

7) the ion activity coefficient is equal 1,

8) there is no flux into solvent through the membrane [33].

The phase-boundary potential approach is widely accepted to explain the response of ion-selective electrodes. Thus, the measured potential actually arises from charge separation at the nanometre dimension of the solution-membrane interface and depends on the activity of the primary ion (the analyte). In the sample solution, the energy required for charge separation is provided by the chemical driving force (Gibbs free energy). Due to the selectivity of the ion-selective membrane, the primary ion can freely disperse into and out of the membrane phase. When the chemical driving forces balance the opposing electrical Coulomb forces, the free diffusion of the charged ions reaches electrochemical equilibrium. An electrical double layer is formed at the interface between the solution and the membrane, which rebuilds with the electrical potential difference. When the activity of the primary ion changes, the equilibrium will be re-established and the phase boundary potential (EPB) also changes. If the above approximations are considered and the activity of the primary ion in the membrane phase is constant, the EPB depends only on the activity of the primary ion in the solution. Therefore, the measured EMF can be simplified with the well-known Nernst equation (2):

$$EMF = E^0 + \frac{2.303RT}{zF}\log a_i \qquad (2)$$

E^0 stands for the standard potential of EMF gained when primary ion activity is equal to one, R is gas constant, F is Faraday constant, T is absolute temperature, z is the valence of primary ion and a is primary activity of ion i [7].

2.2.2. Ion selective electrodes, characteristics

Once the composition of the ion-selective electrode is established and the potential response meets the requirements of the Nernst equation, some properties should be defined to determine the applicability of the sensor. They are listed and explained in the following text.

Calibration curve is a plot of the output signal (potential) as a function of analyte concentration (in fact activity, but for dilute solutions activity can be equalized to concentration). Considering Nernst's equation, it is noticeable that potentiometric ion-selective electrodes have a linear relationship when the potential is plotted with respect to the logarithmic value of the ion activity (or concentration) [34].

Sensitivity is the slope of the calibration curve, the galvanic potential difference between the ion-selective electrode and the external reference electrode as a function of the logarithm of the analyte ion activity [34]. According to IUPAC, Nernstian response implies ideal sensitivity but not necessarily ideal selectivity [35].

Selectivity is the ability of an ion-selective electrode to determine a particular species without affection of any other species present in the sample mixture [22]. According to IUPAC, the selectivity coefficient is determined by Nickolsky-Eisman [34] and experimentally it can be defined with different methods. Some of them are Separate Solution Method (SSM), Matched Potential Method (MPM) and Fixed Interference Method (FIM) [22,34].

Limit of detection: according to IUPAC, the definition of the limit of detection for potentiometric measurements differs from the one for other methods because of the fundamental differences in the nature of ISE response (logarithmic response). Therefore, the practical lower limit of detection is considered to be the activity (or concentration) of the analyte at the intersection of the extrapolated linear segments of the mid-range and the final low concentration level of the calibration plot [35]. For most ion-selective electrodes its value is around $1 \cdot 10^{-6}$ mol L^{-1} [6].

Linear working range is determined by plotted calibration graphs and defined as the range in which the data points on calibration curve do not deviate by more of 2 mV from linearity [6].

Hysteresis and Reproducibility: according to IUPAC, hysteresis (electrode memory) is a kinetic process that occurs when there is a difference in the measured potential first observed in a solution containing analyte and the second observation with the same analyte

concentration but after the electrode has been exposed to a different analyte concentration. *Reproducibility*, on the other hand, is defined as the standard deviation of electrode potential data measured in solutions with different analyte concentrations (after removing and washing or wiping both electrodes). Thus, if hysteresis occurs, reproducibility would be poor [35].

Response time: according to IUPAC, the time elapsing between the moment when an ion-selective electrode and a reference electrode are brought into contact with a sample solution, or when the activity of the ion of interest in a solution is changed, and the first moment when the slope $\Delta E/\Delta t$ becomes equal to a limit value selected on the basis of experimental conditions or accuracy requirements [35]. It can also be defined as the time it takes for the ion in the sample solution to equilibrate with the sensing part of the membrane [6].

pH working range: concentration of analyte of generally $1 \cdot 10^{-2}$ mol L^{-1} in buffer solutions from pH 2 to 12 are prepared and their potentials are measured. The range in which no significant change of potential is established as pH changes [6].

Lifetime: defined as the time period in which there is no significant difference in the slope of the potential difference in dependence of ten-fold concentration change of analyte [6].

2.2.3. Ion-selective electrodes, classification

According to the IUPAC classification, there are three main groups of ion-selective electrodes: primary ISEs, composite or multiple membrane (multilayer) ISEs, and all solid-state electrodes. Primary ion-selective electrodes include crystalline and non-crystalline electrodes. Crystalline electrodes contain mobile ions with one sign and solid sites with opposite sign. They can be homogeneous or heterogeneous. If the membrane of ISE is a crystalline material made from either a single compound or a homogeneous mixture of compounds, it is a homogeneous crystalline electrode. Heterogeneous membrane electrodes are made from an active substance mixed with an inert matrix or deposited on hydrophobized graphite or conductive epoxy resin to form a heterogeneous sensor membrane. Non-crystalline electrode, ion-selective membranes are formed from a support matrix containing a cationic or anionic ion exchanger, a plasticising solvent and possibly an uncharged selectivity enhancing species. Metal contact or all solid state electrodes are those without an internal electrolyte solution and charge transfer occurs in the membrane by ionic and electronic conductivity [35].

According to the novelties in ion-selective electrodes field, in more recent literature, when describing ion-selective electrodes, some authors divided them by the membrane material, according to the construction or some other feature. In the reference [22] authors mentioned few membrane types which includes glass, crystalline (in ref. [36] referred as precipitate-based electrodes) which can be monocrystalline and polycrystalline and polymeric membranes, and two electrode embodiments based on inner contact which can be liquid or solid.

2.3. Ion-selective electrodes for ferric cations determination

Iron is one of the few elements most abundant in the world. It is used in many aspects of human life. First of all, it is important to mention its indispensability in the human organism. Namely, it is an integral part of all cells in the body. Its influence on oxygen transport processes, cell growth and division, and many other biological processes necessary for the functioning of the immune system and energy production is particularly important. Although iron is necessary for the normal development and function of the human body, a deviation of its concentration from the reference values in the body, whether an excess or a deficiency, affects the development of numerous disorders and consequently diseases. Excessive storage of iron in the human body can cause a number of damages to the liver and kidneys, and there are studies that link the occurrence of Huntington's disease, Parkinson's disease and even Alzheimer's disease to excess iron in the body. On the other hand, iron deficiency or problems with iron absorption lead to anaemia. Therefore, the development of new analytical tools for accurate, selective and rapid measurement of iron concentrations would be of great help both as a diagnostic tool for human metabolic disorders and as a tool for research and a better understanding of iron metabolism [37]. Besides the human body, iron and its compounds also play an important role in the steel industry, in the manufacture of water pipes and in the production of paints and plastics. It is common to find iron in wastewater from industrial facilities. Furthermore, since iron alloys are used for tanks and pipelines worldwide, an increased occurrence of iron in drinking water is not uncommonly due to corrosion process [38]. Since iron accelerates the growth of bacteria that derive their energy from the oxidation of iron, a timely indication of elevated iron levels in drinking water is extremely important [25].

There are many publications on poly(vinyl)chloride (PVC) matrix used for the preparation of ferric selective electrodes. As mentioned above, apart from PVC, these membranes usually contain ionophores, plasticizers and lipophilic additives in their composition. The most commonly used plasticizers in the literature are: dioctyl phthalate (DOP), dioctyl sebacate (DOS), 2-nitrophenyl octyl ether (o-NPOE), nitrobenzene (NB), dioctylphenylphophonate (DOPP), dibutyl phthalate (DBP) and tricresyl phosphate (TCP). Lipophilic additives can improve some of the most important properties of membranes such as selectivity, stability, and response time. Some of the lipophilic additives used are: tetradodecylamonium tetrakis(4-chlorophenyl)borate (TDATpClPB), potassium tetrakis(4-chlorophenyl)borate (KTpClPB),

sodium tetrakis(3,5-bis(trifluoromethyl) phenyl borate and sodium tetraphenylborate (NaTPB). The usual approach in the application of PVC membranes focuses on finding the most suitable composition ratio of and material for all the above components. To a less percentage, carbon paste and screen-printed electrodes are used for the same purpose.

Some of the ion-selective electrodes designed primary for the ferric cations determination using the potentiometry method are explained and listed in following text and in Table 1. The literature presented is based on discoveries published in the last decade. The Table 1. lists the sensing materials of the membranes, their matrix and the type of inner contact with some of the most important and commonly defined ISE properties such as the slope of the calibration curve, the linear range and the detection limit. In line with the focus of this doctoral thesis, special attention was paid in the literature and in Table 1. to whether ISEs are modified with nanoparticles and if so, which ones are used.

Gupta et al. [39] as a sensing material for iron(III) cations determination proposed S-methyl (N-methylcarbamoyloxy) thioacetimidate (Methomyl) in PVC holder. Among eleven different membrane compositions, membrane composed of 1% ionophore, 33% PVC, 1% NaTPB and 65% of dioctylphthalate (DOP) showed slope of 21.2 mV dec^{-1} in range from $9.1 \cdot 10^{-6}$ to 10^{-1} mol L^{-1}.

Effect of different membrane compositions as well as the nature and amount of plasticizer added (DOS, DPB, NPOE and DOP) was tested in six membranes used for ferric cations determination and published by Ozer et al. in ref [40]. Authors developed a new miniaturized electrode with solid contact and Fe(II) phthalocyanine as a neutral carrier. Among six different composited membranes, the one with 32% PVC, 64% dioctylsebacte, 3% Fe(II) phthalocyanine and 1% potassium tetrakis(p-chlorophenyl) borate showed best results. Nernstian slope of 26.04 ± 0.95 mV per decade in linear range $1 \cdot 10^{-6} - 1 \cdot 10^{-1}$ mol L^{-1} was recorded.

Yari et al. [41] reported the design and application of a new PVC electrode based on (E)-N'((2-hydroxyphthalen-3-yl) methylene benzohydrazide as a reliable complexing agent for determination of Fe^{3+}. Ten different composited membranes were tested and best response results showed the one with 30% PVC, 64% of plasticizer (NB) and 3% of additive. For this membrane, in linear range from $5 \cdot 10^{-9}$ to $1 \cdot 10^{-2}$ M Nernstian slope of 19.9 ± 0.3 mV per decade was accomplished. Analytical applicability was tested by determination of ferric cations in

tap, mineral, river and waste water. Results showed good agreement with those obtained with AAS method.

Active component 9-ethylacetonaphtho [1,2 b-]quinoxaline (EANQ) was synthesized and used for PVC membrane in order to maintain electrode selective for ferric cations by Mizani et al. [42]. The authors reported how among sixteen different membranes with changed composition rates and nature of additives and plasticizers of membrane, the one with 33% PVC, 58% NPOE, 4% NaTPB and 5% of EANQ showed best response with Nernstian slope of 19.5 ± 0.3 mV dec^{-1}, linear range from $2.3\cdot10^{-7}$ to $5\cdot10^{-2}$ mol L^{-1} and limit of detection $9.6\cdot10^{-8}$ mol L^{-1}.

Wang et al. [43] presented potentiometric sensor for Fe^{3+} ions determination based on N,N'-bis(2,6-diisopropylphenyl)-1,4-diaza-1,3-butadiene as a suitable carrier incorporated in PVC matrix. Membrane constructed of 33% PVC, 66% DOS and 1% ionophore exhibited a linear potential response in concentration range from $1\cdot10^{-6}$ to $1\cdot10^{-2}$ mol L^{-1} with a slope of 19.9 ± 0.3 mV per decade and $4.5\cdot10^{-7}$ mol L^{-1} limit of detection.

Saber et al. [44] reported a highly selective and sensitive iron(III) membrane electrode for fast monitoring of trace level Fe^{3+} based on norfloxacin (NOR) as a neutral carrier. Ionophore was incorporated in PVC matrix with addition of two different plasticizers: o-NPOE or DOP. Ion-selective electrode constructed with o-NPOE showed a slope of 19.58 ± 0.2 mV dec^{-1} in linear range of $1\cdot10^{-5}-1\cdot10^{-1}$ mol L^{-1} and limit of detection $(5\pm1)\cdot10^{-6}$ mol L^{-1}. Same linear range and limit of detection was established for electrode with DOP as plasticizer while slope of 19.27 ± 0.2 mV dec^{-1} was established. Both sensors showed possibility of application for determinig Fe^{3+} in real samples.

Haputhanthri et al. [45] proposed use of piperine as neutral ionophore for ferric cations determination. Electrode presented showed linear response over concentration range from $1\cdot10^{-4}$ to 1 mol L^{-1} and a slope of 20.5 mV dec^{-1}. The lower detection limit was found to be $6\cdot10^{-5}$ mol L^{-1}. Vlascici et al. [46] constructed ionophore:PVC:plasticizer = 1:33:66 composed membrane in Fluka electrode body. Three different porphyrines were used as ionophores and among them, 5-(4-carboxyphenyl-10,15,20-tris(4-phenoxyphenyl)-porphyrin plasticized with bis(2-ethylhexyl)sebacate showed best results towards iron(III) cations determination. Linear range for this electrode was from 10^{-7} to 10^{-1} mol L^{-1} and a slope 21.6 mV per decade. Limit of detection was established at the point of intersection of the

extrapolated linear mid-range and final low concentration level segments of the calibration plot and it amounted $(8.6\pm0.4)\cdot10^{-8}$ mol L^{-1}.

A symmetrical tetradentate Schiff base ligand as membrane active center incorporated in PVC matrix with solid inner contact was proposed by Bita et al. [47]. The electrode exhibited Nernstian slope of 19.5 mV dec^{-1} in ferric concentration range of $3\cdot10^{-6}-1.3\cdot10^{-2}$ mol L^{-1} with limit of detection of $1.2\cdot10^{-6}$ mol L^{-1}. The applicability of the sensor was investigated by determination of ferric cations in pharmaceutical, biological and water samples where high recovery values in comparison with Atomic Adsorption Spectrometry (AAS) results were obtained. Solid contact was accomplished by dipping platinum disc into a mixture of ionophore, additive and PVC solution in tetrahydrofuran (THF).

Morin-Fe^{2+} Shiff base complex was used as an ionophore in ref. [48] reported by Ozer et al. New miniaturized solid-state contact PVC electrode with mentioned ionophore and four different plasticizers (NPOE, DOS, DBP and DOP) for Fe^{3+} determination were prepared. The results showed that membrane composited of PVC, DOC, ionophore, and KTpClPB in percentages of 32%, 63.5%, 5%, 4% and 0.5% recpectively, have widest linear concentration range of $1\cdot10^{-6}-1\cdot10^{-1}$ mol L^{-1} and lowest limit of detection of $4.5\cdot10^{-7}$ mol L^{-1} with super Nernstian slope of 56.14 ± 0.22 mV per decade. The proposed electrode was applied for ferric cations determination in acid mine drainage and soil samples. Obtained potentiometric results were compared with results of inductively coupled plasma (ICP-OES) analysis and the results were aggreable.

Isildak et al. [49] presented all solid state PVC membrane with 2-hydroxymethyl-15-crown-5 ionophore as suitable sensor for Fe^{3+} determination. Detection limit for this sensor was about $1.2\cdot10^{-6}$ mol L^{-1} and in linear range $(8\cdot10^{-6}-1\cdot10^{-1})$ mol L^{-1} a slope of -34.6 mV per decade was reported.

Badakhshan et al. [25] also reported using of crown ether as a ionophore for iron(III) determination. Benzo-18-crown-6 was used with combination of different plasticizers and lipophilic additives in PVC matrix. Membrane constructed from b-18C-6:PVC:o-NPOE=4:30:65.5:0,5 mg exhibited best response results towards ferric cations with desired Nernstian slope of 19.51 ± 0.10 mV per decade and limit of detection of $8\cdot10^{-7}$ mol L^{-1}. Proposed method was validated with Atomic Adsorption Spectroscopy method (AAS).

Another crown ether ionophore (18 crown 6) was used in combination with ZnO nanorods and plasticizer DOPP in PVC matrix and showed sensitivity of 70.2 ± 2.81 mV per decade for

ferric cations concentration. Khun et al. [50] reported linear range was between 10^{-5} and 10^{-2} mol L^{-1}. Other than ZnO nanorods, other nanocomposites such as multi-walled carbon nanotube (MWCNT) was used in ferric selective membrane composition in papers reported from Mittal et al. [51] , Shariyati et al. [52] and Ghohari et al. [53]. They are often used for ensuring ion-to electron transfer. Mittal et al. in their research with mentioned nanotubes modified developed ionophore, (E)-3-((2(2-(2-aminoethylamino)ethylamino)ethylimino)methyl)-4H-chromen-4-one (IFE(III)) in PVC matrix with plasticizer and aditive and tested it for sensing ferric cations. Among twelve different membrane compositions, the one with 3% of ionophore, 33% PVC, 62% o-NPOE, 2% NaTBP and 0.5% MWCNTs showed most desired properties of linear range $1 \cdot 10^{-2} - 1 \cdot 10^{-6}$ and slope 16 mV dec^{-1}. This embodiment of electrode was with liquid inner contact. Shariyati et al. and Ghohari et al. in their researches among MCWNTs used nanosilica and reported use of modified carbon paste electrodes (MCPEs) for determination of ferric cations [52,53]. In ref. [52] di-tertbutylazocarboxylate (TBADC) was used as an ionophore and it was mixed and homogenized with MCWNTs, graphite powder, paraffin oil and nanosilica which is used for helping the extraction of ions on surface of prepared carbon paste electrode (CPE). Sensor with composition containing of 4% TBADC, 0.3% nanosilica, 30% paraffin oil, 62.7% graphite powder and 3% MWCNTs showed extraordinary characteristics. Nernstian slope recorded was 19.9±0.4 mV per decade in linear range from $1 \cdot 10^{-9}$ to $1 \cdot 10^{-2}$ mol L^{-1} and limit of detection $8 \cdot 10^{-10}$ mol L^{-1} for ferric cation concentration. In ref. [53] authors prepared carbon paste electrode with 5% of 1,4-diaminoanthraquinone (DAQ) as ionophore, 25% paraffin oil as binder, 0.5% nanosilica, 1% MCWNTs and 68.5% graphite powder as inert matrix material. This newly constructed sensor showed Nernstian response towards Fe^{3+} of 19.7±0.7 mV dec^{-1} in linear range between $1 \cdot 10^{-8}$ and 10^{-2} mol L^{-1}. Described homogenous paste was packed into a tip of tube containing a copper layer for ensuring electrical contact.

Bandi et al. [54] constructed a novel polymeric membranes (PMEs) using three different ionophores and their response to ferric cations was discussed. They prepared a coated graphite electrode (CGE) with same composition and results were compared. Best results were obtained with N-((3-methylthiophene-2yl)methylene)tjhiazol-2-amine in CGE which showed a most wider working concentration range of $8.3 \cdot 10^{-8} - 1 \cdot 10^{-1}$ mol L^{-1} and lower detection limit of $2.3 \cdot 10^{-8}$ mol L^{-1} with a near Nernstian slope of 19.5±0.4 mV per decade. Motlagh et al. [55] also reported comparison between PVC and CGE electrode but with 1-phenyl-3-pyridin-2-yl-thiourea (PPT) as active center for ferric cations determination. Among 15

different membrane compositions with changing of parameters of ratio and nature of plasticizers and additive, membrane composited of 30% PVC, 64% DBP, 2% NaTPB and 5% PPT was used in preparation both polymeric membrane (PME) and coated graphite electrodes. Results obtained were Nernstian slope of 20.02 ± 0.8 (CGE) and 19.9 ± 0.4 (PME) mV dec^{-1}. Linear range for CGE was $3\cdot10^{-7}-1\cdot10^{-2}$ mol L^{-1} and for PME $6.9\cdot10^{-7}-1\cdot10^{-2}$ mol L^{-1}.

Ali et al. [26] in their study focused on synthesis of a nano Fe(III)-Sud complex and using it for constructing modified carbon paste electrodes (MCPEs) and screen printed electrodes (SPEs) for ferric cations determination. Since the ionophore is the most important sensing component in every ion-selective electrode, they prepared five modified CPEs and SPEs in order to determine best electrode composition. The proportions of Fe(III)-Sud ionophore varied as 5, 7.5, 10, 12.5, and 15 mg. Testing results showed that the highest (best) Nernstian slope and wide linear range was obtained with 7.5 mg and 10 mg of ionophore for MSPE and MCPE sensors, respectively. Both electrodes were prepared with TCP as plasticizer and slopes of 19.73 ± 0.82 mV dec^{-1} with usable range $2.5\cdot10^{-9}-10^{-2}$ mol L^{-1} and 18.57 ± 0.32 mV dec^{-1} with range of $10^{-8}-10^{-2}$ mol L^{-1} were obtained for MSPE and MCPE, respectively. Proposed sensors were applied for Fe^{3+} determination in different water samples and results were compared with ones obtained with AAS analysis.

Ali et al. [56] also for ferric cations determination reported ion-selective screen printed and carbon paste sensors but based on 2-methyl-6-(4-methylenecyclohex-2-e-1-yl)hept-2-en-4-one (MMCHH) ionophore. Addition of different plasticizers (o-NPOE, TCP, DOP, DBP and DOS) were studied. Best results were obtained for electrodes with o-NPOE and TCP plasticizers. MSPEs contained of ionophore, plasticizer, PVC and carbon powder while MCPEs were constructed of ionophore, plasticizer and graphite powder. MCPEs (el. I and el. II) with TCP and o-NPOE respectively showed a wide linear ranges and Nernstian slopes (see Table 1.). MSPEs (el. III and el. IV) also exhibited very good results shown in detail in Table 1.

In reference [57] Ali et al. presented possibility of ferric cations determination with screen printed electrode based on Fe-phosphotungstate as ion-associate and TCP as plasticizer. The working electrode was composited of iron-phosphotungstate, TCP, PVC and carbon powder. Among seven electrodes with different percentage of ionophore in composition, electrode with 12.5 mg of it showed best response with Nernstian slope of 19.20 ± 0.73 mV per decade,

linear range from $1 \cdot 10^{-7}$ to $2.5 \cdot 10^{-2}$ mol L^{-1} and limit of detection $1.57 \cdot 10^{-7}$ mol L^{-1}. This electrode showed long lifetime and good stability.

In addition to publications dealing primarily with the development of ion-selective electrodes for iron(III) cations, these have also been successfully determined with some other selective electrodes, such as the fluoride ion-selective electrode [58] where authors even used Fe_xO_y nanoparticles as modification of electrode.

Earlier literature described the possibility of determining iron(III) cations with a cooper selective electrode based on CuS and Ag_2S precipitates [59]. Another research published with Ag_2S in role of conductor was by Duzgun et al. [60] where authors used $AgFeS_2$-FeS_x mixture for the same purpose and showed that this electrode exhibited linear Nernstian response with a slope 18.7 ± 0.8 mV over the range from 10^{-1} to 10^{-5} mol L^{-1} ferric cations concentration.

Table 1. A review of some literature research on potentiometric ion-selective electrodes for the determination of iron cations in the last decade

Active center	Nanosized modif.	Matrix/ contact state	Linear range (mol L^{-1})	Limit of detection (mol L^{-1})	Slope (mV dec^{-1})	Ref.
Methomyl	−	PVC/liquid	$9.1 \cdot 10^{-6} - 1 \cdot 10^{-1}$	−	21.2	[39]
Fe(II) phthalocyanine	−	PVC/solid	$1 \cdot 10^{-6} - 1 \cdot 10^{-1}$	$1.8 \cdot 10^{-7}$	26.04±0.95	[40]
(E)−N'−((2−hydroxynaphthalen−3−yl)methylene) benzohydrazide	−	PVC/liquid	$5 \cdot 10^{-9} - 1 \cdot 10^{-2}$	$1 \cdot 10^{-9}$	19.9±0.3	[41]
9−ethylacetaonaphtho(1,2−B)quinoxaline	−	PVC/liquid	$2.3 \cdot 10^{-7} - 5 \cdot 10^{-2}$	$9.6 \cdot 10^{-8}$	19.5±0.3	[42]
N,N'−bis(2,6−diisopropylphenyl)−1,4−diaza−1,3−butadiene	−	PVC/liquid	$1 \cdot 10^{-6} - 1 \cdot 10^{-2}$	$4.5 \cdot 10^{-7}$	19.9±0.3	[43]
Norfloxacin (el I)	−	PVC/liquid	$1 \cdot 10^{-5} - 1 \cdot 10^{-1}$	$(5 \pm 1) \cdot 10^{-6}$	19.58±0.2	[44]
Norfloxacin (el II)	−	PVC/liquid	$1 \cdot 10^{-5} - 1 \cdot 10^{-1}$	$(5 \pm 1) \cdot 10^{-6}$	19.27±0.2	[44]
Piperine	−	PVC/liquid	$1 \cdot 10^{-4} - 1$	$6 \cdot 10^{-5}$	20.5	[45]
5−(4−carboxyphenyl)−10,15,20−tris(4−phenoxyphenyl)−porphyrin	−	PVC/liquid	$10^{-7} - 10^{-1}$	$(8.6 \pm 0.4) \cdot 10^{-8}$	21.6	[46]
Schiff base ligand	−	PVC/solid	$3 \cdot 10^{-6} - 1.3 \cdot 10^{-2}$	$1.2 \cdot 10^{-6}$	19.5	[47]
Morin−Fe^{2+} Schiff base	−	PVC/solid	$1 \cdot 10^{-6} - 1 \cdot 10^{-1}$	$4.5 \cdot 10^{-7}$	56.14±0.22	[48]
2−hydroxymethyl−15−crown−5	−	PVC/solid	$8 \cdot 10^{-6} - 1 \cdot 10^{-1}$	$1.2 \cdot 10^{-6}$	−34.6	[49]
b−18C6	−	PVC/liquid	$1 \cdot 10^{-6} - 1 \cdot 10^{-1}$	$8 \cdot 10^{-7}$	19.51±0.10	[25]

18 crown 6	ZnO nanorods	PVC/−	$1 \cdot 10^{-5} - 1 \cdot 10^{-2}$	$5 \cdot 10^{-6}$	70.2 ± 2.81	[50]
IFE(III)	MWCNT	PVC/liquid	$1 \cdot 10^{-6} - 1 \cdot 10^{-2}$	$5 \cdot 10^{-7}$	16	[51]
TBADC	MWCNT and nanosilica	Graphite powder and paraffin oil/solid	$1 \cdot 10^{-9} - 1 \cdot 10^{-2}$	$8 \cdot 10^{-10}$	19.9 ± 0.4	[52]
DAQ	MWCNT and nanosilica	Graphite powder and paraffin oil/solid	$1 \cdot 10^{-8} - 1 \cdot 10^{-2}$	$5 \cdot 10^{-9}$	19.7 ± 0.7	[53]
N−((3−methylthiophene−2yl)methylene)thiazol−2−amine	−	Graphite rod/solid	$8.3 \cdot 10^{-8} - 1 \cdot 10^{-1}$	$2.3 \cdot 10^{-8}$	19.5 ± 0.4	[54]
1−phenyl−3−pyridin−2−yl−thiourea	−	PVC/liquid	$6.9 \cdot 10^{-7} - 1 \cdot 10^{-2}$	$3.9 \cdot 10^{-7}$	19.9 ± 0.4	[55]
1−phenyl−3−pyridin−2−yl−thiourea	−	Graphite rod/solid	$3 \cdot 10^{-7} - 1 \cdot 10^{-2}$	$2 \cdot 10^{-7}$	20.2 ± 0.8	[55]
Nano Fe(III)−Sud complex	Nanosized ionophore	PVC/solid	$2.5 \cdot 10^{-9} - 1 \cdot 10^{-2}$	$2.5 \cdot 10^{-9}$	19.73 ± 0.82	[26]
Nnao Fe(III)−Sud complex	Nanozized ionophore	Carbon powder	$1 \cdot 10^{-8} - 1 \cdot 10^{-2}$	$1 \cdot 10^{-8}$	18.57 ± 0.32	[26]
MMCHH (el. I)	−	PVC and	$4.3 \cdot 10^{-7} - 10^{-2}$	$4.3 \cdot 10^{-7}$	18.5 ± 0.9	[56]

		carbon powder/solid				
MMCHH (el. II)	−	PVC and carbon powder/solid	$4.3 \cdot 10^{-7} - 10^{-2}$	$4.3 \cdot 10^{-7}$	19.3 ± 0.5	[56]
MMCHH (el. III)	−	Graphite powder/−	$1 \cdot 10^{-7} - 10^{-2}$	$1 \cdot 10^{-7}$	19.1 ± 0.2	[56]
MMCHH (el. IV)	−	Graphite powder/−	$1 \cdot 10^{-7} - 10^{-2}$	$1 \cdot 10^{-7}$	19.8 ± 0.5	[56]
Fe−phosphotungstate	−	PVC and carbon powder/solid	$1 \cdot 10^{-7} - 2.5 \cdot 10^{-2}$	$1.57 \cdot 10^{-7}$	19.20 ± 0.73	[57]

2.4. Nanoparticles (NPs) synthesis processes, classification and characterization

Nanotechnology as a science field that deals with preparation of 1−100 nanometers sized particles has gained a huge attention and development over time [61]. One of the first literature sources for preparing and size measurements of gold nanoparticles was published in early years of 20th century [62] while nanotechnology golden era became in the 1980s with fullernes discoveries and advanced with carbon nanotubes development [63]. Nanotechnology with all its aspects has entered many areas of human life, but one of the most important discoveries and application research was on attached to nanoparticles with anti-cancer properties [64]. Nanoparticles exhibit completely different and unique physical, chemical and biological properties according to same matter properties at higher size scale. These phenomena are related to the larger surface area to volume ratio, which is 35-40% higher compared to larger particles or atoms, resulting in strong surface reactivity as it is size dependent. Greater reactivity or stability in a chemical process, improved mechanical strength, etc. have also enabled the multifunctionality of nanoparticles [65].

Synthesis processes

There are various methods for the synthesis of nanoparticles, which are divided into two main categories: bottom-up and top-down synthesis methods. The bottom-up method, e.g., the constructive method, is the assembly of atoms into clusters and eventually into nanoparticles. The top-down method, e.g. the destructive method, on the other hand, involves breaking down a bulk material into nanoscale particles [61]. Top-down methods thus include the techniques of Mechanical milling, Laser ablation and Sputtering. Bottom-up methods are divided into four groups of techniques: Solid phase (Physical vapour deposition and Chemical vapour deposition), Liquid phase (Sol-gel method, Chemical reduction, Hydrothermal method and Solvothermal method), Gas phase (Spray pyrolysis, Laser ablation and Flame pyrolysis), Biological e.g. green synthesis methods (accelerated bacterial, fungal, yeast, algal or plant extracts) and other methods (Electrodeposition methods, Microwave-assisted methods, Precipitation methods with supercritical fluid and Ultrasound techniques) [66].

Among the many synthesis methods, hydrothermal is one of the most useful and widely used for the synthesis of metal and metal oxide nanoparticles. These reactions take place in an aqueous medium at high temperature (usually above 200°C) and high pressure conditions. In such an environment, the metal cations precipitate in the form of polymeric hydroxides, which are dehydrated over time and form metal oxide crystal structures. Due to the extremely

low solubility of the obtained metal oxides in aqueous medium, oversaturation occurs and very fine crystals can be produced. To obtain the desired shape or size of the synthesised particles, parameters such as temperature, pressure, reaction time, type and concentration of precursors can be changed. The particle size and size distribution are thus related to the concentration of the precursor and the reaction time. The influence of temperature is explained by two processes: nucleation and crystal growth. At higher temperatures, nucleation is faster than crystal growth, so the particles obtained have a small size. Larger particles are obtained by a longer reaction time, where crystal growth becomes the decisive factor. Hydrothermally formed crystals have a high density without porosity and are homogeneous in composition. The main advantages of the hydrothermal synthesis method are thus: homogeneous nucleation process, small sized particles, narrow particle distribution, single-phase product, controlled particle morphology and high-purity powders [67,68].

Nowadays, microwave techniques are preferred to thermal heating in the production of nanoparticles. The first publications on microwave synthesis methods date back to 1986 [69,70]. Although microwave radiation was first used in organic chemistry, the number of papers dealing with microwave-assisted synthesis of inorganic substances is growing rapidly. Although many papers (especially in the early years) domestic microwaves, today the use of dedicated equipment is highly recommended. The use of domestic microwaves was associated with some uncertainties, such as irradiation power and reaction temperature, so there was a lack of reproducibility and also a major safety problem. In contrast, modern, commercially available microwave reactors for chemical synthesis have built-in magnetic stirrers and direct temperature and pressure monitoring by various probes and sensors. They are also connected to a computer that enables the regulation of temperature and pressure. [71]. Microwave chemistry is based on the efficient absorption of microwave energy and its conversion into heat. Since the energy of a microwave photon at a frequency of 2.45 GHz is only $1 \cdot 10^{-5}$ eV, it is obvious that it is not sufficient to break chemical bonds [71,72]. It is thus obvious that microwave-assisted synthesis processes are based on efficient heating of materials and not on the initiation of chemical reactions by direct absorption of high-energy electromagnetic radiation. This heating process involves two processes: dipolar polarisation and ionic conduction. They are the result of the electrical component of an electromagnetic field [73]. Irradiation of a sample with microwaves causes the dipoles or ions in the electric field to align. Since electromagnetic radiation creates an oscillating field, they are constantly trying to realign themselves in the electric field, resulting in molecular friction and energy loss in the

form of heat due to molecular friction and dielectric loss (the amount of microwave energy supplied that is lost in the sample in the form of heat). In the case of ionic conduction, a much stronger effect, heat is generated by the oscillation of the dissolved charged particles back and forth under the influence of microwave radiation, colliding with neighbouring molecules [71]. In the nanoparticles synthesis processes, microwave irradiation is applied to liquid−phase synthesis techniques [71,74]. Microwave-assisted synthesis of nanoparticles has many advantages over conventional hydrothermal methods. They relate to the reduction of reaction time, energy savings, good dispersion of particles, high phase purity, high homogeneity in stoichiometry and small particle size [75].

Surface modification with surfactants

Numerous properties of particles depend on their size. With nano-sized materials, the proportion of surface atoms increases and thus their reactivity, while at the same time their stability decreases, so that they have a strong tendency to agglomerate. Surface modification of nanoparticles can take place in two ways: physically (by physiosorption) or chemically (by covalent bonds). Physical modification is usually achieved by surfactants or macromolecules adsorbed on the surface of the nanoparticles [76]. Surfactants are organic compounds consisting of a head group with affinity to polar phases and a tail that is non-polar. Since they consist of two parts with opposite polarities, a surfactant solution is thermodynamically unstable due to the repulsive force between the hydrophobic tail of the surfactant and the polar medium [77]. Thus, in the hybrid system of surfactant and nanoparticles, the hydrophobic surfactant tails direct themselves to the surface of the nanoparticles via electrostatic or van der Waals forces, while the hydrophilic head is in contact with the polar solvent. Due to the potential advantage of surfactants in adjusting the surface/interfacial tensions between solid and liquid interfaces and further improving dispersion stability, surfactants can be a key agent in the synthesis of nanoparticles with well-controlled geometries. Thus, when the agglomeration process of nanoparticles is studied, surfactants can reduce the interaction between particles and disable agglomeration due to the decrease in physical forces [76,77]. The surface of metal oxide nanoparticles can be modified with different types of coupling agents (surfactants) in order to improve their surface properties and achieve specific application possibilities [76]. They are classified in four main groups: carboxylic acids, polymers, silanes and organophosphorus molecules [76].

Classification

The general classification of nanoparticles includes organic, inorganic and carbon-based particles. Organic nanoparticles (dendrimers, micelles, liposomes, ferittin, etc.) are commonly known as polymeric nanoparticles. They are biodegradable, non-toxic and some of them, such as micelles and liposomes, are sensitive to thermal and electromagnetic radiation. They are ideal candidates for drug delivery, making them an important component of biomedicine. Inorganic nanoparticles include those based on metals and on metal oxides. Carbon-based nanoparticles are composed entirely of carbon and are classified into five subgroups: Fullerenes, graphene, carbon nanotubes, carbon nanofibers and carbon black [61].

Characterization

In addition to the synthesis procedures and classification of nanoparticles, it is also important to mention the characterisation procedures and techniques used to characterise the products obtained. Various nanoparticles have been characterised using Infrared spectroscopy (IR), as it provides discriminating information due to the excitation of inherently specific fundamental vibrational transitions of the molecular species present in the sample. [78]. Since size is one of the most important features of nanoparticles, it is usually measured using a Scanning Electron Microscope (SEM) or a Transmission Electron Microscope (TEM). These techniques can be used to determine whether the particles belong to the nano or micro size scale. Nanoparticles can occur in different shapes and surface structures, such as spherical, flat, cylindrical, tubular, conical or irregular. Thanks to the imaging methods mentioned above (SEM and TEM), it is possible to determine particle shape. The presence of impurities in the nanoparticles obtained can reduce efficiency, lead to secondary reactions and cause contamination. For this reason, it is important to determine the composition of the sample, which is usually carried out with X-ray Photoelectrode Spectroscopy (XPS), while crystallography information is obtained with Powder X-ray diffraction (PXRD). The surface-to-volume ratio is the cause of many properties of nanoparticles. Therefore, the surface area can be measured with the Brunauer–Emmett–Teller (BET) analysis, while the zeta potentiometer is used to measure the surface charge [61].

2.5. Metal oxide nanoparticles, structure and synthesis methods

Among all nano-sized materials, metal oxides are the most perspective and attractive candidates from a scientific and technological point of view. Due to their diverse applications, e.g., in biomedicine, optics and electronics, their synthesis processes and their influence on properties are the focus of numerous scientific studies [76].

As mentioned in the previous section, there are many different synthesis methods, but metal oxide nanoparticles are most commonly synthesised by the following methods;

1) co-precipitation methods, which rely on supersaturating a solution with the substance that forms the precipitate,

2) microemulsion techniques, which include two types: direct (oil dispersed on water) and inverse (water dispersed in water) and

3) solvothermal/hydrothermal methods, previously explained in detail and most commonly used [76].

In the following text, structure of chosen metal oxides nanoparticles and their synthesis methods are explained. The literature review presented in Table 2. gives a systematic overview of the conditions of microwave synthesis, the surfactants and precursors used, the shape and crystalline phase of the products obtained, for nanoparticles of iron oxides and aluminium oxide and oxide hydroxides. Data presented in Table 2. apply only on papers where microwave synthesis was successfully applied for pure phase and nano-sized product.

Iron oxides nanoparticles

It has been established existence of different iron oxides and oxide−hydroxides; goethite, lepidocrocite, akaganeite, schwertmannite, feroxyhyte, ferrihydrite, bernalite, hematite, magnetite, maghemite etc.

Hematite is the oldest known and the most stable member of the iron oxide family and is widely distributed in rocks and soils. It is blood red when finely divided, or grey and black when coarsely crystalline [79]. In the crystal structure, ferric ions occupy two-thirds of the octahedral positions surrounded by an oxygen lattice in almost perfect hexagonal, close-packed form. It is n−type semiconductor with a band gap of 2.3 eV at ambient conditions [68].

Magnetite (Fe_3O_4 or $FeO \cdot Fe_2O_3$) is, among all the natural minerals of the earth, the one with the strongest magnetism. It stands out from other iron oxides because it contains both Fe^{2+} and Fe^{3+} ions. The structure of magnetite is a cubic inverse spinel consisted of a cubic close-packed arrangement of oxide ions, with the tetrahedral site occupied by Fe^{3+} cations surrounded by four oxygen atoms, while the octahedral site is occupied by Fe^{2+} and Fe^{3+} ions surrounded by six oxygen atoms, so that Fe^{3+} ions are present in both the tetrahedral and octahedral sites. In addition to its magnetism, magnetite also shows interesting electrical properties due to a small band gap (0.1 eV). Also, the fast electron hopping between Fe^{2+} and Fe^{3+} ions causes its conductivity [68].

The most commonly used methods for the synthesis of iron oxide nanoparticles are:

1) coprecipitation, thermal decomposition,
2) hydrothermal or solvothermal synthesis,
3) pyrolysis,
4) microwave assisted synthesis.

There are a large number of publications dealing with microwave synthesis of iron oxide nanoparticles. This is quite expected considering the range of applications of these nanoparticles and the time and energy saved by using microwave ovens [80]. Review papers published systemised literature of iron oxides synthesis by method [81] or time [80].

Alumina and boehmite nanoparticles

Aluminum oxide, (Alumina, Al_2O_3) can occur in 8 different crystal structures; α, χ, ρ, η, κ, θ, δ and γ. Other forms that can occur are called transitions Al_2O_3 and are formed during the thermal decomposition of aluminium thryhydroxides under various conditions [82]. Among all of them, α-Al_2O_3 is the most stable one and his structure is also known as corundum. Aluminium hydroxides and oxide hydroxides crystal phases known are: monocyclic gibbsite (γ−Al(OH)₃), orthorombic boehmite (γ−AlOOH), orthorombic diaspore (α−AlOOH) and monoclinic bayerite (α−Al(OH)₃) [83]. Most commonly, nanosized alumina particles are synthesized by following methods: bal milling, precipitation, hydrothermal synthesis, sol-gel method and vapour phase reaction [84].

Table 2. Literature data of microwave synthesized hematite, magnetite, alumina and boehmite nanoparticles

Metal oxide nanoparticle	Precursor	Base	Surfactant	Solvent	Conditions	Shape	Ref.
$\alpha-Fe_2O_3$	$FeCl_3$	$H_2O_2^+$ hydrazine	PEG[1]	Water	100 °C/10 min	ellipsoid	[85]
$\alpha-Fe_2O_3$	$FeSO_4 \cdot 7H_2O$	NaOH	PEG	water	100 °C /10 min	sphere	[86]
$\alpha-Fe_2O_3$	$FeCl_3 \cdot 6H_2O$	NaOH	−	water	500 W microwave and then calcination	spherical	[87]
$\alpha-Fe_2O_3$	$FeCl_3 \cdot 6H_2O$	NaOH	−	Water and ethanol	0.5 MPa temp.	anisotropic	[88]
$\alpha-Fe_2O_3$	$K_3(Fe_3(CN)_6)$	N_2H_4	CMC[2]	Water	160°C /60 min	Various shapes	[89]
Fe_3O_4	$FeSO_4 \cdot 7H_2O$	NH_3	−	water	80°C/multiple synthesis times tested	spherical	[90]
Fe_3O_4	$FeCl_3 \cdot 6H_2O$	Na−acetate	P123[3]	Ethylene glycol	160°C/15−60 min	nanoroses	[91]
Fe_3O_4	$FeCl_3 \cdot 6H_2O$	NH_4Ac	−	Ethylene glycol	260°C/ 15 min and then kept at same	aggregates	[92]

					temperature for 2 h		
Fe_3O_4	$FeSO_4 \cdot 7H_2O$	NH_3	−	water	$100°C$/8 min and then kept at same temperature for 15 min	−	[93]
Fe_3O_4	$FeCl_3 \cdot 6H_2O$ and $FeCl_2 \cdot 4H_2O$	NH_3	−	water	$80°C$/30 min	−	[94]
$AlOOH \rightarrow \gamma Al_2O_3$	$AlCl_3 \cdot 6H2O$	NaOH	$CTAB^4$	Water and methanol	$160°C$/30 min+ calcination after synthesis at $500°C$	nanostructured microspheres	[95]
$\alpha-Al_2O_3$	$Al(NO_3)_3 \cdot 9H_2O$	−	urea	−	900 W; 2.45 GHz; 3−5 min (domestic MW)	spherical	[96]

[1] Polyethylene glycol[2] Sodium carboxymehtyl cellulose
[3] PEO-PPO-PEO (poly(ethylene oxide) (PEO) and poly(propylene oxide) (PPO)
[4] Cetyltrimethyl ammonium bromide

2.6. Electrodes modified with metal oxides nanomaterials

Nanomaterials play an important role in the modification of electrochemical sensors due to their unique physical and chemical properties. This is especially related to their large surface-to-volume ratio, good conductivity, excellent electrocatalytic activity and high mechanical strength [97]. Nanomaterials are present in ion-selective electrode modifications in the form of solid contacts, nanomaterials dispersed directly in ion-selective membranes, ionophor modified nanomaterials dispersed in ion-selective membranes and nanomaterial-based potentiometric sensor membranes [97].

Metal oxides as ionic compounds consist of positive metal and negative oxygen ions, and the electrostatic interactions between them lead to the formation of ionic bonds. Therefore, the d-shells of metal oxides may not be completely filled, resulting in some properties that make them good candidates for use in electronic devices. Some of these are: high dielectric constants, superconductivity, reactive electronic transitions and good electrical and optical properties [98]. Considering the thermodynamic aspect of decreasing material particle size, it is known how the total free energy of a nanoparticle is the sum of the free energy of the mass and the surface of the nanoparticle. Unlike macromaterials, the surface energy of nanoparticles is a large component of the total free energy and thus the surface free energy and surface tension are important components for the overall phase stability of nanoparticles. The size-dependent particle properties are thus the electronic properties, the shape, the surface properties and the possibility of aggregation [99]. According to mentioned, metal oxide nanoparticles occupy a unique and important position among the many different types of nanomaterials due to their significant physical and chemical properties, which allow them to be employed in electroanalysis, engineering and biomedical applications [98].

Thus, the most important properties of metal oxide nanoparticles that make them suitable for electrochemical sensing are their high surface-to-volume ratio, surface reaction activity, chemical stability, non-toxicity, ability to facilitate electron transfer, and catalytic activity due to the high proportion of atoms on the surface with free valences compared to the total number of atoms [100,101]. Electrochemical use of metal oxide nanomaterials have a wide range of applications, from heavy metals determination [102] to biosensors [103].

The ability of metal oxide nanoparticles to increase the sensitivity and specificity of sensors for the detection of molecules results from the increase in electrode surface area available for

electron exchange or enzyme immobilisation. In addition to individual types of metal oxides used to modify electrodes, the use of mixed metal oxides has become increasingly common due to the synergistic effects resulting from the close electronic interaction of the components. [104].

Metal oxide nanoparticles are an important component of electrodes with enzymes in their composition. Enzymes are required for specific and sensitive detection of analytes despite the presence of interfering species. Since enzymes usually do not have direct electrical communication with electrodes, their immobilization is essential. If the enzymes are immobilized on the surface of an unmodified electrode, this could lead to their denaturation because the structure of the proteins is not compatible with the electrode surface. By facilitating electron transfer between the enzyme and the electrode, the metal oxide nanoparticles provide a suitable environment for the enzymes to function, enabling higher selectivity towards the analyte. [100,105].

However, most modifications of electrodes by nanoparticles refer to electrodes analysed by voltammetric methods. Nanomaterials in potentiometry have found their application in the last two decades, mainly as transducers in solid contact ISE [106].

2.6.1. Electrodes modified with iron oxides nanoparticles

Iron oxides and oxide hydroxide nanoparticles occupy a unique and very important position among the other metal oxides in terms of their application in the modification of electrochemical sensors. As already mentioned with metal oxides in general, these nanoparticles can have completely different properties due to the different surface area, which are not observed on a larger scale with the same matter [99]. Due to the greater density of reactive sites per unit surface area, a larger area for the adsorption of analyte molecules on the electrode surface is achieved, so that the increased reactivity for the adsorption of cations [107] and electron transfer [108] are reported. More efficient charge transfer makes iron oxide nanoparticles promising candidates for electrochemical sensors and thus enables improvement of sensor performances such as selectivity, sensitivity and detection limit [109].

Among all of iron oxide and oxide hydroxide phases, hematite and magnetite are the most perspective ones for ion-selective electrodes modification [101]. As explained in the previous sections, the oxidation state of iron in the hematite phase is +3, while in the magnetite phase there are two oxidation states, +2 and +3. Two different oxidation states enable electron hopping between Fe^{2+} and Fe^{3+} and thus increase the electrical conductivity even at room

temperature [102]. Also, the magnetic properties can be used for separation of analytes [100]. Hematite-based nanomaterials also have some exceptional properties that make them advantageous for modifying electroanalysis. Some of these are:

1) attractive photo(electrocatalytic) properties that provide alternatives to valuable nanomaterials for numerous energy conversion reactions,
2) superior energy storage capabilities,
3) long-term sustainability,
4) non-toxicity,
5) low cost,
6) high availability,
7) high theoretical specific capacity.

Although there are many papers reported with using only iron oxides as electrode modificators [110-112], in some researches, they are combined with some other materials. For improving the efficiency of working electrode, specially conductivity, in some cases, iron oxide−metal core shell nanostructures are used [113,114]. Among metals, iron oxide nanoparticles are often combined with carbonaceous materials which enable homogenous nanoparticles dispersion, prevent the aggregation and enhance the electrocatalytic process [115-118]. Also, in molecularly imprinted electrochemical sensor, iron oxide nanoparticles are modified with polyaniline [119-121] or some other polymer [122]. Iron oxide nanoparticles including magnetite, maghemite and hematite are considered as promising electrode active materials for lithium ion batteries due to their low cost, high capacity and environmental friendliness [123].

In Table 3 is presented literature review on iron oxide (Fe_2O_3) nanoparticles in the modification of ion-selective electrodes. The main properties of the analyte, electrode composition and sensors are clearly shown. To observe the frequency of use of the potentiometric method to measure the electrode potential, the reported method is also indicated. In addition, the sensors modified exclusively with pure hematite (α- Fe_2O_3) phase are highlighted.

Table 3. Literature data of electrodes modified with iron oxide nanoparticles (Fe_2O_3)

Analyte	Electrode modification	Linear range (mol L^{-1})	Limit of detection (mol L^{-1})	Method	Ref.
Zn^{2+}	Bi/Fe$_2$O$_3$/G[1]/GCE[2]	$1.53 \cdot 10^{-8} - 1.53 \cdot 10^{-6}$	$1.68 \cdot 10^{-9}$	V[3]	[116]
Cd^{+}	Bi/Fe$_2$O$_3$/G/GCE	$8.9 \cdot 10^{-9} - 8.9 \cdot 10^{-7}$	$7.2 \cdot 10^{-10}$	V	[116]
Pb^{2+}	Bi/Fe$_2$O$_3$/G/GCE	$4.83 \cdot 10^{-9} - 4.83 \cdot 10^{-7}$	$3.38 \cdot 10^{-10}$	V	[116]
Nitrite	Fe$_2$O$_3$/rGO[4]/GCE	$5 \cdot 10^{-8} - 7.8 \cdot 10^{-4}$	$1.5 \cdot 10^{-8}$	DPV[5]	[124]
H_2O_2	Fe$_2$O$_3$/ITO[6]	$1 \cdot 10^{-6} - 3.6 \cdot 10^{-4}$	$3 \cdot 10^{-7}$	A[7]	[125]
Dopamine	EPGE[8]-SWCNT[9]-Fe$_2$O$_3$	$3.2 \cdot 10^{-6} - 3.18 \cdot 10^{-5}$	$3.6 \cdot 10^{-7}$	SWV[10]	[126]
H_2O_2	Amorphous Fe$_2$O$_3$/CPE[11]	$0 - 8.5 \cdot 10^{-3}$	$2 \cdot 10^{-5}$	A	[112]
N−acetyl−L cysteine	Fe$_2$O$_3$@CoHCF[12]/csMCPE[13]	$1.22 \cdot 10^{-5} - 6.67 \cdot 10^{-5}$	$2.05 \cdot 10^{-7}$	LSV[14]	[127]
N−acetyl−L cysteine	Fe$_2$O$_3$@CoHCF/csMCPE	$2 \cdot 10^{-5} - 4.32 \cdot 10^{-4}$	$2.092 \cdot 10^{-8}$	A	[127]
L−cysteine	Fe$_2$O$_3$/N−GR[15]/CPE	$2 \cdot 10^{-7} - 4.98 \cdot 10^{-5}$ and $5 \cdot 10^{-5} - 4 \cdot 10^{-4}$	$1 \cdot 10^{-7}$	A	[128]
Nitrate	Ag@Fe$_2$O$_3$/SPCE[16]	$0 - 1 \cdot 10^{-3}$	$3 \cdot 10^{-5}$	A	[129]
Ascorbic acid	Fe$_2$O$_3$/graphene nanocomposite/GCE	$5.7 \cdot 10^{-4} - 3.97 \cdot 10^{-3}$	$5.34 \cdot 10^{-7}$	CV[17]	[130]
Rutin	Fe$_2$O$_3$/rGO	$1.5 \cdot 10^{-8} - 1.8 \cdot 10^{-5}$	$9.8 \cdot 10^{-9}$	DPV	[131]

Gallic acid	CS−Fe$_2$O$_3$−ERGO[18]/GCE	10^{-6}−$5 \cdot 10^{-5}$	$1.5 \cdot 10^{-7}$	DPV	[132]
Ivabradine	Fe$_2$O$_3$@MWCNTs[19]/MIP[20]/CPE	$1 \cdot 10^{-3}$−$1 \cdot 10^{-8}$	$9.8 \cdot 10^{-8}$	P[21]	[133]
Hidroquinone	CHIT[22]/α−Fe$_2$O$_3$−NG[23]/ITO	$3 \cdot 10^{-9}$−$3.3 \cdot 10^{-6}$	$1.09 \cdot 10^{-9}$	PEC[24]	[134]
Ammonia	α−Fe$_2$O$_3$/CNTs[25]	−	−	−	[135]
H$_2$O$_2$	α−Fe$_2$O$_3$/GCE	$5 \cdot 10^{-6}$−$9.25 \cdot 10^{-5}$	$1.3 \cdot 10^{-6}$	A	[136]
Honokiol	Fe$_2$O$_3$−RGO/GCE	$1.5 \cdot 10^{-8}$−$3.3 \cdot 10^{-5}$	$9.64 \cdot 10^{-9}$	DPV	[137]
Magnolol	Fe$_2$O$_3$−RGO/GCE	$7.5 \cdot 10^{-8}$−$2.6 \cdot 10^{-5}$	$1.05 \cdot 10^{-8}$	DPV	[137]

[1] Graphene
[2] Glassy carbon electrode
[3] Voltammetry
[4] Reduced graphene oxide
[5] Differential pulse voltammetry
[6] Indium tin oxide
[7] Amperometry
[8] Edge-plane pyrolytic graphite electrode
[9] Single wall carbon nanotubes
[10] Square wave voltammetry
[11] Carbon paste electrode
[12] Cobalt hexacyanoferrate
[13] Modified carbon paste electrode
[14] Linear sweep voltammetry
[15] N-doped graphene
[16] Screen printed electrode
[17] Cyclic voltammetry
[18] Electrochemically reduced graphene oxide
[19] Multi walled carbon nanotubes
[20] Molecularly imprinted polymer
[21] Potentiometry
[22] Chitosan
[23] N-doped graphene
[24] Photoelectrochemical
[25] Carbon nanotubes

In Table 4 is presented same approach as in Table 3. for literature review of electrodes modified with magnetite (Fe_3O_4).

Table 4. Literature data of electrodes modified with magnetite

Analyte	Electrode modification	Linear range (mol L^{-1})	Limit of detection (mol L^{-1})	Method	Ref.
Nitrite	Ag−Fe_3O_4−GO[1]/GCE[2]	$5\cdot10^{-7}$−$7.2\cdot10^{-4}$ and $7.2\cdot10^{-4}$−$8.15\cdot10^{-3}$	$1.7\cdot10^{-7}$	A[3]	[138]
Catechol	AuNPs[4]/Fe_3O_4−APTES[5]−GO/GCE	$2\cdot10^{-6}$−$1.45\cdot10^{-4}$	$8\cdot10^{-7}$	A	[139]
Hydrokinone	AuNPs/Fe_3O_4−APTES−GO/GCE	$3\cdot10^{-6}$−$1.37\cdot10^{-4}$	$1.1\cdot10^{-6}$	A	[139]
NADH	Fe_3O_4/rGO[6]/GCE	$2\cdot10^{-6}$−$1.5\cdot10^{-5}$ and $1.5\cdot10^{-5}$−$1.9\cdot10^{-4}$	$4\cdot10^{-7}$	A	[140]
H_2O_2	Indiumtinoxide electrode modified with Fe_3O_4 NPs	$2\cdot10^{-4}$−$2\cdot10^{-3}$	$1\cdot10^{-5}$	A	[111]
Glutathione	Fe_3O_4@PANI[7]/rGO	$5\cdot10^{-7}$−$5\cdot10^{-5}$	$3\cdot10^{-9}$	DPV[8]	[121]
Hydrazine	MBCPE[9]/Fe_3O_4NPs/DPB[10]	$1\cdot10^{-7}$−$1.2\cdot10^{-5}$	$1.8\cdot10^{-8}$	DPV	[141]
Catechol	Fe_3O_4−MWCNT[11]/GCE	$5\cdot10^{-7}$−$5.5\cdot10^{-6}$	$5.38\cdot10^{-8}$	A	[142]
As^{3+}	AuNPs/Fe_3O_4/GCE	$1.33\cdot10^{-9}$−$2.67\cdot10^{-7}$	$1.29\cdot10^{-11}$	SWV[12]	[143]
Dopamine	Doped PPy[13]/Fe_3O_4/rGO/GCE	$7.9\cdot10^{-9}$−$2\cdot10^{-6}$	$2.33\cdot10^{-9}$	DPV	[144]
L−cysteine	Pt−Fe_3O_4/rGO/GCE	$1\cdot10^{-4}$−$1\cdot10^{-3}$	$1.01\cdot10^{-5}$	DPV	[145]

Glucose	Glucose oxidase on the Fe$_3$O$_4$/chitosan composite	$1\cdot10^{-6}$–$3\cdot10^{-2}$	–	P[14]	[146]
Isoniazid	Fe$_3$O$_4$/CPE	$1\cdot10^{-5}$–10^{-10}	$3.09\cdot10^{-13}$	P	[147]
Chlorhexidine digluconate	GCE/Fe$_3$O$_4$/CS[15]	$2.1\cdot10^{-9}$–$2.09\cdot10^{-7}$	$5.7\cdot10^{-9}$	SWV	[148]
Methyl parathion	Fe$_3$O$_4$@ZrO$_2$/MGCE[16]	$7,6\cdot10^{-8}$–$9.12\cdot10^{-5}$	$1.52\cdot10^{-8}$	SWV	[149]
Olanzapine	Fe$_3$O$_4$@Ag/CPE	$3.9\cdot10^{-7}$–$1.38\cdot10^{-6}$ and $1.38\cdot10^{-6}$–$3.84\cdot10^{-5}$	$1.8\cdot10^{-9}$	DPV	[150]

[1] Graphene oxide
[2] Glassy carbon electrode
[3] Amperometry
[4] Au nanoparticles
[5] 3-Aminopropyl triethoxysilane
[6] Reduced graphene oxide
[7] Polyaniline nanofiber
[8] Differential pulse voltammetry
[9] Magnetic bar carbon paste electrode
[10] 2-(3,4-dihydroxyphenyl) benzothiazole
[11] Multi walled carbon nanotubes
[12] Square wave voltammetry
[13] Polypyrrole
[14] Potentiometry
[15] Chitosan
[16] Magnetic glassy carbon electrode

Although there are many research papers using iron oxide nanoparticles to modify electrodes, few of them refer to the potentiometric analysis method. Thus, the nanomaterials are much less employed in potentiometric sensors than in voltammetric ones. Moreover, many publications have reported the use of iron oxide nanomaterials (in the form of Fe_2O_3) in the modification of electrodes, but only a few of them contain the pure hematite phase [128,130,134-136].

2.6.2. Electrodes modified with alumina and boehmite nanoparticles

Membranes based on nanoporous alumina particles are used as biosensors to detect many viruses, proteins or pathogens, and high selectivity properties have been reported [151]. It is also taken into consideration as electrode material for lithium batteries [152]. In electrodes modifications presented in Table 5, these nanoparticles are often used in combination with ZnO nanoparticles. Main reason for their use in electrochemical analysis and combination with other metal oxide nanoparticles is their ability of increasing long term stability as structural promoter of the catalyst system [153,154]. Although it is insulator, its high mechanical strength and compressive strength [155] makes them attractive candidates for improving the mechanical properties of the sensor which could lead to prolonging its durability.

To the best of my knowledge, boehmite nanoparticles have not been used in any electrode modification. Nevertheless, in reference [156] $\gamma-AlOOH@SiO_2/Fe_3O_4/GCE$ microspheres electrode is used for determination of Zn^{2+}, Cd^{2+}, Pb^{2+}, Cu^{2+} and Hg^{2+} ions in drinking water.

Table 5. Literature data of electrodes modified with alumina nanoparticles

Analyte	Electrode modification	Linear range (mol L^{-1})	Limit of detection (mol L^{-1})	Method	Ref.
NADH	Al$_2$O$_3$−GO[1]/CPE[2]	$3 \cdot 10^{-5}$–$3.3 \cdot 10^{-4}$	$4.5 \cdot 10^{-6}$	DPV[3]	[157]
Dopamine	ZnO−Al$_2$O$_3$/GCE[4]	$5 \cdot 10^{-6}$–$7 \cdot 10^{-4}$	$2 \cdot 10^{-6}$	DPV	[154]
Vitamin E	Au/PAn[5]/γ−Al$_2$O$_3$	−	$6 \cdot 10^{-8}$	DPV	[158]
Methyldopa	ZnO/Al$_2$O$_3$/SPE[6]	$1 \cdot 10^{-6}$–$1 \cdot 10^{-4}$	$5 \cdot 10^{-7}$	DPV	[153]
Hydrochlorothiozide	ZnO/Al$_2$O$_3$/SPE	$1 \cdot 10^{-7}$–$1 \cdot 10^{-4}$	$8 \cdot 10^{-8}$	DPV	[153]
Salycil acid	ZnO/Al$_2$O$_3$/SPE	$5 \cdot 10^{-7}$–$8 \cdot 10^{-5}$	$2.5 \cdot 10^{-7}$	DPV	[159]
Acetaminophen	Al$_2$O$_3$−Au/PDDA[7]/rGO[8]/GCE	$2 \cdot 10^{-7}$–$2 \cdot 10^{-4}$	$6 \cdot 10^{-9}$	DPV	[160]
Melatonin	PdNP@Al$_2$O$_3$/CPE	$6 \cdot 10^{-8}$–$1.4 \cdot 10^{-4}$	$2.1 \cdot 10^{-8}$	DPV	[155]
Dopamine	PdNP@Al$_2$O$_3$/CPE	$5 \cdot 10^{-8}$–$1.45 \cdot 10^{-4}$	$3.6 \cdot 10^{-9}$	DPV	[155]
Acetaminophen	PdNP@Al$_2$O$_3$/CPE	$4 \cdot 10^{-8}$–$1.4 \cdot 10^{-4}$	$2.1 \cdot 10^{-8}$	DPV	[155]
Ascorbic acid	ZnO/Al$_2$O$_3$ nanocomposite/SPE	$1 \cdot 10^{-6}$–$1 \cdot 10^{-4}$	$6 \cdot 10^{-7}$	DPV	[161]

[1] Graphene oxide
[2] Carbon paste electrode
[3] Differential pulse voltammetry
[4] Glassy carbon electrode
[5] Polyaniline
[6] Screen printed electrode
[7] Poly(diallyldimethylammonium chloride)
[8] Reduced graphene oxide

3. DISCUSSION

Article 1 presents the development of a new potentiometric sensor based on ferric phosphate precipitate for the determination of ferric cations. In addition to the proposed development of an ion-selective membrane, a newly designed electrode body was developed and compared with the one used in this and previous research. The development of the ion-selective membrane started with the precipitation of iron(III) phosphate and silver sulphide as two main components of the presented sensor. Both precipitates were obtained in our laboratory, while commercially available polytetrafluoroethylene (PTFE) was used as matrix. A detailed description of the experimental procedure for the preparation of the powders used as well as their XRD characterization can be found in the *Materials and Methods* section of Article 1.

After the precipitation process, different ratios of the three aforementioned membrane components were weighed and pressed under 625 MPa pressure for two hours to form 10 mm diameter pellets or ion-selective membranes. Similar to the approaches in the literature review, it was important to establish ideal membrane composition for successful determination of iron(III) cations. Therefore, the membranes were prepared by increasing or decreasing each of the three main components in order to establish importance and influence of each component. Detailed information on the composition of the membranes can be found in Table 1 in Article 1. Membranes M1−M5 were prepared with decreasing amounts of ferric phosphate and increasing amounts of silver sulphide to determine the smallest active site ratio required to obtain a potentiometric response towards ferric cations. Membranes M6−M10 were made with a slightly decreasing proportion of PTFE to find the ideal proportion for maintaining all mechanical properties while avoiding the insulating effect on the conduction process through the membrane. Membranes M11−M14 were prepared without PTFE in their composition. The M14 membrane was constructed with ferric phosphate only, while M15 was composed of iron(III) phosphate and PTFE. These two membranes therefore did not contain silver sulphide and therefore Ag_2S contributions can be concluded from their response. All fifteen prepared membranes were inserted into electrode body 1 (EB1), embodiment with solid inner contact through a stainless steel disc. This electrode body has been used in previous research. The schematic and digital photograph are shown in Figure 1 and Figure 2 in Article 1, respectively. The membrane testing was carried out under acidic and alkaline conditions. It was established that membrane M1 at pH 1 showed best response, most closely to the requirements of Nernst's equation. Membranes M2−M15 showed no indication of being able to determine ferric cations (Table 3 in Article 1). Under alkaline conditions, at pH 13, the membranes were tested for the determination of phosphate ions and none of them showed

Nernstian response. From the graphical (Figure 8 and Figure 9 in Article 1) and numerical (Table 2 in Article 1) representation of the M1 membrane test results, it is obvious that this sensor was successful in the determination of ferric cations with a slope of -20.63 ± 0.63 mV dec^{-1} and a detection limit of $2.64\cdot10^{-5}$ mol L^{-1} in ferric chloride solution, while in ferric nitrate solution a slope of -18.76 ± 1.01 mV dec^{-1} and a detection limit of $4.54\cdot10^{-4}$ mol L^{-1} were obtained. However, it can be seen from the graphical representation that the reproducibility of the potentials was not satisfactory. This was probably a consequence of the incomplete adhesion between the membrane and the stainless-steel disc, which led to the "loss" of part of the charge. And this, along with the need for miniaturisation, was the main reason for producing a new electrode body that would ensure better charge transfer.

The design of electrode body 2 (EB2) is based on the print screen electrodes mechanism, but manufactured in our laboratory without sophisticated equipment, large investments or inaccessible components, so that any laboratory could manufacture it on its own. The EB2 (Figure 3 and 4 in Article 1) was designed with a copper layer on an epoxy plate, which was important for charge transfer to the millivoltmeter. The copper layer was connected to the millivoltmeter via a wire. The ion-selective membrane M1 was inserted into the electrode body with conductive graphite adhesive. Before drying, the adhesive was in a liquid state, so that a complete interaction was established between the membrane and the copper layer. After the adhesive had dried in the air, the copper layer was protected from the influence of the test solution with a non-conductive polish. The sensor made in this way was tested towards possibility of determination of ferric cations. The results confirmed the hypotheses made, as the deviation of the three E^0 potential values were significantly lower than with the membrane used in EB1. Figure 10 and Figure 11 (Article 1) show that the calibration curves overlapped satisfactorily. The results agreed well within one and within three days. The membrane in EB2 also showed a Nernstian response with a slope of -19.421 ± 1.70 mV dec^{-1} and a detection limit of $1.43\cdot10^{-4}$ mol L^{-1}.

Further experiments with the proposed sensor were the determination of the selectivity and the application of the sensor in real samples. The selectivity coefficients were examined using the matched potential method and the results are shown in Table 5 in Article 1. The interference of Al^{3+}, Ba^{2+}, Ca^{2+} and Mg^{2+} was investigated. The most influential interference was caused by Al^{3+}, but if these ions are present less than 50.4 times with regards to an iron(III) concentration of $5\cdot10^{-4}$ mol L^{-1} , the determination of iron(III) cations should still be possible. Other ions caused less significant interference. The determination of ferric cations

with membrane M1 was successfully performed in standard solution of Fe^{3+} with recovery values of 101.2%, 98.2% and 98.9% for added $m(Fe^{3+})$ =0.84 mg, 1.64 mg and 8.37 mg, respectively. For establishing the possibility of a wider application of the presented M1 membrane, it was tested towards the determination of iron(III) cations in real samples. Two pharmaceuticals, Tardyferon and Heferol, prepared by a microwave digestion process, were used as real samples. The potentiometric results were compared with those obtained with Ultraviolet Visible Spectrophotometric (UV/VIS) analysis carried out with complexation of ferric cations with 5-sulphosalicylic acid. The compared results were aggregable and the determined recovery value for Tardyferon® was 98.6% and for Heferol® 106.5%.

Article 2 presents a synthesis method for the preparation of iron oxides and hydroxides. This article is mainly devoted to the study and clear explanation of the conditions for microwave-assisted hydrothermal synthesis and the complete characterisation of the products obtained. The influence of the synthesis temperature as well as the addition of the surfactant cetyltrimethylammonium bromide (CTAB) is studied in detail. Table 1 in Article 2 lists ten different synthesised samples with detailed experimental conditions. The main principle for establishing the synthesis conditions was based on changing the parameters of temperature and CTAB concentration, while the concentration of the precursor ($FeCl_3$), the pH of the medium (~13.5) and the synthesis duration time remained constant.

The temperature effect could be observed for samples RS1, RS2 and RS3 as they were synthesised at 150°C, 200°C and 250°C, respectively, and without the addition of surfactant. The same temperature layout was used for the synthesis of samples S1−S3, but these samples were prepared with the addition of 1% CTAB. Samples S4−S6 were synthesized under the same temperature (200°C) but with an addition of 0.25%, 0.5% and 2.5% CTAB, respectively. Sample S7 was synthesized with the same amount of CTAB as sample S6, but at a higher temperature (250°C).

All synthesized products were characterised in detail using various techniques: Fourier infrared spectroscopy (FTIR), powder X-ray diffraction (PXRD) and field emission scanning electron microscopy (FE-SEM). The data obtained with FTIR analysis provides information about the molecular species present in the sample, while PXRD analysis provides accurate information about the composition and crystallography of the sample. The estimated mass fractions of the identified phases were calculated using the Rietveld algorithm. The shapes and surface structures of the particles are observed using the FE-SEM analysis technique.

In Figure 1 in Article 2 are represented FTIR spectra of three reference samples (RS1, RS2 and RS3) as well as of S1, S2 and S3 samples synthesized with addition of 1% CTAB. Samples RS1 and S1, synthesized under temperature of 150°C showed the same IR bands, assigned to the formation of goethite and hematite phases and they refer to the in-plane bending band (δOH) at 893 cm^{-1} and out-of-plane bending band (γOH) at 795 cm^{-1} typical for goethite phase, as well as bands visible at 536 cm^{-1} and 461 cm^{-1} which indicated hematite (α-Fe$_2$O$_3$) phase.

In Figure 2 in Article 2, PXRD patterns of RS1 and S1 samples showed the presence of both goethite and hematite phases but according to the results of structure refinements, RS1 sample contained of ~40wt.% α-Fe$_2$O$_3$ and ~60wt.% α-FeOOH while sample S1, where 1% of CTAB was added, consisted of ~20wt.% α-Fe$_2$O$_3$ and ~80wt.% α-FeOOH. So, it was obvious how, in this case, addition of certain amount of surfactant slowed down the rate of goethite to hematite transformation process.

The FTIR spectra of the reference sample synthesized at 200°C (RS2) in Figure 1 (Article 2) and the PXRD pattern in Figure 3 (Article 2) show the formation of a pure hematite phase, while the FTIR spectra of the S2 sample show peaks at 893 cm^{-1} and 799 cm^{-1} assigned to the goethite phase and peaks at 546 cm^{-1} and 471 cm^{-1} indicating the presence of a hematite phase. The PXRD pattern together with the quantitative analyses confirmed that the S2 sample consists of ~40 wt% α-Fe$_2$O$_3$ and ~60 wt% α-FeOOH. As mentioned, it is evident that the addition of CTAB, as in the RS1 and S1 samples, slows down the phase transformation of goethite to hematite. At a temperature of 250 °C, the addition of CTAB had no effect on the transformation of goethite to hematite, as the FTIR and PXRD analyses of samples RS3, S3 and S7 confirmed the composition of the pure hematite phase (Figures 1, 4 and 6 in Article 2).

When considering the influence of the addition of CTAB concentration, the samples synthesized under the same temperature value (200°C) are observed. As shown in Table 2 in Article 2, the addition of 0.25% CTAB (sample S4) had no significant influence on the mentioned process of transformation of goethite into hematite. Nevertheless, it is evident from the quantitative analysis in Table 2 in Article 2 that the larger amount of CTAB added to samples S4−S6 resulted with smaller mass fraction of hematite phase.

The FE− SEM images (Figure 7 in Article 2) for the RS1 sample show the presence of nanorods typical of goethite and irregular particles typical for hematite formed in alkaline media. In the S1 sample, with CTAB addition, an increased proportion of goethite nanorods

46

and smaller irregular hematite particles are visible. In sample RS2 only irregular hematite particles can be seen, while in sample S2 goethite nanorods together with hematite particles are recognized. The FE-SEM images for samples RS3, S3 and S7 (Figure 8 in Article 2) show the presence of irregular hematite particles with an estimated size of several tens of nanometres to 1 µm. According to the mentioned, the addition of CTAB did not affect on the size and shape of hematite particles in the synthesized samples.

Article 3 is composed of two main parts and their combination in form of improvement sensor proposed in Article 1. The first part of Article 3 is thus devoted to the synthesis processes and characterisation of the nanoparticles used for the modification of the ion-selective electrodes whose properties are presented in the second part. The sensor is also modified with (nano)particles, whose synthesis process and characterisation are presented in detail in Article 2. Thus, the solid-state ion-selective membrane with solid inner contact embedded in electrode body 2 (EB2; Article 1) was modified with (nano)particles of hematite (sample RS3, presented in Article 2), nanoparticles of magnetite, boehmite and alumina to achieve an ideal membrane composition for the determination of ferric cations (Article 3). This article is thus a combination of the simplicity of the potentiometric technique and the improvement of sensor properties through its modification with nanostructured materials. The combination of the advantages of these two scientific fields is presented in this article, but also, considering the combination of all three articles, this doctoral thesis as a whole.

A microwave-assisted hydrothermal synthesis method was used to obtain all nanoparticles. The detailed experimental conditions are presented in Table 1 and Table 2 in Article 3 for boehmite, alumina and magnetite, respectively. Boehmite nanoparticles were synthesized using $Al_2(SO_4)_3 \cdot 18\ H_2O$ as precursor at a temperature of 200°C for 30 minutes. After drying, part of the sample was calcinated at a temperature of 800°C to obtain alumina nanoparticles. Magnetite was synthesized from $FeCl_2 \cdot 4H_2O$ and $FeCl_3$ with the addition of ammonium solution at a temperature of 200°C for 10 minutes. The approach of characterisation of the synthesised nanoparticles in this Article was similar to that in Article 2. Accordingly, the first technique used for characterisation was FTIR. The FTIR spectra of boehmite (Figure 1 in Article 3) showed peaks at 1067 cm^{-1} and 1159 cm^{-1}, which are characteristic for symmetric and asymmetric Al−O−H bending, respectively, and peaks at 737 cm^{-1}, 610 cm^{-1} and 476 cm^{-1} occurred from Al−O vibrations. The PXRD pattern in Figure 2 in Article 3 confirms that these are crystalline (γ-AlOOH) particles, which are then analysed by FE-SEM (Figure 3 in Article 3) and EDS (Figure 4 in Article 3). The boehmite nanoparticles appear in needle

shaped structure and their estimated size is less than 20 nm in diameter. The EDS data confirmed atomic ratio of Al and O in good agreement for the boehmite phase. For the alumina nanoparticles, the FTIR spectra (Figure 5 in Article 3) showed a characteristic peak for the stretching of the Al−O bond at 1115 cm^{-1} and peaks at 745 cm^{-1} and 554 cm^{-1} due to the symmetric stretching and bending vibrations of the Al−O−Al bond, respectively. The PXRD pattern of the alumina nanoparticles (Figure 6 in Article 3) showed an indication of hexagonal Al_2O_3 formation, but also the appearance of an amorphous phase, so that the proposed sample was poorly crystallised. Nevertheless, needle shaped particles are visible under high magnification with FE-SEM analyses (Figure 7 in Article 3) and EDS data agree well with the atomic ratio of Al and O in the Al_2O_3 phase (Figure 8 in Article 3). The FTIR analyses of the magnetite nanoparticles (Figure 9 in Article 3) show a characteristic Fe−O stretching vibration peak and PXRD analyses (Figure 10 in Article 3) confirm the formation of the phase-pure sample, cubic Fe_3O_4. In FE-SEM images (Figure 11 in Article 3), irregularly shaped aggregates with individual magnetite nanoparticles less than 20 nm in diameter are visible. The EDS data (Figure 12 in Article 3) show the ideal atomic ratio for the magnetite phase.

After successful synthesis and complete characterisation of the nanoparticles, they are used together with hematite particles for the modification of the ion-selective membrane from **Article 1** (membrane M1). The sensor is tested towards determination of ferric cations. Twelve different composited membranes were prepared with different types and proportions (0.25-1%) of nanoparticles, while the ratios of the three main components remained constant (Table 3). In this way, it was possible to establish which (nano)particle phase and in which amount can improve the properties of the ion-selective electrodes.

Membrane MN7 with addition of 0.25% alumina nanoparticles showed a Nernstian response for the determination of ferric cations with a slope of −21.73 mV per decade in the range from $6.25 \cdot 10^{-4}$ to 10^{-2} mol L^{-1}. The addition of 0.5% alumina nanoparticles (MN8) showed a positive effect on the widening of the linear dynamic range for almost a whole decade with a slope of −18.75 mV per decade. Positive effect of a larger amount of added boehmite nanoparticles was not detected. The only membrane with boehmite nanoparticles that showed satisfactory sensitivity to the concentration of ferric cations was the one with 0.25% boehmite in the composition (MN10) and it showed a slope of −18.86 mV dec^{-1} in the linear range of $1.56 \cdot 10^{-4} - 10^{-2}$ mol L^{-1} with a detection limit for ferric cations of $8.38 \cdot 10^{-5}$ mol L^{-1}.

Nevertheless, membranes modified with iron oxide (nano)particles showed much more attractive results in the determination of ferric cations. The addition of 0.25% magnetite nanoparticles affected on expanding linear range from $2.44 \cdot 10^{-6}$ to 10^{-2} mol L^{-1} with a slope of -22.38 mV per decade and a detection limit of $1.85 \cdot 10^{-6}$ mol L^{-1}.

However, the best response showed membrane MN1 with an addition of 0.25% pure hematite phase (nano)particles. This sensor showed an almost identical slope with the Nernst's equation requirement for trivalent cations and it was -19.75 mV dec^{-1}. As mentioned in the introduction, the ideal Nernstian slope for trivalent cations would be -19.73 mV dec^{-1}. The linear range for the determination of ferric cations for this sensor was between $1.22 \cdot 10^{-6}$ mol L^{-1} and 10^{-2} mol L^{-1}. The correlation factor (R^2) for this sensor was also almost ideal and was 0.9925. The detection limit is $1.01 \cdot 10^{-6}$ mol L^{-1}. Due to the very attractive properties of the MN1 sensor, it was applied for the determination of iron(III) cations in a laboratory prepared iron(III) solution as well as in the standard solutions of Fe^{3+} cations within three cycles (Tables 6 and 7 in Article 3). The recovery values are always calculated in the same way, regardless of whether the calculations are performed for trivalent or monovalent ions. However, when looking closely at the calculated and measured potential values for the determination of ferric cations in standard solution samples, it becomes clear that even a small deviation in the potential measurement can lead to a much larger deviation in the recovery values than would be the case for monovalent cations. Nevertheless, the MN1 membrane still showed high recovery values between the determined and the reference value for ferric cations (99.4%, 106.7%, 93.6% and 101.1%).

The morphology of the tested MN1 sensor surface was examined using the FE-SEM technique. At 500× magnification, a very heterogeneous surface can be seen while at 10000× magnification, different sizes and particle agglomerations are noticeable.

To summarise the discussion, Table 6 in Article 3 shows the main contributions of all three articles represented as well as their relevance to the doctoral thesis as a whole.

Table 6. Summary of individual contributions for presented articles (Article 1, Article 2 and Article 3) with united scientific contribution for doctoral thesis as a whole

Main individual scientific contributions		
Article 1	**Article 2**	**Article 3**
- establishment of the the ideal composition of the three basic ion-selective membrane components ($FePO_4$, Ag_2S and PTFE) for the successful determination of iron cations, - proposal for a new electrode body design (EB2), - obtaining a sensor for the successful determination of iron(III) cations with a slope of -20.53 ± 0.63 mV dec^{-1} and a detection limit of $2.41\cdot10^{-5}$ mol L^{-1} for the M1 membrane in EB1, - obtaining a sensor for the successful determination of ferric cations with a slope of -19.42 ± 1.70 mV dec^{-1} and a detection limit of detection $1.43\cdot10^{-4}$	- establishment of the ideal synthesis conditions for the synthesis of pure hematite (nano)particles synthesis (RS3) - study of the influence of temperature conditions on size, shape and composition of the obtained products, - study of the influence of CTAB addition on size, shape and composition of the obtained products, - detailed characterisation of all obtained products.	- establishment of ideal synthesis conditions for the synthesis of boehmite, alumina and magnetite nanoparticles, - detailed characterisation of all nanoparticle products obtained, - modification of ion-selective membranes with boehmite, alumina, magnetite and hematite nanoparticles, - obtaining six (MN1, MN2, MN4, MN7, MN8 and MN10) ion-selective membranes inserted into electrode body EB2 for successful determination of ferric cations, - successful determination of ferric cations in standard solutions with high recoveries corresponding to the

mol L^{-1} for membrane M1 in EB2, • successful application of sensor M1 inserted in EB2 for determination of ferric cations in pharmaceutical samples.		reference value of ferric cation concentration.
United scientific contribution		

The ion-selective membrane (M1) presented in **Article 1**, modified with (nano)particles of pure hematite phase (**Article 2**) and inserted into the electrode body (EB2) presented in **Article 1**, showed improved properties compared to membranes modified with other nanoparticles or without any modification. The membrane (MN1) modified with hematite presented in **Article 3** showed Nernstian response with a slope of -19.75 mV dec^{-1} in the linear range from $1.2 \cdot 10^{-6}$ to 10^{-2} mol L^{-1} and a detection limit of $1.01 \cdot 10^{-6}$ mol L^{-1} for the determination of ferric cations. Comparing the properties of the MN1 membrane with those of the M1 membrane in EB1 or EB2, it is clear that modification of the sensor with nanoparticles leads to an extension of the linear range, better sensitivity and a lower detection limit.

4. CONCLUSION

Ion-selective electrodes as a simple and affordable analytical tool for the precise and accurate determination of analytes have good prospects for wider application. The combination of the simplicity of the potentiometric technique with the modernisation through nanotechnology and the new design of the electrode body is explained in detail in this doctoral thesis.

An ion-selective electrode based on iron ferric phosphate with addition of silver sulphide and polytetrafluoroethylene in the ratio $FePO_4:Ag_2S:PTFE=1:1:2$ was successfully used for the determination of iron(III) cations. This sensor showed Nernstian slope of -20.53 ± 0.63 mV dec^{-1} and a detection limit of $2.41 \cdot 10^{-5}$ mol L^{-1}. Although the sensor obtained a slope in good agreement with the Nernstian equation for trivalent cations, the poor repeatability of the results was the main reason for fabricating a new electrode body with a miniaturised design which provided better charge transfer. Membrane inserted in the newly developed electrode body responded to concentration changes of ferric cations with a slope of -19.421 ± 1.70 mV dec^{-1} and a detection limit of $1.43 \cdot 10^{-4}$ mol L^{-1} was determined. It showed a good response not only to ferric cations in a solution containing ferric cations alone, but also in the presence of some other interfering species. This sensor was successfully used for the determination of ferric cations in two different pharmaceuticals and high recoveries were obtained (98.6% and 106.5%). It became clear that although the repeatability of the potential measurement is much better with the new electrode body, the detection limit was in the concentration range where there was still room for improvement.

Four different types of nanoparticles were used to increase the sensitivity of the sensor. Since the main components of the sensor, iron phosphate and silver sulphide, as well as the process of integrating the ion-selective membrane into a newly developed electrode body were carried out in our laboratory, the nanoparticles used for sensor modification were also synthesized in our laboratory. The nanoparticle synthesis was carefully performed and explained in detail, focusing on the experimental conditions. The microwave-assisted synthesis method was used for all nanoparticles because it has numerous advantages, such as reduction of reaction time, energy conservation, good particle dispersion, high phase purity, high homogeneity in stoichiometry and small particle size. Special attention was paid to the synthesis of iron oxides. During the synthesis process, the effects of the synthesis temperature and the addition of the surfactant CTAB were studied in detail and described. The investigation of the

influence of the above parameters was complemented by a number of characterisation techniques such as FTIR, PXRD and FE-SEM analyses.

The samples prepared using $FeCl_3$ as precursor in alkaline media and 20 min synthesis time at a temperature of 150°C gave both goethite (α-FeOOH) and hematite (α-Fe_2O_3) phases, while the pure hematite phase was synthesised at 200°C and 250°C. The effect of the CTAB addition showed a slowing down of the transformation process from goethite to hematite at 200°C, while it did not affect the transformation at 250°C. The FE-SEM analyses showed the presence of goethite nanorods and irregular hematite particles in the samples with heterogeneous phase (RS1, S1, S2) and only irregular hematite particles are visible in samples RS2, RS3, S3 and S7. The addition of surfactants had no effect on the size and shape of hematite particles. The estimated particle size for hematite was in the range of several tens of nanometres to one micrometre. In addition to hematite, pure magnetite phases, boehmite and alumina nanoparticles are also synthesised. The $Al_2(SO_4)_3 \cdot 18H_2O$ was used as a precursor for the synthesis of boehmite nanoparticles and the synthesis process was carried out at a temperature of 200°C and a duration of 30 minutes. The calcination process of boehmite particles at 800°C resulted in obtaining alumina nanoparticles. Magnetite was synthesised at the same temperature but in a synthesis time of 20 minutes using $FeCl_3$ and $FeCl_2 \cdot 4H_2O$ as precursors. The characterisation of the obtained products was carried out in a similar way as for hematite. Pure phases of boehmite and magnetite were synthesised, while for alumina the presence of hexagonal Al_2O_3 and amorphous phase was found. The FE-SEM analyses for the boehmite and alumina samples showed the needle shape with an estimated size of less than 20nm in diameter. For the magnetite samples, irregularly shaped aggregates are visible, but the size of the individual particles within the aggregates is smaller than 20nm.

All presented nanoparticles (except goethite) are used for ion-selective electrode modification to obtain a fast and reliable sensor for the determination of ferric cations. The modified membranes consisted of 0.25% iron phosphate, 0.25% silver sulphide and 0.50% polytetrafluoroethylene, while the percentage of nanoparticles in the membranes varied from 0.25%−1%. Although six modified membranes showed satisfactory response to iron(III) cations, the best results were obtained with a pure− phase hematite modification. The addition of 0.25% hematite (nano)particles to the membranes affected higher sensitivity, wider linear range and lower detection limit compared to the values of the above parameters in the unmodified membranes. The results of ferric determination with membrane MN1 showed a nearly perfect Nernstian slope of −19.75 mV dec^{-1}, a linear range from $1.22 \cdot 10^{-6}$ to 10^{-2} mol

L^{-1} and detection limit of $1.01 \cdot 10^{-2}$ mol L^{-1}. This sensor was successfully used for the determination of ferric cations in three different standard concentrations and the recoveries of the potentiometric measurements towards reference values were 106.7%, 93.6% and 101.1%.

The careful synthesis and detailed characterisation of the nanoparticles thus made it possible to determine which phase composition is most suitable for the modification of membranes for ion-selective electrodes in order to obtain a suitable sensor for the determination of iron(III) cations in wide concentration range, with high sensitivity and low detection limit.

5. BIBLIOGRAPHY

1.   B. Perret, Chemical sensors. An introduction for scientists and engineers, Vol. 392, Springer, New York, 2008, str. 21-22

2.   A. Hulanicki, S. Glab, F. Ingman, Chemical sensors: definitions and classification, Pure Appl. Chem. 63 (1991) 1247-1250

3.   J. Wang, Analitical Electrochemistry, John Wiley & Sons, Inc., New Jersey, 2006, str. 201-245

4.   J. Janata, Principles of chemical sensors, Springer Science & Business Media, New York, 2010, str. 138-144

5.   E. Zdrachek, E. Bakker, Potentiometric sensing, Anal. Chem. 91 (2018) 2-26

6.   Ö. Isildak, O. Özbek, Application of Potentiometric Sensors in Real Samples, Crit. Rev. Anal. Chem. 51 (2021) 218-231

7.   Y. Z. Shao, Y. B. Ying, J. F. Ping, Recent advances in solid-contact ion-selective electrodes: functional materials, transduction mechanisms, and development trends, Chem. Soc. Rev. 49 (2020) 4405-4465

8.   J. Hu, A. Stein, P. Bühlmann, Rational design of all-solid-state ion-selective electrodes and reference electrodes, TrAC, Trends Anal. Chem. 76 (2016) 102-114

9.   K. H. Lubert, K. Kalcher, History of electroanalytical methods, Electroanalysis 22 (2010) 1937-1946

10.   I. Kolthoff, H. Sanders, Electric potentials at crystal surfaces, and at silver halide surfaces in particular, J. Am. Chem. Soc. 59 (1937) 416-420

11.   R. P. Buck, E. Lindner, Peer reviewed: tracing the history of selective ion sensors, Anal. Chem. 73 (2001) 88-97

12.   M. S. Frant, J. W. Ross, Jr., Electrode for sensing fluoride ion activity in solution, Science 154 (1966) 1553-1555

13.   P. Oggenfuss, W. Morf, U. Oesch, D. Ammann, E. Pretsch, W. Simon, Neutral-carrier-based ion-selective electrodes, Anal. Chim. Acta 180 (1986) 299-311

14.   J. W. Ross, Calcium-selective electrode with liquid ion exchanger, Science 156 (1967) 1378-1379

15.   X.-G. Li, X.-L. Ma, M.-R. Huang, Lead (II) ion-selective electrode based on polyaminoanthraquinone particles with intrinsic conductivity, Talanta 78 (2009) 498-505

16.   M.-R. Huang, X.-W. Rao, X.-G. Li, Y.-B. Ding, Lead ion-selective electrodes based on polyphenylenediamine as unique solid ionophores, 85 (2011) 1575-1584

17.   R. W. Cattrall, H. Freiser, Coated wire ion-selective electrodes, Anal. Chem. 43 (1971) 1905-1906

18.   M. Frant, J. W. Ross, Use of a total ionic strength adjustment buffer for electrode determination of fluoride in water supplies, Anal. Chem. 40 (1968) 1169-1171

19.   F. Faridbod, P. Norouzi, R. Dinarvand, M. R. Ganjali, Developments in the Field of Conducting and Non-conducting Polymer Based Potentiometric Membrane Sensors for Ions Over the Past Decade, Sensors 8 (2008) 2331-2412

20.   M. Cuartero, G. A. Crespo, All-solid-state potentiometric sensors: A new wave for in situ aquatic research, Curr. Opin. Electrochem. 10 (2018) 98-106

21.   E. Zdrachek, E. Bakker, Potentiometric Sensing, Anal. Chem. 91 (2019) 2-26

22.   K. N. Mikhelson, Ion-selective electrodes, Vol. 81, Springer, Berlin, 2013, str. 5-31

23.   R. De Marco, G. Clarke, ELECTRODES | Ion-Selective Electrodes. In Encyclopedia of Electrochemical Power Sources, Garche, J., Ed. Elsevier: Amsterdam, 2009; pp. 103-109.

24.   J. Ding, W. Qin, Recent advances in potentiometric biosensors, TrAC, Trends Anal. Chem. 124 (2020) 115803

25.   S. Badakhshan, S. Ahmadzadeh, A. Mohseni-Bandpei, M. Aghasi, A. Basiri, Potentiometric sensor for iron (III) quantitative determination: experimental and computational approaches, BMC Chem. 13 (2019) 1-12

26.   T. A. Ali, W. H. Mahmoud, G. G. Mohamed, Construction and characterization of nano iron complex ionophore for electrochemical determination of Fe(III) in pure and various real water samples, Appl. Organomet. Chem. 33 (2019) 17

27.   A. Prkic, J. Giljanovic, M. Bralic, Direct Potentiometric Determination of N-acetyl-L-cysteine (NAC) in Real Samples by Using "home made" Iodide ISE, Int. .J Electrochem. Sc. 6 (2011) 5388-5395

28.   R. W. Cattrall, Chemical Sensors, Oxford University Press, New York, 1997, str.

29.   A. Rajbhandari, A. Yadav, K. Manandhar, R. Pradhananga, Characterization and applications of silver sulphide based membrane electrodes, Sci. World (Kathmandu, Nepal) 7 (2009) 19-23

30.   S. Ikeda, N. Matsuda, G. Nakagawa, K. Ito, Studies on solid-state mixed sulfide active materials for ion-selective electrodes, Solid State Ionics 3 (1981) 197-201

31.   E. Pungor, K. Tóth, Ion-selective membrane electrodes. A review, Analyst 95 (1970) 625-648

32.   Y. G. Vlasov, New solid-state ion-selective electrodes—Sensors for chemical analysis

of solutions, Fresenius' Zeitschrift für analytische Chemie 335 (1989) 92-99

33. J. Bobacka, A. Ivaska, A. Lewenstam, Potentiometric ion sensors, Chem. Rev. 108 (2008) 329-351

34. F. Criscuolo, M. I. N. Hanitra, I. Taurino, S. Carrara, G. D. Micheli, All-Solid-State Ion-Selective Electrodes: A Tutorial for Correct Practice, IEEE Sens. J. 21 (2021) 22143-22154

35. R. P. Buck, E. Lindner, Recommendations for nomenclature of ionselective electrodes (IUPAC Recommendations 1994), Pure Appl. Chem. 66 (1994) 2527-2536

36. H. Freiser, Ion-selective electrodes in analytical chemistry, Springer Science & Business Media, 1978, str.

37. M. Becuwe, P. Rouge, C. Gervais, D. Cailleu, M. Courty, A. Dassonville-Klimpt, P. Sonnet, E. Baudrin, Calix[4]arene-modified silica nanoparticles for the potentiometric detection of iron (III) in aqueous solution, C. R. Chim. 15 (2012) 290-297

38. H. A. Zamani, M. T. Hamed-Mosavian, E. Hamidfar, M. R. Ganjali, P. Norouzi, A novel iron (III)-PVC membrane potentiomeric sensor based on N-(2-hydroxyethyl) ethylenediamine-N, N', N"-triacetic acid, Mater. Sci. Eng. C 28 (2008) 1551-1555

39. V. K. Gupta, B. Sethi, N. Upadhyay, S. Kumar, R. Singh, L. P. Singh, Iron (III) Selective Electrode Based on S-Methyl N-(Methylcarbamoyloxy) Thioacetimidate as a Sensing Material, Int. J. Electrochem. Sc. 6 (2011) 650-663

40. T. Ozer, I. Isildak, A New Fe (III)-Selective Membrane Electrode Based on Fe (II) Phthalocyanine, J. Electrochem. Sci. Technol. 10 (2019) 321-328

41. A. Yari, M. Bagheri, M. Ghazizadeh, A Novel Iron(III) Potentiometric Sensor Based on (E)-N '-((2-hydroxynaphthalen-3-yl)methylene)benzohydrazide, Int. J. Electrochem. Sc. 11 (2016) 6597-6608

42. F. Mizani, M. R. Ganjali, F. Faridbod, S. Esmaeilnia, A Novel Iron(III) Selective Potentiometric Sensor Based on 9-Ethylacenaphtho [1, 2-B]Quinoxaline, Int. J. Electrochem. Sc. 8 (2013) 10473-10486

43. H. Wang, Z. Yan, S. Zhang, X. Wen, Y. Kang, Construction and performance characteristics of polymeric membrane electrode based on iPr2Ph-DAD for the selective determination of Fe3+ ion, Desalin. Water Treat. 57 (2016) 18120-18130

44. A. L. Saber, A. M. Hameed, A. A. Sayqal, H. Alessa, A. Alharbi, Iron-selective Poly(Vinyl Chloride) Membrane Electrode Based on Norfloxacin as a Neutral Carrier, Int. J. Electrochem. Sc. 13 (2018) 10076-10087

45. M. C. Haputhanthri, H. R. Perera, A Novel Potentiometric Ion Selective Electrode

Based on Piperine for the Determination of Fe(III) Ions, J. Anal. Chem. 76 (2021) 129-134

46. D. Vlascici, E. Fagadar-Cosma, I. Popa, V. Chiriac, M. Gil-Agusti, A Novel Sensor for Monitoring of Iron(III) Ions Based on Porphyrins, Sensors 12 (2012) 8193-8203

47. S. Bita, S. O. Sadati, A. Soleymanpour, F. Amouzad, Highly Selective Solid Contact Sensor for Low Level Concentration Measurements of Iron(III) in Pharmaceutical and Biological Media, J. Anal. Chem. 73 (2018) 1202-1208

48. T. Ozer, I. Isildak, Potentiometric Studies of a New Solid-state Contact Iron(III)-Selective Electrode Based on Morin-Fe2+ Shiff Base Complex., Int. J. Electrochem. Sc. 13 (2018) 11375-11387

49. O. Isildak, O. Durgun, All-Solid-State PVC Membrane Fe (III) Selective Electrode based on 2-Hydroxymethyl-15-crown-5, Int. J. Eng. Appl. Sci. 2 (2015) 257963

50. K. Khun, Z. H. Ibupoto, S. M. U. Ali, C. O. Chey, O. Nur, M. Willander, Iron ion sensor based on functionalized ZnO nanorods, Electroanalysis 24 (2012) 521-528

51. S. K. Mittal, S. Kumar, N. Kaur, Enhanced Performance of CNT-doped Imine Based Receptors as Fe (III) Sensor Using Potentiometry and Voltammetry, Electroanalysis 31 (2019) 1229-1237

52. M. Shariyati, H. A. Zamani, A. Dehnavi, M. R. Abedi, Construction of a Fe3+ Carbon Paste Electrode Based on Multi-walled Carbon Nanotubes (MWCNTs)/Nanosilica, Int. J. Electrochem. Sci. 9 (2014) 8320-8329

53. H. Ghohari, H. A. Zamani, F. Joz-Yarmohammadi, M. Ebrahimi, M. R. Abedi, Application of 1,4-Diaminoanthraquinone as a New Sensing Material for Fabrication of a Iron(III)-Selective Modified Carbon Paste Electrode, Russ. J. Electrochem. 54 (2018) 747-754

54. K. R. Bandi, A. K. Singh, A. Upadhyay, Construction and performance characteristics of polymeric membrane electrode and coated graphite electrode for the selective determination of Fe3+ ion, Mater. Sci. Eng. C 36 (2014) 187-193

55. M. G. Motlagh, M. A. Taher, A. Ahmadi, PVC membrane and coated graphite potentiometric sensors based on 1-phenyl-3-pyridin-2-yl-thiourea for selective determination of iron(III), Electrochim Acta 55 (2010) 6724-6730

56. T. A. Ali, G. G. Mohamed, A. H. Farag, Electroanalytical studies on Fe (III) ion-selective sensors based on 2-methyl-6-(4-methylenecyclohex-2-en-1-yl) hept-2-en-4-one ionophore, Int. J. Electrochem. Sci 10 (2015) 564-578

57. T. A. Ali, A. A. Farag, G. G. Mohamed, Potentiometric determination of iron in

polluted water samples using new modified Fe(III)-screen printed ion selective electrode, J. Ind. Eng. Chem. 20 (2014) 2394-2400

58. J. Radić, M. Bralić, M. Kolar, B. Genorio, A. Prkić, I. Mitar, Development of the New Fluoride Ion-Selective Electrode Modified with Fe(x)O(y) Nanoparticles, Molecules 25 (2020) 5213

59. Y. Fung, K. Fung, Determination of iron (III) with a copper selective electrode, Anal. Chem. 49 (1977) 497-499

60. E. Duzgun, M. Tastekin, O. Atakol, A new modified Fe(III)-selective solid membrane electrode, Rev Anal Chem 27 (2008) 83-90

61. S. Anu Mary Ealia, M. P. Saravanakumar, A review on the classification, characterisation, synthesis of nanoparticles and their application, IOP Conf. Ser.: Mater. Sci. Eng. 263 (2017) 032019

62. S. Elhag, Chemically Modified Metal Oxide Nanostructures Electrodes for Sensing and Energy Conversion, Vol. 1827, Linköping University Electronic Press, 2017, str.

63. J. Hulla, S. Sahu, A. Hayes, Nanotechnology: History and future, Hum. Exp. Toxicol. 34 (2015) 1318-1321

64. J. Kreuter, Nanoparticles—a historical perspective, Int. J. Pharm. 331 (2007) 1-10

65. M. S. Chavali, M. P. Nikolova, Metal oxide nanoparticles and their applications in nanotechnology, SN Appl. Sci. 1 (2019) 1-30

66. P. G. Jamkhande, N. W. Ghule, A. H. Bamer, M. G. Kalaskar, Metal nanoparticles synthesis: An overview on methods of preparation, advantages and disadvantages, and applications, J. Drug Delivery Sci. Technol. 53 (2019) 101174

67. A. Tavakoli, M. Sohrabi, A. Kargari, A review of methods for synthesis of nanostructured metals with emphasis on iron compounds, Chem. Pap. 61 (2007) 151-170

68. K. Movlaee, M. R. Ganjali, P. Norouzi, G. Neri, Iron-Based Nanomaterials/Graphene Composites for Advanced Electrochemical Sensors, Nanomaterials (Basel, Switzerland) 7 (2017)

69. R. Gedye, F. Smith, K. Westaway, H. Ali, L. Baldisera, L. Laberge, J. Rousell, The use of microwave ovens for rapid organic synthesis, Tetrahedron Lett. 27 (1986) 279-282

70. R. J. Giguere, T. L. Bray, S. M. Duncan, G. Majetich, Application of commercial microwave ovens to organic synthesis, Tetrahedron Lett. 27 (1986) 4945-4948

71. I. Bilecka, M. Niederberger, Microwave chemistry for inorganic nanomaterials synthesis, Nanoscale 2 (2010) 1358-1374

72. M. Nuchter, B. Ondruschka, W. Bonrath, A. Gum, Microwave assisted synthesis - a critical technology overview, Green Chem. 6 (2004) 128-141

73. C. O. Kappe, Controlled Microwave Heating in Modern Organic Synthesis, Angew. Chem., Int. Ed. 43 (2004) 6250-6284

74. M. Tsuji, Microwave-Assisted Synthesis of Metallic Nanomaterials in Liquid Phase, ChemistrySelect 2 (2017) 805-819

75. R. Rosa, C. Ponzoni, C. Leonelli, Direct Energy Supply to the Reaction Mixture during Microwave-Assisted Hydrothermal and Combustion Synthesis of Inorganic Materials, Inorganics 2 (2014) 191-210

76. S. Mallakpour, M. Madani, A review of current coupling agents for modification of metal oxide nanoparticles, Prog. Org. Coat. 86 (2015) 194-207

77. S. M. Shaban, J. Kang, D.-H. Kim, Surfactants: Recent advances and their applications, Composites Communications 22 (2020) 100537

78. Á. I. López-Lorente, B. Mizaikoff, Recent advances on the characterization of nanoparticles using infrared spectroscopy, TrAC, Trends Anal. Chem. 84 (2016) 97-106

79. R. M. Cornell, U. Schwertmann, The iron oxides: structure, properties, reactions, occurrence, and uses, VCH, Weinheim; New York, 2003, str. 1-7

80. I. Fernandez-Barahona, M. Munoz-Hernando, F. Herranz, Microwave-Driven Synthesis of Iron-Oxide Nanoparticles for Molecular Imaging, Molecules 24 (2019)

81. A. Nikam, B. Prasad, A. Kulkarni, Wet chemical synthesis of metal oxide nanoparticles: a review, CrystEngComm 20 (2018) 5091-5107

82. T. Shirai, H. Watanabe, M. Fuji, M. Takahashi, Structural properties and surface characteristics on aluminum oxide powders, (2010)

83. V. Barrón, J. Torrent, Iron, manganese and aluminium oxides and oxyhydroxides. In Minerals at the Nanoscale, Mineralogical Society of Great Britain and Ireland: 2013.

84. R. Ruiz Jh, R. Lopez Sy, Synthesis of α-Al2O3 Nanopowders at Low Temperature from Aluminum Formate by Combustion Process, J. Mater. Sci. Eng. 05 (2016)

85. W. W. Wang, Y. J. Zhu, M. L. Ruan, Microwave-assisted synthesis and magnetic property of magnetite and hematite nanoparticles, J. Nanopart. Res. 9 (2007) 419-426

86. S. Guru, D. Mishra, S. S. Amritphale, S. Joshi, Influence of glycols in microwave assisted synthesis of ironoxide nanoparticles, Colloid Polym. Sci. 294 (2016) 207-213

87. T. Nurhayati, F. Iskandar, M. Abdullah, Khairurrijal. Syntheses of Hematite (alpha-Fe2O3) Nanoparticles Using Microwave-Assisted Calcination Method. In Proceedings

of Symposium on Nanotechnology Applications in Energy and Environment (NAEE 2012), Bandung, INDONESIA, Sep 20-21; pp. 197-203.

88. L. Hu, A. Percheron, D. Chaumont, C. H. Brachais, Microwave-assisted one-step hydrothermal synthesis of pure iron oxide nanoparticles: magnetite, maghemite and hematite, J. Sol-Gel Sci. Technol. 60 (2011) 198-205

89. C. W. Kim, M. J. Kang, T. K. Van, Y. S. Kang, A selective morphosynthetic approach for single crystalline hematite through morphology evolution via microwave assisted hydrothermal synthesis, J. Ind. Eng. Chem. 53 (2017) 341-347

90. K. P. Ananth, S. P. Jose, K. S. Venkatesh, R. Ilangovan, Size Controlled Synthesis of Magnetite Nanoparticles Using Microwave Irradiation Method, J. Nano Res. 24 (2013) 184-193

91. Z. Ai, K. Deng, Q. Wan, L. Zhang, S. Lee, Facile Microwave-Assisted Synthesis and Magnetic and Gas Sensing Properties of Fe(3)O4 Nanoroses, J. Phys. Chem. C 114 (2010) 6237-6242

92. C. Y. Li, Y. J. Wei, A. Liivat, Y. H. Zhu, J. F. Zhu, Microwave-solvothermal synthesis of Fe3O4 magnetic nanoparticles, Mater. Lett. 107 (2013) 23-26

93. C. S. Xavier, C. A. Paskocimas, F. V. da Motta, V. D. Araujo, M. J. Aragon, J. L. Tirado, P. Lavela, E. Longo, M. R. B. Delmonte, Microwave-assisted Hydrothermal Synthesis of Magnetite Nanoparticles with Potential Use as Anode in Lithium Ion Batteries, Mater. Res.-Ibero-am. J. Mater. 17 (2014) 1065-1070

94. E. Kostyukhin, Synthesis of magnetite nanoparticles upon microwave and convection heating, Russ. J. Phys. Chem. A 92 (2018) 2399-2402

95. L. Zhang, Y.-J. Zhu, Microwave-Assisted Solvothermal Synthesis of AlOOH Hierarchically Nanostructured Microspheres and Their Transformation to γ-Al2O3 with Similar Morphologies, The Journal of Physical Chemistry C 112 (2008) 16764-16768

96. K. Laishram, R. Mann, N. Malhan, A novel microwave combustion approach for single step synthesis of alpha-Al2O3 nanopowders, Ceram Int 38 (2012) 1703-1706

97. T. Yin, W. Qin, Applications of nanomaterials in potentiometric sensors, TrAC, Trends Anal. Chem. 51 (2013) 79-86

98. M. Willander, H. Alnoor, S. Elhag, Z. H. Ibupoto, E. S. Nour, O. Nur, Comparision between different metal oxide nanostructures and nanocomposites for sensing, energy generation, and energy harvesting, Vol. 9749, SPIE, 2016, str.

99. V. H. Grassian, When size really matters: size-dependent properties and surface

chemistry of metal and metal oxide nanoparticles in gas and liquid phase environments, The Journal of Physical Chemistry C 112 (2008) 18303-18313

100. W. Q. Lim, Z. Gao, Metal oxide nanoparticles in electroanalysis, Electroanalysis 27 (2015) 2074-2090

101. J. M. George, A. Antony, B. Mathew, Metal oxide nanoparticles in electrochemical sensing and biosensing: a review, Microchim. Acta 185 (2018) 358

102. S. Sawan, R. Maalouf, A. Errachid, N. Jaffrezic-Renault, Metal and metal oxide nanoparticles in the voltammetric detection of heavy metals: A review, TrAC, Trends Anal. Chem. 131 (2020) 116014

103. A. Chen, S. Chatterjee, Nanomaterials based electrochemical sensors for biomedical applications, Chem. Soc. Rev. 42 (2013) 5425-5438

104. X. Zhang, S. Yu, W. He, H. Uyama, Q. Xie, L. Zhang, F. Yang, Electrochemical sensor based on carbon-supported NiCoO2 nanoparticles for selective detection of ascorbic acid, Biosens. Bioelectron. 55 (2014) 446-451

105. E. Katz, I. Willner, J. Wang, Electroanalytical and Bioelectroanalytical Systems Based on Metal and Semiconductor Nanoparticles, Electroanalysis 16 (2004) 19-44

106. M. Trojanowicz, Impact of nanotechnology on design of advanced screen-printed electrodes for different analytical applications, TrAC, Trends Anal. Chem. 84 (2016) 22-47

107. A. J. Anschutz, R. L. Penn, Reduction of crystalline iron(III) oxyhydroxides using hydroquinone: Influence of phase and particle size, Geochem. Trans. 6 (2005)

108. A. S. Madden, M. F. Hochella Jr, A test of geochemical reactivity as a function of mineral size: Manganese oxidation promoted by hematite nanoparticles, Geochim. Cosmochim. Acta 69 (2005) 389-398

109. A. S. Agnihotri, A. Varghese, M. Nidhin, Transition metal oxides in electrochemical and bio sensing: A state-of-art review, Applied Surface Science Advances 4 (2021) 100072

110. B. Fang, G. Wang, W. Zhang, M. Li, X. Kan, Fabrication of Fe3O4 Nanoparticles Modified Electrode and Its Application for Voltammetric Sensing of Dopamine, Electroanalysis 17 (2005) 744-748

111. Z. Zhang, H. Zhu, X. Wang, X. Yang, Sensitive electrochemical sensor for hydrogen peroxide using Fe3O4 magnetic nanoparticles as a mimic for peroxidase, Microchim. Acta 174 (2011) 183-189

112. J. Hrbac, V. Halouzka, R. Zboril, K. Papadopoulos, T. Triantis, Carbon Electrodes

Modified by Nanoscopic Iron(III) Oxides to Assemble Chemical Sensors for the Hydrogen Peroxide Amperometric Detection, Electroanalysis 19 (2007) 1850-1854

113. S. X. Luo, Y. H. Wu, H. Gou, Y. Liu. A novel electrochemical sensor for the analysis of salbutamol in pork samples by using NiFe2O4 nanoparticles modified glassy carbon electrode. In Proceedings of Advanced Materials Research; pp. 1279-1282.

114. N. S. Osman, N. Thapliyal, W. S. Alwan, R. Karpoormath, T. Moyo, Synthesis and characterization of Ba0.5Co0.5Fe2O4 nanoparticle ferrites: application as electrochemical sensor for ciprofloxacin, J. Mater. Sci.: Mater. Electron. 26 (2015) 5097-5105

115. T. Madrakian, S. Maleki, M. Heidari, A. Afkhami, An electrochemical sensor for rizatriptan benzoate determination using Fe3O4 nanoparticle/multiwall carbon nanotube-modified glassy carbon electrode in real samples, Materials Science and Engineering: C 63 (2016) 637-643

116. S. Lee, J. Oh, D. Kim, Y. Piao, A sensitive electrochemical sensor using an iron oxide/graphene composite for the simultaneous detection of heavy metal ions, Talanta 160 (2016) 528-536

117. Y. Zhang, Y. Cheng, Y. Zhou, B. Li, W. Gu, X. Shi, Y. Xian, Electrochemical sensor for bisphenol A based on magnetic nanoparticles decorated reduced graphene oxide, Talanta 107 (2013) 211-218

118. C. Hou, W. Tang, C. Zhang, Y. Wang, N. Zhu, A novel and sensitive electrochemical sensor for bisphenol A determination based on carbon black supporting ferroferric oxide nanoparticles, Electrochim. Acta 144 (2014) 324-331

119. T. Wen, W. Zhu, C. Xue, J. Wu, Q. Han, X. Wang, X. Zhou, H. Jiang, Novel electrochemical sensing platform based on magnetic field-induced self-assembly of Fe3O4@Polyaniline nanoparticles for clinical detection of creatinine, Biosens. Bioelectron. 56 (2014) 180-185

120. S. Chandra, H. Lang, D. Bahadur, Polyaniline-iron oxide nanohybrid film as multi-functional label-free electrochemical and biomagnetic sensor for catechol, Anal. Chim. Acta 795 (2013) 8-14

121. W. Zhu, G. Jiang, L. Xu, B. Li, Q. Cai, H. Jiang, X. Zhou, Facile and controllable one-step fabrication of molecularly imprinted polymer membrane by magnetic field directed self-assembly for electrochemical sensing of glutathione, Anal. Chim. Acta 886 (2015) 37-47

122. S. Kumar, P. Karfa, S. Patra, R. Madhuri, P. K. Sharma, Molecularly imprinted star

polymer-modified superparamagnetic iron oxide nanoparticle for trace level sensing and separation of mancozeb, RSC Adv. 6 (2016) 36751-36760

123. L. Chen, G. Wang, J. Xie, P. Rai, J. Lee, G. Mathur, V. Varadan, Study of the electrochemical properties of magnetite, maghemite and hematite nanoparticles for their applications in lithium ion batteries, Vol. 8691, SPIE, 2013, str.

124. S. Radhakrishnan, K. Krishnamoorthy, C. Sekar, J. Wilson, S. J. Kim, A highly sensitive electrochemical sensor for nitrite detection based on Fe2O3 nanoparticles decorated reduced graphene oxide nanosheets, Appl. Catal., B 148-149 (2014) 22-28

125. M. Yuan, J. Li, Y. Yu, Y. Fu, A. Fong, J. Hu, Fabrication of a Fe2O3Nanoparticles Implantation-modified Electrode and its Applications in Electrochemical Sensing, Electroanalysis 28 (2015) 954-961

126. A. S. Adekunle, B. O. Agboola, J. Pillay, K. I. Ozoemena, Electrocatalytic detection of dopamine at single-walled carbon nanotubes–iron (III) oxide nanoparticles platform, Sens. Actuators, B 148 (2010) 93-102

127. H. Heli, S. Majdi, N. Sattarahmady, Ultrasensitive sensing of N-acetyl-l-cysteine using an electrocatalytic transducer of nanoparticles of iron(III) oxide core–cobalt hexacyanoferrate shell, Sens. Actuators, B 145 (2010) 185-193

128. S. Yang, G. Li, G. Wang, D. Deng, L. Qu, A novel electrochemical sensor based on Fe2O3 nanoparticles/N-doped graphene for electrocatalytic oxidation of L-cysteine, J. Solid State Electrochem. 19 (2015) 3613-3620

129. M. Bonyani, A. Mirzaei, S. G. Leonardi, A. Bonavita, G. Neri, Electrochemical Properties of Ag@iron Oxide Nanocomposite for Application as Nitrate Sensor, Electroanalysis 27 (2015) 2654-2662

130. Z. Yu, H. Li, J. Lu, X. Zhang, N. Liu, X. Zhang, Hydrothermal synthesis of Fe2O3/graphene nanocomposite for selective determination of ascorbic acid in the presence of uric acid, Electrochim. Acta 158 (2015) 264-270

131. Y. Wu, C. Hu, M. Huang, N. Song, W. Hu, Highly enhanced electrochemical responses of rutin by nanostructured Fe2O3/RGO composites, Ionics 21 (2015) 1427-1434

132. F. Gao, D. Zheng, H. Tanaka, F. Zhan, X. Yuan, F. Gao, Q. Wang, An electrochemical sensor for gallic acid based on Fe2O3/electro-reduced graphene oxide composite: Estimation for the antioxidant capacity index of wines, 57 (2015) 279-287

133. F. M. Abdel-Haleem, E. Gamal, M. S. Rizk, A. Madbouly, R. M. El Nashar, B. Anis, H. M. Elnabawy, A. S. G. Khalil, A. Barhoum, Molecularly Imprinted Electrochemical Sensor-Based Fe2O3@MWCNTs for Ivabradine Drug Determination in

Pharmaceutical Formulation, Serum, and Urine Samples, Front. Bioeng. Biotechnol. 9 (2021) 16

134.   L. Dai, X. Du, D. Jiang, W. Chen, M. Zhu, K. Wang, Ultrafine α-Fe2O3 nanocrystals anchored on N-doped graphene: a nanomaterial with long hole diffusion length and efficient visible light-excited charge separation for use in photoelectrochemical sensing, 184 (2017) 137-145

135.   P. Muthukumaran, C. Sumathi, J. Wilson, C. Sekar, S. Leonardi, G. Neri, Fe2O3/Carbon nanotube-based resistive sensors for the selective ammonia gas sensing, Sens. Lett. 12 (2014) 17-23

136.   X. Li, Y. Lei, X. Li, S. Song, C. Wang, H. Zhang, Morphology-controlled synthesis of α-Fe2O3 nanostructures with magnetic property and excellent electrocatalytic activity for H2O2, Solid State Sci. 13 (2011) 2129-2136

137.   W. Hu, W. Zhang, Y. Wu, W. Qu, Self-assembly and hydrothermal technique syntheized Fe2O3-RGO nanocomposite: The enhancement effect of electrochemical simultaneous detection of honokiol and magnolol, J. Electroceram. 40 (2018) 1-10

138.   B.-Q. Li, F. Nie, Q.-L. Sheng, J.-B. Zheng, An electrochemical sensor for sensitive determination of nitrites based on Ag–Fe3O4–graphene oxide magnetic nanocomposites, Chem. Pap. 69 (2015) 911-920

139.   S. Erogul, S. Z. Bas, M. Ozmen, S. Yildiz, A new electrochemical sensor based on Fe3O4 functionalized graphene oxide-gold nanoparticle composite film for simultaneous determination of catechol and hydroquinone, Electrochim. Acta 186 (2015) 302-313

140.   H. Teymourian, A. Salimi, S. Khezrian, Fe3O4 magnetic nanoparticles/reduced graphene oxide nanosheets as a novel electrochemical and bioeletrochemical sensing platform, Biosens. Bioelectron. 49 (2013) 1-8

141.   A. Benvidi, S. Jahanbani, B.-F. Mirjalili, R. Zare, Electrocatalytic oxidation of hydrazine on magnetic bar carbon paste electrode modified with benzothiazole and iron oxide nanoparticles: Simultaneous determination of hydrazine and phenol, Chin. J. Catal. 37 (2016) 549-560

142.   H. Huang, X. Liu, X. Zhang, W. Liu, X. Su, Z. Zhang, Fabrication of New Magnetic Nanoparticles (Fe3O4) Grafted Multiwall Carbon Nanotubes and Heterocyclic Compound Modified Electrode for Electrochemical Sensor, Electroanalysis 22 (2010) 433-438

143.   H. Cui, W. Yang, X. Li, H. Zhao, Z. Yuan, An electrochemical sensor based on a

magnetic Fe3O4 nanoparticles and gold nanoparticles modified electrode for sensitive determination of trace amounts of arsenic(iii), Anal. Methods 4 (2012) 4176-4181

144. Y. Wang, Y. Zhang, C. Hou, M. Liu, Ultrasensitive electrochemical sensing of dopamine using reduced graphene oxide sheets decorated with p-toluenesulfonate-doped polypyrrole/Fe3O4 nanospheres, Microchim. Acta 183 (2016) 1145-1152

145. Y. Wang, W. Wang, G. Li, Q. Liu, T. Wei, B. Li, C. Jiang, Y. Sun, Electrochemical detection of L-cysteine using a glassy carbon electrode modified with a two-dimensional composite prepared from platinum and Fe3O4 nanoparticles on reduced graphene oxide, Microchim. Acta 183 (2016) 3221-3228

146. K. Khun, Z. H. Ibupoto, J. Lu, M. S. Alsalhi, M. Atif, A. A. Ansari, M. Willander, Potentiometric glucose sensor based on the glucose oxidase immobilized iron ferrite magnetic particle/chitosan composite modified gold coated glass electrode, Sens. Actuators, B 173 (2012) 698-703

147. R. Shabani, Z. Lakhaiy Rizi, R. Moosavi, Selective Potentiometric Sensor for Isoniazid Ultra-Trace Determination Based on Fe3O4 Nanoparticles Modified Carbon Paste Electrode (Fe3O4/CPE), Int. J. Nanosci. Nanotechnol. 14 (2018) 241-249

148. C. P. Sousa, R. C. de Oliveira, T. M. Freire, P. B. A. Fechine, M. A. Salvador, P. Homem-de-Mello, S. Morais, P. de Lima-Neto, A. N. Correia, Chlorhexidine digluconate on chitosan-magnetic iron oxide nanoparticles modified electrode: Electroanalysis and mechanistic insights by computational simulations, Sens. Actuators, B 240 (2017) 417-425

149. N.-N. Li, T.-F. Kang, J.-J. Zhang, L.-P. Lu, S.-Y. Cheng, Fe3O4@ZrO2 magnetic nanoparticles as a new electrode material for sensitive determination of organophosphorus agents, Anal. Methods 7 (2015) 5053-5059

150. M. Arvand, S. Orangpour, N. Ghodsi, Differential pulse stripping voltammetric determination of the antipsychotic medication olanzapine at a magnetic nano-composite with a core/shell structure, RSC Adv. 5 (2015) 46095-46103

151. N. Baig, M. Sajid, T. A. Saleh, Recent trends in nanomaterial-modified electrodes for electroanalytical applications, TrAC, Trends Anal. Chem. 111 (2019) 47-61

152. J. Qiu, M. Zhao, Q. Zhao, Y. Xu, L. Zhang, X. Lu, H. Xue, H. Pang, Aluminum-based materials for advanced battery systems, Sci. China Mater. 60 (2017) 577-607

153. R. Zaimbashi, H. Beitollahi, M. Torkzadeh-Mahani, Simultaneous Electrochemical Sensing of Methyldopa and Hydrochlorothiazide using a Novel ZnO/Al2O3 Nanocomposite Modified Screen Printed Electrode, Anal. Bioanal. Electrochem. 9

(2017) 1008-1020

154. M. Reza Ganjali, Voltammetric Determination of Dopamine Using Glassy Carbon Electrode Modified with ZnO/Al2O3 Nanocomposite, Int. J. Electrochem. Sci. (2018) 2519-2529

155. N. Soltani, N. Tavakkoli, F. Shahdost-fard, H. Salavati, F. Abdoli, A carbon paste electrode modified with Al2O3-supported palladium nanoparticles for simultaneous voltammetric determination of melatonin, dopamine, and acetaminophen, Microchim. Acta 186 (2019) 13

156. Y. Wei, R. Yang, Y. X. Zhang, L. Wang, J. H. Liu, X. J. Huang, High adsorptive gamma-AlOOH(boehmite)@SiO2/Fe3O4 porous magnetic microspheres for detection of toxic metal ions in drinking water, Chem. Commun. 47 (2011) 11062-11064

157. M. M. Mekawy, R. Y. A. Hassan, P. Ramnani, X. J. Yu, A. Mulchandani, Electrochemical detection of dihydronicotinamide adenine dinucleotide using Al2O3-GO nanocomposite modified electrode, Arab. J. Chem. 11 (2018) 942-949

158. M. H. Parvin, J. Arjomandi, J. Y. Lee, gamma-Al2O3 nanoparticle catalyst mediated polyaniline gold electrode biosensor for vitamin E, Catal. Commun. 110 (2018) 59-63

159. M. Reza Ganjali, Determination of Salicylic Acid by Differential Pulse Voltammetry Using ZnO/Al2O3 Nanocomposite Modified Graphite Screen Printed Electrode, Int. J. Electrochem. Sci. (2017) 9972-9982

160. J. B. Li, W. Y. Sun, X. J. Wang, H. M. Duan, Y. H. Wang, Y. L. Sun, C. F. Ding, C. N. Luo, Ultra-sensitive film sensor based on Al2O3-Au nanoparticles supported on PDDA-functionalized graphene for the determination of acetaminophen, Anal. Bioanal. Chem. 408 (2016) 5567-5576

161. M. Reza Ganjali, Highly Sensitive Voltammetric Sensor for Determination of Ascorbic Acid Using Graphite Screen Printed Electrode Modified with ZnO/Al2O3 Nanocomposite, Int. J. Electrochem. Sci. (2017) 3231-3240

6. APPENDICES

Article 1

A. Paut, A. Prkić, I. Mitar, P. Bošković, D. Jozić, M. Jakić, T. Vukušić, Potentiometric Response of Solid-State Sensors Based on Ferric Phosphate for Iron(III) Determination, Sensors, 21 (2021), 5.

Author Contributions:

Conceptualization; Andrea Paut, Ante Prkić, and Ivana Mitar

Methodology; Ante Prkić

Software; Perica Bošković

Validation; Tina Vukušić and Andrea Paut

Formal analysis; Dražan Jozić and Miće Jakić

Investigation; Andrea Paut

Resources; Ante Prkić

Data curation; Ivana Mitar

Writing-original draft preparation; Andrea Paut

Writing-review and editing; Andrea Paut, Ivana Mitar and Dražan Jozić

Visualization; Andrea Paut

Supervision; Ante Prkić

Project administration; Ante Prkić

Funding acquisition; Ante Prkić

Potentiometric Response of Solid-State Sensors Based on Ferric Phosphate for Iron(III) Determination

Andrea Paut [1], Ante Prkić [1,*], Ivana Mitar [2], Perica Bošković [2], Dražan Jozić [3], Miće Jakić [4] and Tina Vukušić [5]

1   Department of Analytical Chemistry, Faculty of Chemistry and Technology, University of Split, R. Boškovića 35, 21000 Split, Croatia; andrea.paut@ktf-split.hr
2   Department of Chemistry, Faculty of Science, University of Split, R. Boškovića 33, 21000 Split, Croatia; imitar@pmfst.hr (I.M.); pboskovic@pmfst.hr (P.B.)
3   Department of Inorganic Technology, Faculty of Chemistry and Technology, University of Split, R. Boškovića 35, 21000 Split, Croatia; drazan.jozic@ktf-split.hr
4   Department of Organic Technology, Faculty of Chemistry and Technology, University of Split, R. Boškovića 35, 21000 Split, Croatia; mice.jakic@ktf-split.hr
5   Faculty of Chemistry and Technology, University of Split, R. Boškovića 35, 21000 Split, Croatia; tinavukusic@gmail.com
*   Correspondence: ante.prkic@ktf-split.hr

Abstract: A novel ion-selective electrode with membranes based on iron(III) phosphate and silver sulfide integrated into a completely new electrode body design has been developed for the determination of iron(III) cations. The best response characteristics with linear potential change were found in the iron(III) concentration range from 3.97×10^{-5} to 10^{-2} mol L^{-1}. The detection limit was found to be 2.41×10^{-5} mol L^{-1} with a slope of -20.53 ± 0.63 and regression coefficient of 0.9925, while the quantification limit was 3.97×10^{-5} M. The potential change per concentration decade ranged from -13.59 ± 0.54 to -20.53 ± 1.56 for Electrode Body 1 (EB1) and from -17.28 ± 1.04 to -24 ± 1.87 for Electrode Body 2 (EB2), which is presented for the first time in this work. The prepared electrode has a long lifetime and the ability to detect changes in the concentration of iron cations within 20 s. Membrane M1 showed high recoveries in the determination of iron cations in iron(III) standard solutions (98.2–101.2%) as well as in two different pharmaceuticals (98.6–106.5%). This proves that this type of sensor is applicable in the determination of ferric cations in unknown samples, and the fact that all sensor parts are completely manufactured in our laboratory proves the simplicity of the method.

Keywords: ion-selective electrode; potentiometry; iron(III) cations

1. Introduction

Ion-selective electrodes (ISEs) represent a small electrochemical sensor that can determine ion activity in various sample matrices without pretreatment. Potentiometry stands out as a non-destructive electroanalytical method with the possibility of application in a wide range of sensor performances [1]. Although liquid-contact ion-selective membranes are well developed and commercially available in a number of embodiments, their impossibility of miniaturization, special storage requirements, the sensitivity of inner filings toward evaporation the possibility of volume changes, and delamination of the sensing membrane, make solid-state electrodes preferred ion-selective sensors [2–5]. The possibility of developing this type of sensor with the characteristics of high selectivity and sensitivity and with the simplicity of implementation, low cost, and durability makes them attractive for use in ion determination in biological, chemical, environmental, and industrial samples [6].

Numerous solid-state ion-selective membranes with different compositions and performances for the determination of metal ions are known. Since iron is a ubiquitous metal in

various biological processes and has found numerous industrial applications in steel, water pipes, paints, plastics, and the medical industry, it was not only desirable but necessary to develop a suitable method for rapid, efficient, and cost-effective iron determination. Some of the human health disorders are closely related to the imbalance of iron concentration in the human body, such as iron deficiency causes anemia, while iron accumulation can lead to the occurrence of hemochromatosis diseases [7].

Iron(III) cations are often detected by atomic absorption spectroscopy [8,9], inductively coupled plasma mass spectrometry [10], and spectrophotometry [11,12]. Although the aforementioned techniques provide accurate results, they are less accessible to the general population due to the necessary pretreatment of samples and sophisticated, expensive equipment that requires a trained analyst to use.

Considering different types of potentiometric sensors, ferric cations are mostly determined with membranes based on conductive polymers [7,13–23], carbon materials electrodes [24,25], and to a small extent with those based on iron salts [26].

In this work, a new homemade solid-contact ion-selective membrane based on sparingly soluble ferric phosphate is presented for the determination of Fe^{3+} cations in acidic media. To obtain a membrane selective for a particular ion, it is necessary to have a compound in the membrane composition that forms a stable complex or a sparingly soluble salt with the analyte. That compound represents the active centers of the sensors, and in this research is the iron phosphate precipitated in our laboratory. The other two components are silver sulfide, which is the charge transmitter, and polytetrafluoroethylene (PTFE) as the carrier. In this work, not only a completely new membrane for iron determination was presented, but also a new electrode body with many improved properties compared to the electrode body presented in previous work [27].

2. Materials and Methods

The main components of the membrane, iron(III) phosphate and silver sulfide, were prepared in our laboratory by a precipitation technique, while the polytetrafluoroethylene used was commercially available. The solutions used for both, preparation and testing of the proposed membranes, were prepared in ultrapure water with a declared conductivity of 0.04 μS cm^{-1} (Millipore Simplicity, Billerica, MA, USA). Ferric phosphate powder was prepared by mixing 0.5 mol L^{-1} anhydrous ferric chloride with disodium hydrogen phosphate of the same concentration under acidic conditions. A white-yellow precipitate was formed, which was centrifuged and washed with ultrapure water. After centrifugation, the ferric phosphate was dried in a vacuum dryer at 150 °C. Silver sulfide was also prepared by precipitation technique using silver nitrate and sodium sulfide nonahydrate as reagents. The black precipitate obtained, was then filtered, washed with chloroform and ultrapure water, and dried in a conventional dryer at 60 °C for 2 h. Different ratios of the three membrane components in the 500 mg mixture were homogenized and pressed under 625 MPa for 2 h to form membranes of 10 mm diameter. The compositions of the membrane mixtures are chosen by sequentially increasing or decreasing each of the three major components to investigate their influence. In membranes M1–M5, it was possible to find out which is the smallest percentage of the active substance in the composition to obtain a membrane that is selective towards iron cations. In membranes M6–M10, the percentage of polytetrafluoroethylene was reduced to find the smallest amount necessary to ensure the mechanical compactness of the membrane. Membranes M11–M15 show the importance of the presence of silver sulfide and polytetrafluoroethylene. A similar approach was previously reported [4,5,27,28]. As described, 15 different membranes were prepared and their composition ratios are shown in Table 1.

Table 1. List of all tested membranes.

Sensor Name	Membrane Composition Ratio		
	FePO$_4$	Ag$_2$S	PTFE
M1	1	1	2
M2	1	2	3
M3	1	3	4
M4	1	4	5
M5	1	5	6
M6	1	4	3.33
M7	1	4	2.14
M8	1	4	1.25
M9	1	4	0.56
M10	1	4	0
M11	1	1	0
M12	2	1	0
M13	3	1	0
M14	1	0	0
M15	1	0	1

The XRD analysis of three main membranes components: FePO$_4$, Ag$_2$S, and polytetrafluoroethylene were performed by using Malvern PANalytical Empyrean X-ray diffraction system with the following operating conditions: Cu-Kα, 45 kV voltage and 40 mA current, 0.1050° step size, counting time/step of 88.5 s and a scanning angle 2θ from 5 to 80°. The instrument uses a multicore optics iCore/dCore and detector PIXcel3D-Medipix3 1 × 1 detector. In the procedure of data treatment collected pattern was corrected for systematic errors (external Si standard). The qualitative interpretation of the XRD pattern was made by comparison with standards patterns contained in the database PDF2 (ICDD, PDF2 Released 2020) by using HighScore Plus. Quantitative analysis was made by using the Direct Derivative (DD) quantification method. [28]

The ion-selective membranes for the determination of ferric cations presented in this work were tested in two different embodiments of the electrode body. They differ in terms of electrode size, membrane mobility, and the amount of charge transferred.

The scheme of Electrode Body 1 (EB1) is shown in Figure 1 and the digital photo in Figure 2. It is entirely made of polytetrafluoroethylene, while the contact between the sensor and the millivoltmeter (SevenExcellence, Mettler Toledo, Switzerland-USA) is ensured by a stainless-steel disk connected to the device by a coaxial cable. The use of this electrode body requires a specially designed glass cell that ensures the positioning of the sensor at an angle of 45 degrees.

The Electrode Body 2 (EB2), shown in Figures 3 and 4 (digital photo), is based on the idea of print screen electrodes, it is miniaturized, not limited by the position angle and all tests can be performed in normal laboratory glass.

Although the idea of EB2 is based on the print screen electrodes, to the best of our knowledge, this type of design has not yet been reported. The copper layer on the epoxy plate provides charge transfer between the sensor and the cable connected to the millivoltmeter. Contact between the ion-selective membrane and the copper layer is made possible by a special conductive graphite adhesive. Since the adhesive is in a liquid state before drying, complete adhesion of the sensor to the tile is ensured and no loss of contact occurs. The copper layer is protected from the influence of the solution with a non-conductive layer in the form of a varnish commonly used to coat copper wires in cables.

A double silver-silver chloride electrode (Reference plus, Mettler Toledo) was used as the reference electrode in both cases. Both electrodes (reference and indicator electrodes) were immersed together in a solution containing ions of interest in a double-walled glass vessel (if EB1) or a conventional laboratory glass (if EB2) on a magnetic stirrer at room temperature.
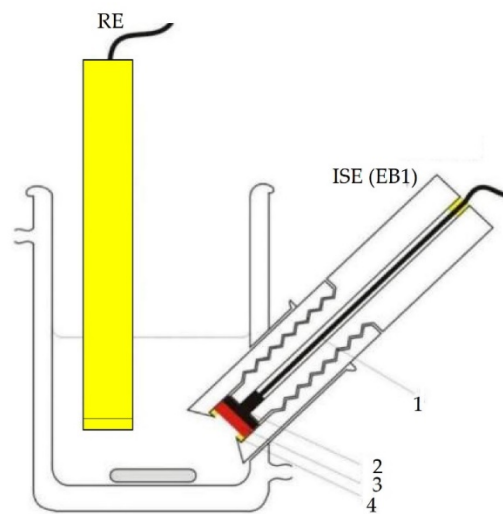
Figure 1. Scheme of ion-selective electrode (ISE(EB1)) and reference electrode (RE); (**1**—coaxial cable, **2**—steel disc, **3**—membrane, **4**—silicon rubber) [27].

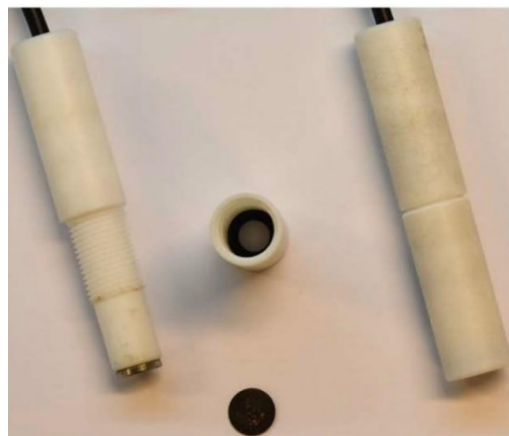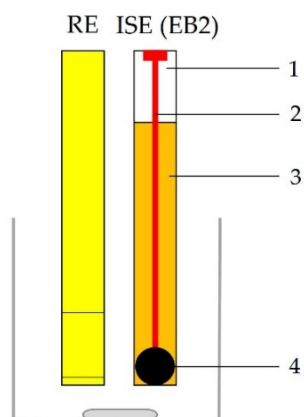**Figure 2.** Digital picture of Electrode Body 1 (EB1).

Figure 3. Scheme of ion-selective electrode (ISE(EB2)) and reference electrode (RE); (**1**—epoxy plate, **2**—copper layer, **3**—non-conductive lack, **4**—ion-selective membrane).

Figure 4. Digital photography of Electrode Body 2 (EB2).

Testing of all the presented membranes in Table 1 was carried out in anhydrous ferric chloride and ferric nitrate nonahydrate solutions at pH 0, 1, and 1.5 because at pH > 2 ferric hydroxide starts to precipitate which could prevent the membrane from responding. The pH of ferric chloride solutions was adjusted with sulfuric acid and ferric nitrate solutions with nitric acid. All sensors were also tested in the disodium hydrogen phosphate solution for the response towards phosphate ions at pH = 13, since under these conditions $(PO_4)^{3-}$ is the dominant form in a solution. The tests were carried out at room temperature by a standard dilution method.

Selectivity is one of the most important properties of an ion-selective electrode. It refers to the ability of the sensor to determine the presence of the analyte (A) over the presence of another (interfering) ion in the solution (B).

The matched potential method (MPM) was used to measure the selectivity coefficient since it was recommended in literature because of the different charge numbers of primary and interfering ions [29]. According to this method, the activity of Fe^{3+} cations was increased from $a_A = 5 \times 10^{-4}$ mol L^{-1} (reference solution) to $a_A' = 5 \times 10^{-3}$ mol L^{-1}, and the potential change (ΔE) was recorded. In the next step, 0.1 mol L^{-1} solution of the interfering ion was added to the Fe^{3+} reference solution until the same potential change (ΔE) was recorded, and the concentration of added the interfering ion is thus a_B. The values of the sensor selectivity coefficient are calculated using the following equation.

$$K_{A,B}^{pot} = \left(a_A' - a_A\right) / a_B$$

The interfering species selected in this work were aluminum nitrate, barium nitrate, calcium nitrate, and magnesium nitrate. These interfering species were selected because of their high ability to form sparingly soluble precipitates with PO_4^{3-} anions ($Al(PO_4)$, $Ba_3(PO_4)_2$, $Ca_3(PO_4)_2$, $Mg_3(PO_4)_2$), according to their Ksp values which are lower than 1×10^{-20}.

To confirm the applicability of the sensor in the determination of ferric cations, a homemade sensor proposed in this work was used to determine Fe^{3+} ions in two different oxidized drugs. The dietary supplements used in this experiment were Tardyferon® and Heferol®, both of which contain ferrous cations as active ingredients. Due to the complex composition of the supplements and the fact that it was necessary to oxidize ferrous cations to ferric cations, samples were prepared by microwave digestion using the Milestone flexiWAVE 480 (Milestone, Italy). One sample per insert was digested with nitric acid and hydrogen peroxide at a pressure of 0.75 MPa and a temperature of 180 °C in the vessel. The digestion process took 1 h. After cooling, a certain volume of the samples was diluted separately in two 100 mL flasks with nitric acid at pH 1.

3. Results

3.1. XRD Characterization

Figures 5–7 show the powder diffraction patterns of the prepared samples of silver sulfide (Ag_2S), ferric phosphate, and used polytetrafluoroethylene for preparation membranes. According to the results of the analysis powder diffraction pattern of specimens denoted as Ag_2S (Figure 5) is visible that its composition is a mixture of three different crystal phases, silver sulfide sulfate (PDF 00-061-0633), silver sulfide (PDF 00-068-0300), and silver (PDF 01-071-4613). The results of the conducted quantitative analysis of the diffraction pattern on the presence of phases silver sulfide sulfate, silver sulfide, and silver, indicate the proportion of phases is 31.0, 60.7, and 8.3 wt%, respectively.
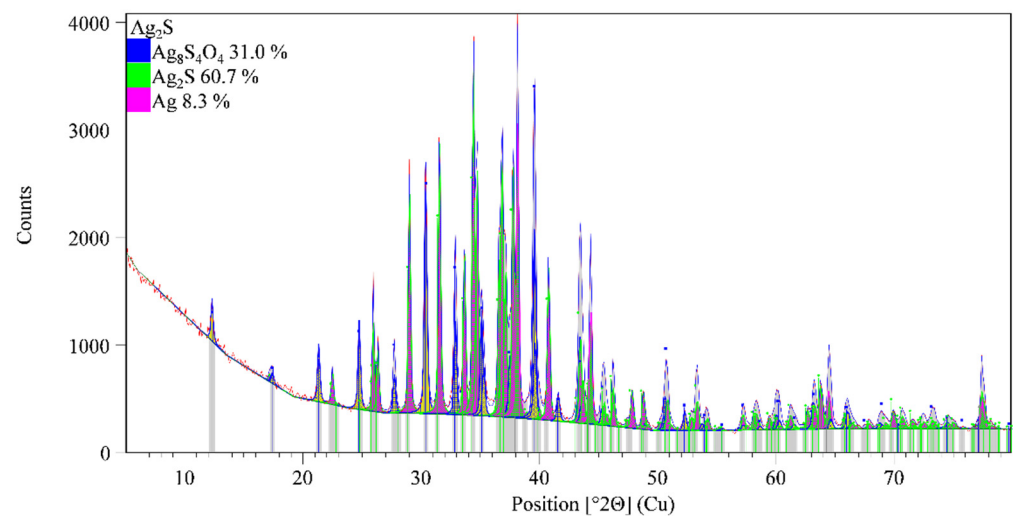
Figure 5. XRD pattern of silver sulfide.

The diffraction pattern of the sample denoted as $FePO_4$ is shown in Figure 6, from the level of intensity background into diffraction patterns is visible high fluorescence which is presented into diffraction pattern which arises from the iron. The appearance of a diffuse diffraction maximum centered at 2Theta value at 8.72° and 29.08° indicates the presence of a structurally disordered phase (structurally ordered phase at the short-range distance). In addition, the sample also shows diffraction maxima that belong to the structurally arranged phases, according to the qualitative analysis diffraction pattern they belong to the NaCl (PDF 01-080-3939), $Fe(H_2PO_4)_3 \cdot 2H_2O$ (PDF 00-043-0104) and $Fe(H_2PO_2)_3$ (PDF 00-001-0181). Figure 7 shows the diffraction pattern of the polytetrafluoroethylene used in the preparation procedure of membranes. Diffraction patterns show that PTFE is a semi-crystalline material that consists of the crystallized phase of polytetrafluoroethylene (PDF 00-061-1415) and the amorphous phase which suggests the appearing the diffuse diffraction maximum centered at 2Theta value at 39°.
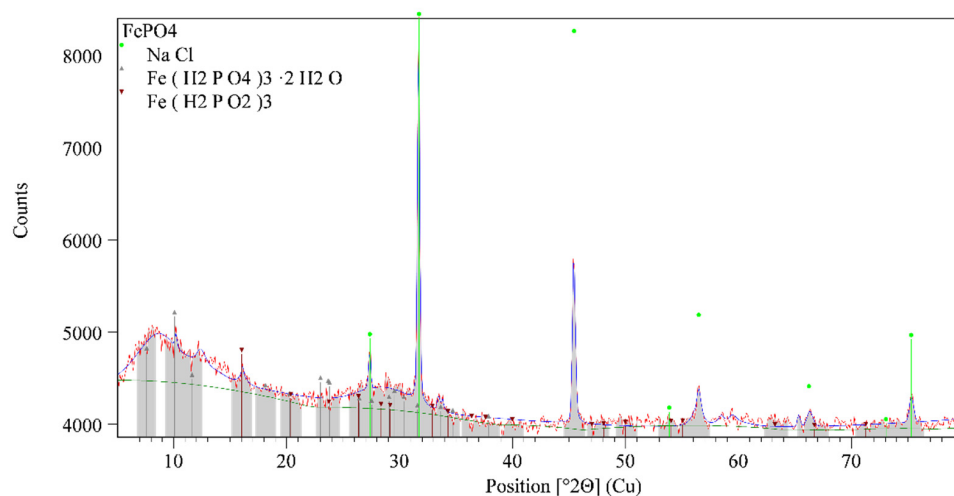
Figure 6. XRD pattern of ferric phosphate ($FePO_4$).
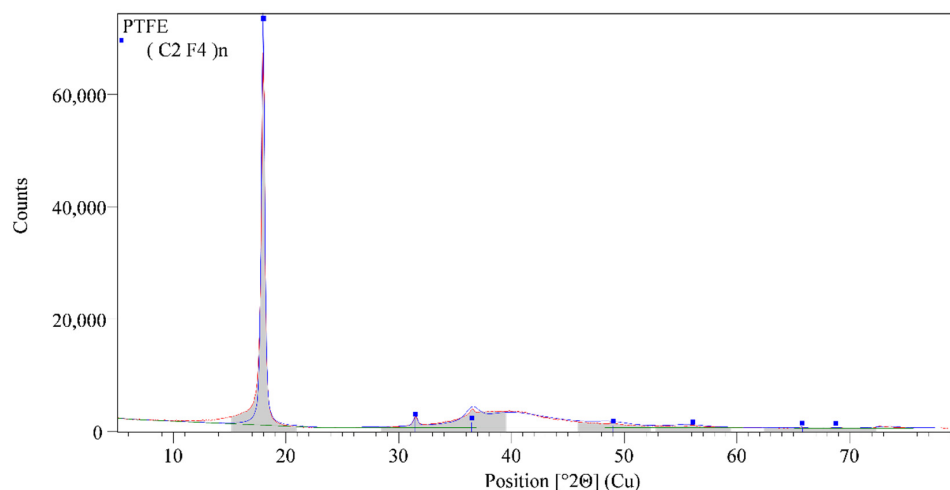
Figure 7. XRD pattern of polytetrafluoroethylene (PTFE).

3.2. Membrane Testing Results

Among the numerous sources of ferric cations, membranes M1–M15 were tested in anhydrous ferric chloride, ferric nitrate nonahydrate, and disodium hydrogen phosphate solution. The main reason for choosing this kind of ferric solution was the possibility of chloride ions to form a sparingly soluble precipitate with the silver ions present in the phase boundary between membrane and solution while nitrate anions do not have this possibility. In this way, the response of the membrane to ferric cations was studied in the presence of interfering (Cl^-) and non-interfering anions ($(NO_3)^-$). The tests were performed with electrode bodies EB1 and EB2. In this way, all sensors were tested for response to ferric and phosphate ions. Membrane M1 with a composition of 25% $FePO_4$, 25% Ag_2S, and 50% PTFE, as it is shown in Table 2 exhibited a linear response to Fe^{3+} cations at pH = 1 with a potential change per decade in good agreement with the theoretical Nernst slope for trivalent cations in both, ferric chloride (Figure 8) and ferric nitrate solutions (Figure 9).

Table 3 shows the slope results of the M2–M15 test membranes in ferric cation solution at pH = 1. Since none of the M2–M15 membranes showed a slope close to −19.6 mV per decade, which would indicate the possibility of determining ferric cations, these membranes were not tested further.

Tests of the sensors for phosphate ions were performed at pH = 13 and none of the 15 membranes showed the same Nernst response towards $(PO_4)^{3-}$ as towards ferric cations at pH values of 0 and 1.5.

Table 2. M1 testing results in EB1.

Testing Solution	Linear Curve No.	Slope $\pm$ SD	LOD	LOQ	R^2
FeCl$_3$ (pH = 1.00)	C1	-20.525 ± 1.56	2.64×10^{-5}	8.97×10^{-5}	0.9720
	C2	-20.528 ± 0.63	2.41×10^{-5}	3.97×10^{-5}	0.9925
	C3	-16.948 ± 0.72	1.31×10^{-5}	2.63×10^{-5}	0.9836
Fe(NO$_3$)$_3$ (pH = 1.00)	C1	-18.271 ± 1.57	1.13×10^{-4}	4.52×10^{-4}	0.9783
	C2	-18.755 ± 1.01	4.54×10^{-4}	1.08×10^{-3}	0.9885
	C3	-13.587 ± 0.54	1.55×10^{-4}	8.20×10^{-4}	0.9954
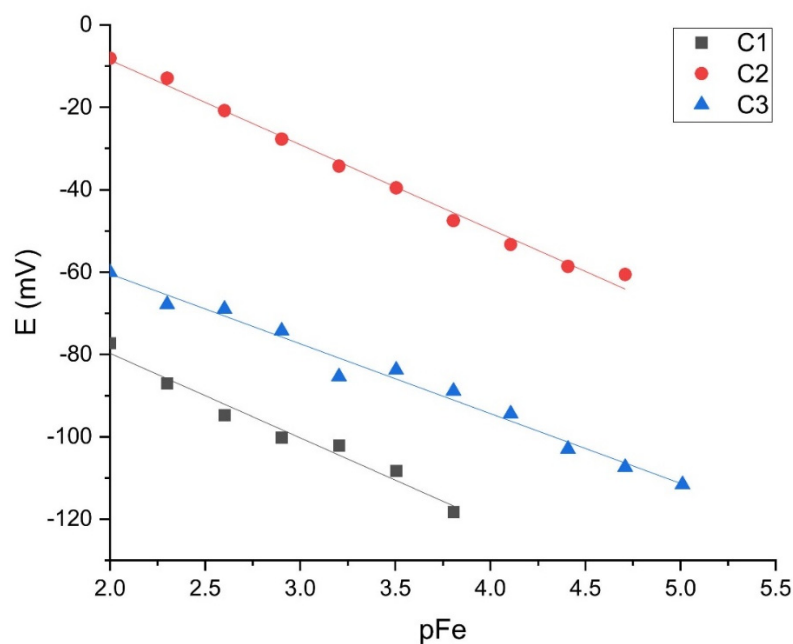
Figure 8. Results were obtained for Fe^{3+} cation determination in the ferric chloride solution using the M1 sensor.
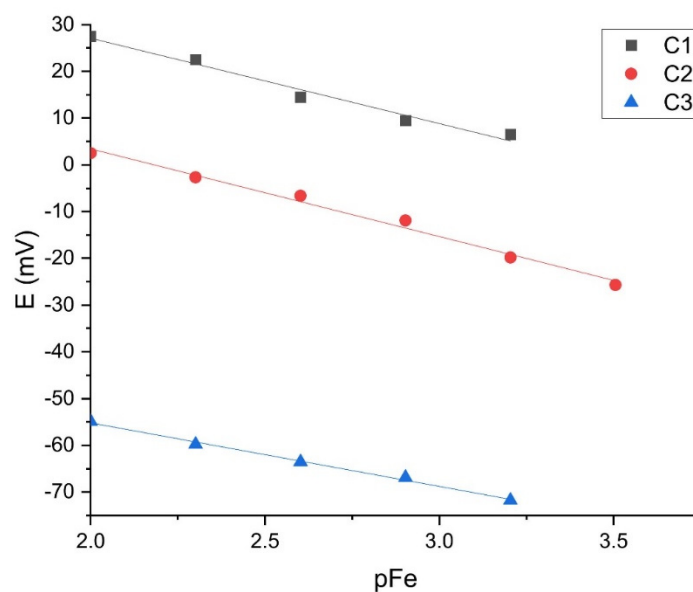
Figure 9. Results obtained for Fe^{3+} cation determination in ferric nitrate solution using the M1 sensor.

Table 3. Results of testing M2–M15 membranes in EB1 towards ferric cations.

Testing Solution	FeCl$_3$ (pH = 1.00)		Fe(NO$_3$)$_3$ (pH = 1.00)	
Sensor	Slope/mV dec^{-1}	R^2	Slope/mV dec^{-1}	R^2
M2	11.49	0.9306	−4.95	0.7662
M3	3.09	0.3982	18.38	0.9176
M4	11.46	0.9900	17.47	0.4835
M5	24.68	0.7874	-	-
M6	11.27	0.9740	5.71	0.9881
M7	−4.42	0.0384	13.09	0.9496
M8	20.56	0.9813	-	-
M9	34.91	0.9193	1.69	0.8627
M10	22.00	0.9612	3.29	0.8586
M11	-	-	5.81	0.8828
M12	-	-	17.19	0.9744
M13	−9.01	0.9392	−27.74	0.8946
M14	–6.48	0.2376	-	-
M15	−6.91	0.9397	−11.02	0.9221

"-"—measurement could not be performed.

Although the membrane M1 tested in EB1 showed linearity in the range ([Fe^{3+}] = 10^{-2}–3.97×10^{-5}) mol L^{-1} with a slope in good agreement with the theoretical Nernst slope for trivalent cations (−20.53 ± 0.63 mV per decade) and a high correlation factor (0.9925), there is no satisfactory repeatability among the measurements which could be caused by a periodic loss of contact between the sensor and the stainless-steel disc.

To ensure complete contact transfer, it was necessary to improve the adhesion of the sensor with the conductor, which is made possible by a special graphite adhesive in the EB2.

The sensor M1, which showed good results in the iron cation solution, was tested with EB2. Figures 10 and 11 show the results of three tests intraday and three interday results. Table 4 shows slopes, LOD, and LOQ values with correlation factors of each curve (C1, C2, C3).
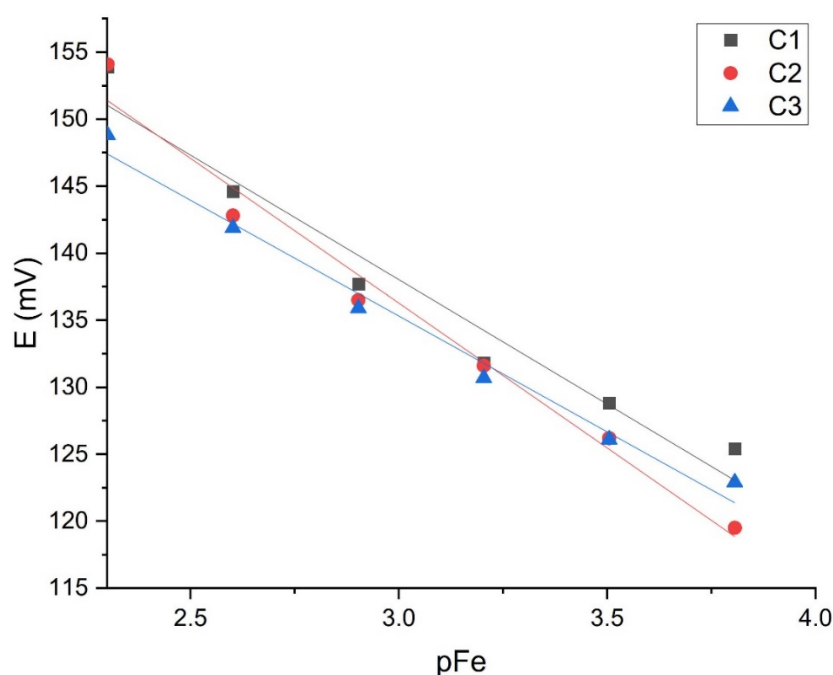
Figure 10. M1 intraday testing (*n* = 3).
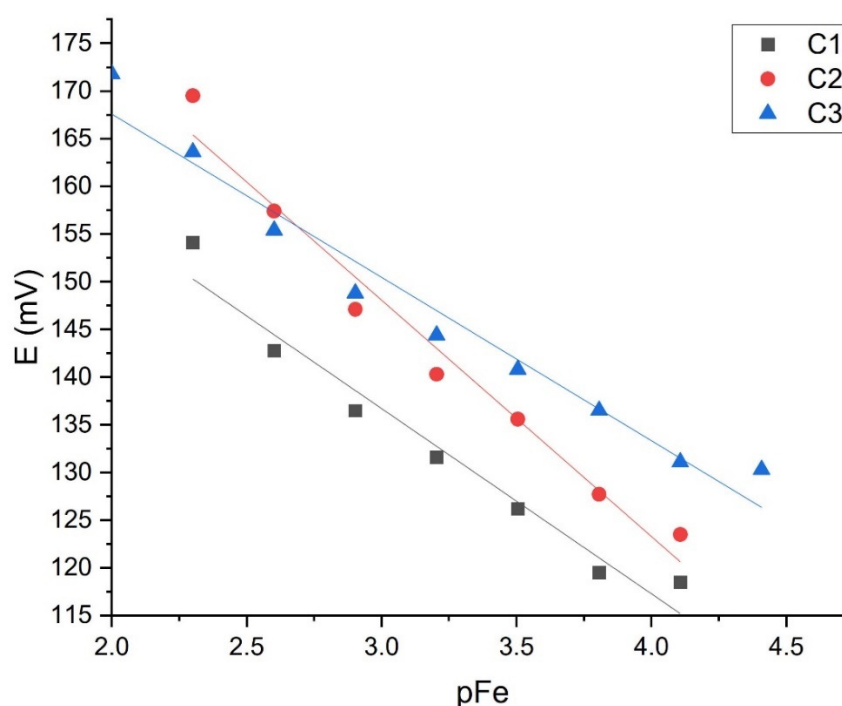
Figure 11. M1 interday testing (*n* = 3).

Table 4. M1 intra- and interday testing results in EB2.

	Intraday Results					Interday Results			
Curve	Slope ± SD/ mV dec^{-1}	R^2	LOD/ mol L^{-1}	LOQ/ mol L^{-1}	Curve	Slope ± SD/ mV dec^{-1}	R^2	LOD/ mol L^{-1}	LOQ/ mol L^{-1}
C1	−18.58 ± 1.99	0.9563	3.27×10^{-4}	1.83×10^{-3}	C1 (day 1)	−18.53 ± 1.83	0.9761	1.21×10^{-4}	3.40×10^{-4}
C2	−19.421 ± 1.70	0.9631	1.43×10^{-4}	5.86×10^{-4}	C2 (day 2)	−24.78 ± 1.87	0.9724	1.31×10^{-4}	4.43×10^{-4}
C3	−17.28 ± 1.04	0.9855	2.38×10^{-4}	6.31×10^{-4}	C3 (day 3)	−19.421 ± 1.7	0.9631	1.43×10^{-4}	5.86×10^{-4}

When comparing three consecutive measurements within one day, the graphical representation of the curves shows obvious high repeatability. The membrane showed a slope of −19.421 ± 1.70 mV per decade with a correlation factor of 0.9631. The detection limit is [Fe^{3+}] = 1.43×10^{-4} mol L^{-1} and limit of quantification [Fe^{3+}] = 5.86×10^{-4} mol L^{-1}.

The M1 tests between days also show high repeatability of results with slopes from −18 ± 1.83 to −24 ± 1.87 mV per decade and correlation factor of from 0.9631 to 0.9761. The detection limit is [Fe^{3+}] = (1.21×10^{-4}–1.43×10^{-4}) and limit of quantification [Fe^{3+}] = (3.40×10^{-4}–5.86×10^{-4}) mol L^{-1}.

From the graphs, it can be seen that the repeatability of the results is much better with EB2. As the results of the M1 membrane test showed the expected response, further experiments were carried out with this sensor only.

3.3. Electrode Selectivity

Table 5 shows the studied interferences with calculated selectivity coefficient values.

Table 5 shows that the values of the selectivity coefficients are very low, indicating high electrode selectivity to ferric cations. Although the presence of aluminum is the main interference for the determination of ferric cations, it is important to note that the concentration of Al^{3+} in a solution must be at least 50.4 times greater than the concentration of Fe^{3+} to cause interference (at [Fe^{3+}] = 5×10^{-4} mol L^{-1}).

Table 5. Logarithmic potentiometric selectivity coefficient values of M1 membrane in Electrode Body 2.

Interfering Species (B)	$\log K^{pot}_{Fe^{3+},B}$
Al^{3+}	−0.74
Ba^{2+}	−1.16
Ca^{2+}	<−1.45
Mg^{2+}	−0.82

3.4. Determination of Iron(III) in Pharmaceuticals

To confirm the applicability of the sensor M1 in the determination of ferric cations in the sample of unknown analyte concentration, it was tested in three different concentrations of Fe^{3+} standard solutions ($Fe(NO_3)_3 \times 9\ H_2O$) at pH = 1. Recovery investigations of prepared membranes were done by using VWR 455532A iron standard for ICP and the results are shown in Table 6.

Table 6. Determination of ferric cations in standard solution at pH = 1.

Added $m(Fe^{3+})$/mg	Determined $m(Fe^{3+})$/mg	Recovery (%)
0.84	0.85	101.2
1.68	1.65	98.2
8.37	8.28	98.9

Since membrane M1 showed high recoveries (98.2–101.2%) in ferric standard solutions, the same sensor was used to determine Fe^{3+} ions in two different oxidized drugs. Samples of Tardyferon® and Heferol® prepared by microwave digestion described in detail above were analyzed potentiometrically for iron cations and the results were compared with those obtained by ultraviolet-visible spectrophotometric analysis. The spectrophotometric determination of iron cations was carried out by complexation with sulfosalicylic acid. Results are shown in Table 7 with calculated recoveries.

Table 7. Determination of ferric cations in digested pharmaceuticals.

Pharmaceutical	Determined $m(Fe^{3+})$ by M1/mg	Determined $m(Fe^{3+})$ by UV/VIS/mg	Recovery (%)
Tardyferon	0.925	0.938	98.6
Heferol	1.283	1.205	106.5

4. Discussion

The theoretical interpretation of the electrochemical behavior of precipitate-based ion-selective electrodes is based on the fundamentals of solubility equilibria and precipitation reactions at the phase boundaries of the electrode membrane. The fundamental reaction considered in this work is the reaction between phosphate ions $(PO_4)^{3-}$ present in the phase boundary between the membrane and the solution, and iron(III) cations present in the solution.

At the beginning of the design of sensors for iron cations, it was necessary to determine the appropriate composition of the three components of the membrane.

Fifteen different membranes were designed, each of which had a completely different composition. M1–M5 sensors were designed by gradually increasing the charge carrier ratio, M6–M10 sensors have the same ratio of $FePO_4$ and Ag_2S but a reduced ratio of PTFE. M11 and M12 sensors are without PTFE in their composition. M2–M11 sensors did not show suitable behavior for trivalent cations. The main reason for the unfavorable behavior of electrochemical potential is the absence of active centers on the membrane surface $(Fe(PO_4)_3)$. Although polytetrafluoroethylene is an insulator and could be considered as interfering due to its inability to contact, the tests of M6–M10 membranes showed that

reducing the amount of polytetrafluoroethylene did not improve the membrane behavior. Also, the tests of M11 and M12 resulted in rupture of the membrane and its one-time use, which is exactly the consequence of the absence of support. The M1 sensor is obviously the perfect combination of the set of active sites, charge transmitters, and carriers that provided a potential change as a function of the change in the activity of the iron cations in accordance with the requirements of the Nernst equation. Positive slope values recorded in a high percentage during the membrane test in ferric chloride solution could be due to the backreaction of the membrane to chloride anions. None of the sensors showed any response to phosphate anions, which is another indication that the M1 sensor is selective only for ferric cations.

After determining the ideal membrane composition, two variants of the electrode body were investigated, of which EB1 was presented in previous papers [4,5,27] and EB2 for the first time in this work. Both bodies were designed in our laboratory. Membrane tests in both bodies showed results in the style of the Nernst equation requirements, such that slopes in the range of -13.59 ± 0.54 to -24.78 ± 1.87 mV per decade were recorded. As explained in the Results section, the graphical representation of the M1 membrane test in the EB2 body shows an almost complete overlap of the three curves (C1, C2, C3) of three consecutive measurements, indicating high repeatability of the results within one day. The curves showing test results within three consecutive days show slightly larger deviations in the E_0 value, but this is also to be expected. For this reason, when determining the concentration of iron cations in a standard or in real samples, the calibration curve must be prepared immediately before the measurement. The main disadvantage of the EB1 design is the non-uniform charge transfer. Namely, since both the membrane and the contact plate are in a solid-state and both have some non-uniformity at the microscopic level, in extreme cases they may touch each other only at one point, while in the other case they may adhere to each other completely. Since the silicone rubber that allows the membrane to be fixed inside the body under the influence of acids can be damaged, it often happens that the solution penetrates the space between the membrane and the stainless-steel disk, further preventing their contact resulting in none or Sub-Nernstian slope. The conductive graphite adhesive used in the construction of the EB2 completely eliminates the aforementioned problem. Other advantages of the EB2 are: minimal saturation, increase in the working area of the sensor, the impossibility of replacing the working and adhesive sides of the membrane as it is solid, no need for special construction of the cell in which the electrodes are located, and general handling is much easier.

The iron ion-selective electrode (M1) described in this work with the possibility of application in two different electrode bodies (EB1 and EB2) showed a linear response towards iron cations in the range $[Fe^{3+}] = 3.97 \times 10^{-5}$ mol $L^{-1} - 1 \times 10^{-2}$ mol L^{-1} with a change of -20.528 ± 0.63 mV per decade and a correlation factor of 0.9925. The sensor showed high selectivity to ferric cations in the presence of numerous interfering species and an average potential stabilization time of 20 s. The presence of aluminum cations caused the greatest interference to the determination of iron cations, which was expected according to the value of the solubility constant, Ksp, of aluminum phosphate, which is 9.84×10^{-21}. However, it is important to emphasize that as mentioned in the Results section, when the concentration of iron cations is 5×10^{-4} mol L^{-1}, the concentration of aluminum cations causing interference must be 50.4 times higher. Other cations (Ba^{2+}, Ca^{2+}, Mg^{2+}) do not cause significant interference and thus do not interfere with the determination of iron(III) cations. The M1 detection limit is $[Fe^{3+}] = 2.41 \times 10^{-5}$ mol L^{-1} and the quantification limit is $[Fe^{3+}] = 3.97 \times 10^{-5}$ mol L^{-1}.

Due to the recoveries of Fe^{3+} determination in the standard solutions (98.2–101.2%), the M1 membrane was tested in real samples and the potentiometric results were compared with the UV/VIS spectrophotometry results. Recoveries of (98.6–106.5%) showed the reliability of using this homemade sensor for real sample analysis.

The time that has passed from the first to the last testing of the M1 membrane was around one year, so the conclusion is that lifetime of the sensor is from 10 to 12 months.

5. Conclusions

The ion-selective electrode, M1 showed a high ability to determine ferric cations in standard and pharmaceutical samples with recovery values ≈100%. Not only the possibility of using an M1 sensor in the real sample was reported but also high selectivity in the presence of many interfering species. This low-priced sensor showed high agreement with the requirements of the Nernst equation for trivalent cations. The potential change was −20.53 ± 0.63 mV per decade, with correlation factor R^2 = 0.9925.

In contrast to many expensive methods for the determination of ferric cations in a sample, this method proved to be affordable and all sensor parts were manufactured entirely in our laboratory, demonstrating the possibility of wide availability.

Sensor M1 proposed in this work is suitable for qualitative and semi-quantitative analysis.

References

1. Bobacka, J.; Ivaska, A.; Lewenstam, A. Potentiometric ion sensors. *Chem. Rev.* **2008**, *108*, 329–351. [CrossRef]
2. Cuartero, M.; Crespo, G.A. All-solid-state potentiometric sensors: A new wave for in situ aquatic research. *Curr. Opin. Electrochem.* **2018**, *10*, 98–106. [CrossRef]
3. Hu, J.; Stein, A.; Bühlmann, P. Rational design of all-solid-state ion-selective electrodes and reference electrodes. *TrAC Trends Anal. Chem.* **2016**, *76*, 102–114. [CrossRef]
4. Prkic, A.; Vukusic, T.; Giljanovic, J.; Sokol, V.; Boskovic, P.; Lavcevic, M.L.; Mitar, I.; Jakic, M. Development of a New Potentiometric Sensor based on home made Iodide ISE Enriched with ZnO Nanoparticles and its Application for Determination of Penicillamine. *Int. J. Electrochem. Sci.* **2018**, *13*, 10894–10903. [CrossRef]
5. Prkic, A.; Vukusic, T.; Mitar, I.; Giljanovic, J.; Sokol, V.; Boskovic, P.; Jakic, M.; Sedlar, A. New sensor based on AgCl containing Iron Oxide or Zinc Oxide Nanoparticles for Chloride Determination. *Int. J. Electrochem. Sci.* **2019**, *14*, 861–874. [CrossRef]
6. Shao, Y.Z.; Ying, Y.B.; Ping, J.F. Recent advances in solid-contact ion-selective electrodes: Functional materials, transduction mechanisms, and development trends. *Chem. Soc. Rev.* **2020**, *49*, 4405–4465. [CrossRef]
7. Ozer, T.; Isildak, I. A New Fe (III)-Selective Membrane Electrode Based on Fe (II) Phthalocyanine. *J. Electrochem. Sci. Technol.* **2019**, *10*, 321–328. [CrossRef]
8. Burguera, J.L.; Burguera, M. Flow-Injection Spectrophotometry Followed by Atomic-Absorption Spectrometry for the Determination of Iron(Ii) and Total Iron. *Anal. Chim. Acta* **1984**, *161*, 375–379. [CrossRef]
9. Carbonell, V.; Sanz, A.; Salvador, A.; de la Guardia, M. Flow injection flame atomic spectrometric determination of aluminium, iron, calcium, magnesium, sodium and potassium in ceramic material by on-line dilution in a stirred chamber. *J. Anal. At. Spectrom.* **1991**, *6*, 233–238. [CrossRef]
10. Vanhoe, H.; Vandecasteele, C.; Versieck, J.; Dams, R. Determination of Iron, Cobalt, Copper, Zinc, Rubidium, Molybdenum, and Cesium in Human-Serum by Inductively Coupled Plasma Mass-Spectrometry. *Anal. Chem.* **1989**, *61*, 1851–1857. [CrossRef]
11. Samadi, A.; Amjadi, M. Halloysite Nanotubes as a New Adsorbent for Solid Phase Extraction and Spectrophotometric Determination of Iron in Water and Food Samples. *J. Appl. Spectrosc.* **2016**, *83*, 422–428. [CrossRef]
12. Jha, A.R.; Mishra, R.K. Solvent-Extraction of the Thiocyanato Mixed-Ligand Complexes of Iron(III) with Various Hydroxyamidines and Spectrophotometric Determination of Iron(III) in Various Biochemical and Biological Samples. *Analyst* **1981**, *106*, 1150–1156. [CrossRef]

13. Isildak, I.; Attar, A.; Demir, E.; Kemer, B.; Aboul-Enein, H.Y. A Novel all Solid-State Contact PVC-Membrane Beryllium-Selective Electrode Based on 4-Hydroxybenzo-15-Crown-5 Ether Ionophore. *Curr. Anal. Chem.* **2018**, *14*, 43–48. [CrossRef]
14. Mizani, F.; Ganjali, M.R.; Faridbod, F.; Esmaeilnia, S. A Novel Iron(III) Selective Potentiometric Sensor Based on 9-Ethylacenaphtho [1, 2-B]Quinoxaline. *Int. J. Electrochem. Sci.* **2013**, *8*, 10473–10486.
15. Bita, S.; Sadati, S.O.; Soleymanpour, A.; Amouzad, F. Highly Selective Solid Contact Sensor for Low Level Concentration Measurements of Iron(III) in Pharmaceutical and Biological Media. *J. Anal. Chem.* **2018**, *73*, 1202–1208. [CrossRef]
16. Yari, A.; Bagheri, M.; Ghazizadeh, M. A Novel Iron(III) Potentiometric Sensor Based on (E)-N ′-((2-hydroxynaphthalen-3-yl)methylene)benzohydrazide. *Int. J. Electrochem. Sci.* **2016**, *11*, 6597–6608. [CrossRef]
17. Mashhadizadeh, M.H.; Shoaei, I.S.; Monadi, N. A novel ion selective membrane potentiometric sensor for direct determination of Fe(III) in the presence of Fe(II). *Talanta* **2004**, *64*, 1048–1052. [CrossRef] [PubMed]
18. Ekmekci, G.; Uzun, D.; Somer, G.; Kalayci, S. A novel iron(III) selective membrane electrode based on benzo-18-crown-6 crown ether and its applications. *J. Membr. Sci.* **2007**, *288*, 36–40. [CrossRef]
19. Vlascici, D.; Fagadar-Cosma, E.; Popa, I.; Chiriac, V.; Gil-Agusti, M. A Novel Sensor for Monitoring of Iron(III) Ions Based on Porphyrins. *Sensors* **2012**, *12*, 8193–8203. [CrossRef]
20. Gupta, V.K.; Sethi, B.; Upadhyay, N.; Kumar, S.; Singh, R.; Singh, L.P. Iron (III) Selective Electrode Based on S-Methyl N-(Methylcarbamoyloxy) Thioacetimidate as a Sensing Material. *Int. J. Electrochem. Sci.* **2011**, *6*, 650–663.
21. Fakhari, A.R.; Alaghemand, M.; Shamsipur, M. Iron(III)-selective membrane potentiometric sensor based on 5,10,15,20-tetrakis(pentafluorophenyl)-21H, 23H-porphyrin. *Anal. Lett.* **2001**, *34*, 1097–1106. [CrossRef]
22. Saber, A.L.; Hameed, A.M.; Sayqal, A.A.; Alessa, H.; Alharbi, A. Iron-selective Poly(Vinyl Chloride) Membrane Electrode Based on Norfloxacin as a Neutral Carrier. *Int. J. Electrochem. Sci.* **2018**, *13*, 10076–10087. [CrossRef]
23. Ozer, T.; Isildak, I. Potentiometric Studies of a New Solid-state Contact Iron(III)-Selective Electrode Based on Morin-Fe2+ Shiff Base Complex. *Int. J. Electrochem. Sci.* **2018**, *13*, 11375–11387. [CrossRef]
24. Ali, T.A.; Mahmoud, W.H.; Mohamed, G.G. Construction and characterization of nano iron complex ionophore for electrochemical determination of Fe(III) in pure and various real water samples. *Appl. Organomet. Chem.* **2019**, *33*. [CrossRef]
25. Ali, T.A.; Mohamed, G.G.; El-Dessouky, M.M.I.; Abou El Ella, S.M.; Mohamed, R.T.F. Modified Carbon Paste Ion Selective Electrodes for the Determination of Iron (III) in Water, Soil and Fish Tissue Samples. *Int. J. Electrochem. Sci.* **2013**, *8*, 1469–1486.
26. Duzgun, E.; Tastekin, M.; Atakol, O. A new modified Fe(III)-selective solid membrane electrode. *Rev. Anal. Chem.* **2008**, *27*, 83–90. [CrossRef]
27. Prkic, A.; Giljanovic, J.; Bralic, M. Direct Potentiometric Determination of N-acetyl-L-cysteine (NAC) in Real Samples by Using "home made" Iodide ISE. *Int. J. Electrochem. Sci.* **2011**, *6*, 5388–5395.
28. Bralić, M.; Prkić, A.; Radić, J.; Pleslić, I. Preparation of Phosphate Ion-Selective Membrane Based on Silver Salts Mixed with PTFE or Carbon Nanotubes. *Int. J. Electrochem. Sci.* **2018**, *13*, 1390–1399. [CrossRef]
29. Umezawa, Y.; Umezawa, K.; Sato, H. Selectivity Coefficients for Ion-Selective Electrodes—Recommended Methods for Reporting K-a,B(Pot) Values—(Technical Report). *Pure Appl. Chem.* **1995**, *67*, 507–518. [CrossRef]

Article 2

I. Mitar, L. Guć, Ž. Soldin, M. Vrankić, A. Paut, A. Prkić, S. Krehula, Stjepko Rapid Microwave Method for Synthesis of Iron Oxide Particles under Specific Conditions, Crystals, 11 (2021), 4.

Author Contributions:

Methodology, Lucija Guć and Andrea Paut

Validation; Ivana Mitar, Željka Soldin, and Martina Vrankić

Formal analysis; Ivana Mitar, Željka Soldin, and Martina Vrankić

Iinvestigation; Ivana Mitar and Stjepko Krehula

Resources; Ivana Mitar

Data curation; Ivana Mitar

Writing-original draft preparation; Ivana Mitar

Writing-review and editing; Ivana Mitar, Lucija Guć, Andrea Paut, Martina Vrankić, and Stjepko Krehula

Visualization; Ivana Mitar and Martina Vrankić

Supervision; Ivana Mitar

Project administration; Ante Prkić and Stjepko Krehula

Funding acquisition; Ivana Mitar, Ante Prkić, and Stjepko Krehula

This paper is published in an open access journal (doi.org/10.3390/cryst11040383)

crystals

MDPI

Article

Rapid Microwave Method for Synthesis of Iron Oxide Particles under Specific Conditions

Ivana Mitar [1,*], Lucija Guć [2], Željka Soldin [3], Martina Vrankić [4], Andrea Paut [5], Ante Prkić [5] and Stjepko Krehula [6]

1 Faculty of Science, University of Split, Ruđera Boškovića 33, 21000 Split, Croatia
2 University of Split, Ruđera Boškovića 31, 21000 Split, Croatia; lucija.guc95@gmail.com
3 Department of Chemistry, Faculty of Science, University of Zagreb, Horvatovac 102a, 10000 Zagreb, Croatia; zeljka@chem.pmf.hr
4 Division of Materials Physics and Center of Excellence for Advanced Materials and Sensing Devices, Ruđer Bošković Institute, Bijenička 54, 10000 Zagreb, Croatia; martina.vrankic@irb.hr
5 Faculty of Chemistry and Technology, University of Split, Ruđera Boškovića 35, 21000 Split, Croatia; andrea.paut@ktf-split.hr (A.P.); prkic@ktf-split.hr (A.P.)
6 Division of Materials Chemistry, Ruđer Bošković Institute, Bijenička 54, 10000 Zagreb, Croatia; krehul@irb.hr
* Correspondence: imitar@pmfst.hr; Tel.: +385-21-691-279

Abstract: The advantages of microwave technology over conventionally conducted experiments are numerous. Some of them are reduction in reaction time, a higher degree of process control, repeatability, and work safety. Microwave synthesis routes require a complete description of the experimental details, instrumentation, and design program of a microwave oven used in the experiments. In this work, microwave-assisted hydrothermal synthesis of hematite (α-Fe$_2$O$_3$) particles from 0.1 M FeCl$_3$ solution in highly alkaline media with heating in a microwave oven at continuous microwave emission of 800 W at 150 °C, 200 °C, and 250 °C for 20 min are presented. Also, the influence of the percentage of the addition of a cationic surfactant, cetyltrimethylammonium bromide (CTAB) on the composition, size, and shape of the final product was investigated. The samples precipitated at 150 °C formed a final product consisting of goethite (α-FeOOH) and hematite particles in contrast to the those precipitated at 200 °C and 250 °C where pure hematite phase was obtained. In these synthesis routes, the CTAB caused to slow down the rate of the goethite-to-hematite transformation process at temperatures at 200 °C but did not affect the transformation at 250 °C.

Keywords: microwave-assisted synthesis; hematite; α-Fe$_2$O$_3$ particles; goethite; α-FeOOH particles; cetyltrimethylammonium bromide; FT-IR spectroscopy; powder X-ray diffraction; FE-SEM

1. Introduction

During the last decades, microwaves have been studied as a source of energy for chemical reactions and processes, mainly for organic synthesis pathways rather than inorganic ones. Although the number of papers dealing with the microwave-assisted synthesis of inorganic nanomaterials has been extensive since the 1990s in all classes of functional materials such as metals, oxides, sulfides, phosphates, and halides, microwave synthesis is not yet where it belongs in science [1]. Advantages of microwave technology over conventionally performed experiments are numerous and well known. Some of them are reducing reaction times and energy costs, suppression of side reactions and, hence, improvement in product yield, purity, better material properties, a higher degree of process control, repeatability, and safety [1,2]. All advantages of microwave technology can be attributed to the efficient internal heating (in-core volumetric heating) by direct coupling of microwave energy with the molecules (solvents, reagents, catalysts) so that the temperature rise is uniform throughout the sample [3].

In many publications, the microwave systems used are usually insufficiently described and details regarding the experimental conditions are relatively scarce. Essential reaction

parameters, such as the power used in the experiments or the temperatures reached, are not given, which is mainly due to the use of domestic microwave ovens. Namely, a domestic microwave oven cannot provide the required information because the irradiation power is controlled by on–off cycles of the magnetron. Therefore, it is not possible to reliably monitor the reaction temperature. Many published papers describe only "full power" or 2.45-GHz power specifications, and very few published synthesis routes can be repeated. There are no literature data on the repeatability of synthesis products prepared using microwave techniques. Reactions carried out in this way cannot be compared with literature data, so such procedures cannot be recommended for scientific purposes, nor can they guarantee the safety of the work. Schütz et al. discussed the difficulty of direct comparison of conditions performed by microwave-assisted synthesis methods [4]. Microwave synthesis routes require a detailed description of the experimental procedure, such as the apparatus, reaction protocol, instrumentation, and design program of a microwave oven used in experiments. The only disadvantage of microwave technology is the high capital cost of professional chemical microwave systems. Modern professional microwave reactors allow autoclave process conditions of 300 °C and 100 bar under carefully controlled and safe operating conditions, with the continuous rotation of samples within the cavity and the possibility of mixing samples within a reaction vessel [2]. These systems allow temperature measurements directly in the microwave field by IR sensors or in the reaction mixture using fiber optic sensors and software that enable temperature control by regulating the microwave power with faster temperature rise and cooling [5].

Iron oxyhydroxides and oxides are widely spread in our environment, while synthetic iron oxides are heavily used in advanced technologies. For this reason, the synthesis of iron oxides is a well-investigated scientific topic. Hematite (α-Fe_2O_3) and goethite (α-$FeOOH$) are the most studied materials due to their diverse applications in many scientific and industrial fields, e.g., as inorganic pigments [6,7]; adsorbents for wastewater treatment [8,9]; abrasives [10]; gas sensors; catalysts [11]; electrochemical sensors [12,13]; and precursors in the manufacture of electronic, magnetic, or optical devices and medical diagnosis or therapy [10,14–17]. The chemical composition, purity, morphology, and size of iron oxide particles are the key features for their application. Each potential application requires different properties of the particles, for example, a stable, switchable, magnetic state of iron oxide particles is necessary for data storage applications, while the stability in the water at pH 7 is crucial for the versatile biomedical applications [16]. The properties of iron oxide particles mainly depend on the preparation method and experimental conditions of the synthesis route. Due to the use of iron oxides in advanced technologies and because they are non-toxic, biocompatible, and cheap to produce, scientists and engineers have investigated various methods for the synthesis of precisely defined iron oxide nano/microstructures. However, designing the iron oxide particles of defined size and morphology for targeted applications is still a major research challenge. In their book, Yue et al. highlighted the great challenge of how to efficiently synthesize iron oxides with controlled morphology, size, and functionality and how to fundamentally understand the formation, growth mechanisms, and structure of iron oxide particles [18]. Machala et al., in their review paper, described parameters affecting polymorphous transformations of iron oxides, which is a great challenge in the study of polymorphism of solid compounds [19].

Among the many available and widely studied methods for the synthesis of hematite and goethite particles (e.g., sol-gel, microemulsion method, thermal decomposition, sono-chemical techniques), hydrothermal techniques were the fastest, easiest, and most widely used pathways for the preparation of these oxides. The hydrothermal routes under different experimental conditions of pressure, temperature, pH medium, reaction time, precursor type, and concentration are well investigated and reported in the literature [6,10,11,14,20–46].

As mentioned earlier, microwave-assisted hydrothermal techniques are still not well investigated because of the high capital cost of professional chemical microwave systems. There are many published papers in the literature describing the microwave-assisted hydrothermal synthesis of iron oxide particles prepared using a domestic microwave oven,

without specifying microwave instrumentation and experimental conditions [12,47–53] or using microwave digestion systems, where the temperature reached is calculated by the temperature/pressure ratio based on the steam tables [47,51–60]. Few published papers described program details of a professional microwave oven, thus providing specific and well-established experimental conditions that could ensure reproducibility [50,56,61–64].

In recent years, the influence of added polysaccharides [65,66], surface-active substances [42,67–73], soluble polymers, and biopolymers [18,20,44,72,74–76] was intensively studied under the influence of various experimental factors in the abovementioned synthesis for iron oxide nano/microstructures. The role of various additives in the synthesis of iron oxide fascinates scientists because of the impact on the morphology of particles: both on the internal properties of particles and the external parameters (e.g., particle morphology, degree of particle aggregation, the size distribution of particles) and polymorphous transformation pathways. Commonly, the additives are used in synthesis as a coating material for particles to design their specific properties for targeted applications [45]. Cole et al. showed the application and advantages of coated iron nanoparticles for magnetic tumor targeting [77]. Kumagai et al. [78] described a simple route for the synthesis of polyethylene glycol (PEG)-coated iron oxide nanoparticles featuring excellent solubility and stability in an aqueous solution.

Microwave-assisted hydrothermal synthesis ensures rapid research of the influence of various additives and their added amount in the synthesis mixture. In 2007, Zhu and co-workers reported the microwave synthesis of Fe_3O_4 nanoparticles and ellipsoidal Fe_2O_3 nanoparticles with a nonionic surfactant, PEG [47]. Yang et al. published the microwave synthesis of spherical nanoporous Fe_3O_4 nanoparticles, also with PEG [79]. Unfortunately, none of the mentioned papers provided microwave instrument-specific experimental conditions that can be easily replicated. Finding a microwave synthesis route that is fast and repeatable could ensure that future studies change only one variable in the synthesis route and examine its effects on the final product.

In this work, the microwave-assisted hydrothermal synthesis of the α-Fe_2O_3 and α-FeOOH was carried out in a highly alkaline medium using $FeCl_3$ precursor. The influence of the added amount of cationic surfactant, cetyltrimethylammonium bromide (CTAB), was investigated. Iron oxide particles synthesized under the specified experimental conditions were in excellent agreement with the literature data. It was found that the control of the experimental conditions can be performed effortlessly and rapidly using a professional microwave oven.

2. Materials and Methods

2.1. Materials

All the required solutions were prepared by dissolving a certain amount of chemicals in ultrapure water. Ultrapure water (declared conductivity of 0.04 μS cm^{-1}) was prepared using the ultrapure water purification system Millipore Simplicity 185, Burlington, MA, USA; resistivity at 25 °C was 18.2 MΩ cm^{-1}.

The following chemicals were used: $FeCl_3 \cdot 6H_2O$ in reagent grade, NaOH (Kemika, Croatia), and cetyltrimethylammonium bromide, CTAB (Alfa Aesar, Ward Hill, MA, USA). Absolute alcohol, pro analysis pure, and 25% ammonium supplied by Gram-mol, Zagreb, Croatia.

2.2. Synthesis

Precipitation experiments were performed at room temperature (RT) in alkali-resistant plastic bottles to avoid contamination by dissolved silicon from glassware. All mixtures were prepared by adding 4 mL of 1 M $FeCl_3$ solution, 32 mL of water, and 4 mL of 8M NaOH solution. For the samples that contained the addition of CTAB, different masses of CTAB were added. After vigorous shaking of each precipitation mixture, the suspension was transferred to a Milestone Teflon-lined, non-stirred pressure vessel. The samples were heated for 20 min in a microwave oven (Milestone, FlexiWave SK15, Sorisole (Bergamo),

Italy, direct temperature control monitor via microwave-transparent fiber optic sensor up to 300 °C, magnetron frequency 2450 MHz, magnetron output 2 × 950 Watt, power supply 230 V, 50–60 Hz) at the prevailing temperature according to a microwave oven program with rotor twist on and continuous microwave emission at 800 W.

Immediately after the reaction time was completed, the autoclaves were cooled utilizing a cooling program of the microwave oven and left inside until the final temperature in the vessels was 25 °C. The mother liquor was separated from the precipitate using the ultrafast centrifuge (Beckman Avanti J-25, Indianapolis, IN, USA). The pH of the mother liquor was measured using a pH meter Mettler Toledo, MP220, Columbus, OH, USA. The precipitates were additionally washed with ultrapure water and ethanol to remove the "neutral" electrolyte and dried in a vacuum oven, Thermo Scientific, 3608–1CE, Waltham, MA, USA at 60 °C overnight.

2.3. FT-IR Spectroscopy

A Shimadzu IR Prestige-21, FTIR-8400S spectrophotometer, Kyoto, Japan, was used to collect the FT-IR spectra. Prior to the analysis, the samples were mixed with spectroscopically pure KBr (Alfa Aesar, Ward Hill, MA, USA) and pressed into pellets. All spectra were processed by the Origin program [80].

2.4. Powder X-ray Diffraction

Powder X-ray diffraction (PXRD) patterns were collected using a *Malvern Panalytical Aeris* XRD diffractometer with CuKα (λ = 1.5406 Å) radiation, Ni filter, and solid-state PIXcel3D-Medipix3 detector. The data were collected in the 2θ range from 15° to 90° with a step size of 0.022°, scan rate 39.53 s/°, $\frac{1}{4}$-inch divergence slit, and 13-mm beam mask. The detector energy discrimination levels were adjusted to suppress the sample fluorescence. The estimated mass fractions of the identified phases [81] were calculated by the Rietveld algorithm [82] using the X'Pert HighScore Plus program [83]. A pseudo-Voigt profile function and a polynomial background model were applied in the structure refinements, whereas the isotropic vibration modes were assumed for all atoms. The crystallite sizes in samples were calculated using the phase fit method (i.e., simultaneously with the Rietveld refinements) based on the change of the profile widths, compared to a standard sample.

2.5. Field-Emission Scanning Electron Microscopy

The morphology of samples was studied using a thermal field-emission scanning electron microscope (FE-SEM) JEOL JSM-7000F, Tokyo, Japan.

3. Results

The experimental conditions for the preparation of the reference samples and samples prepared in the presence of the surfactant CTAB are shown in Table 1. The samples were prepared at different temperatures with the same aging time, 20 min.

Table 1. Experimental conditions for iron oxide particles' preparation.

Sample	1 M FeCl₃ /mL	H₂O /mL	8M NaOH /mL	CTAB * /g	CTAB * /%	T/°C	t/min	pH
RS1	4	32	4			150	20	13.39
RS2	4	32	4			200	20	13.51
RS3	4	32	4			250	20	13.35
S1	4	32	4	0.4	1	150	20	13.39
S4	4	32	4	0.1	0.25	200	20	13.16
S5	4	32	4	0.2	0.5	200	20	13.11
S2	4	32	4	0.4	1	200	20	13.46
S6	4	32	4	1.0	2.5	200	20	13.35
S3	4	32	4	0.4	1	250	20	13.38
S7	4	32	4	1.0	2.5	250	20	13.28

* CTAB (cetyltrimethylammonium bromide).

3.1. Fourier-Transform Infrared Spectroscopy Features and Structural Characterization

The FT-IR spectra of selected reference samples and samples with the addition of 1% CTAB in the precipitation mixture are shown in Figure 1.
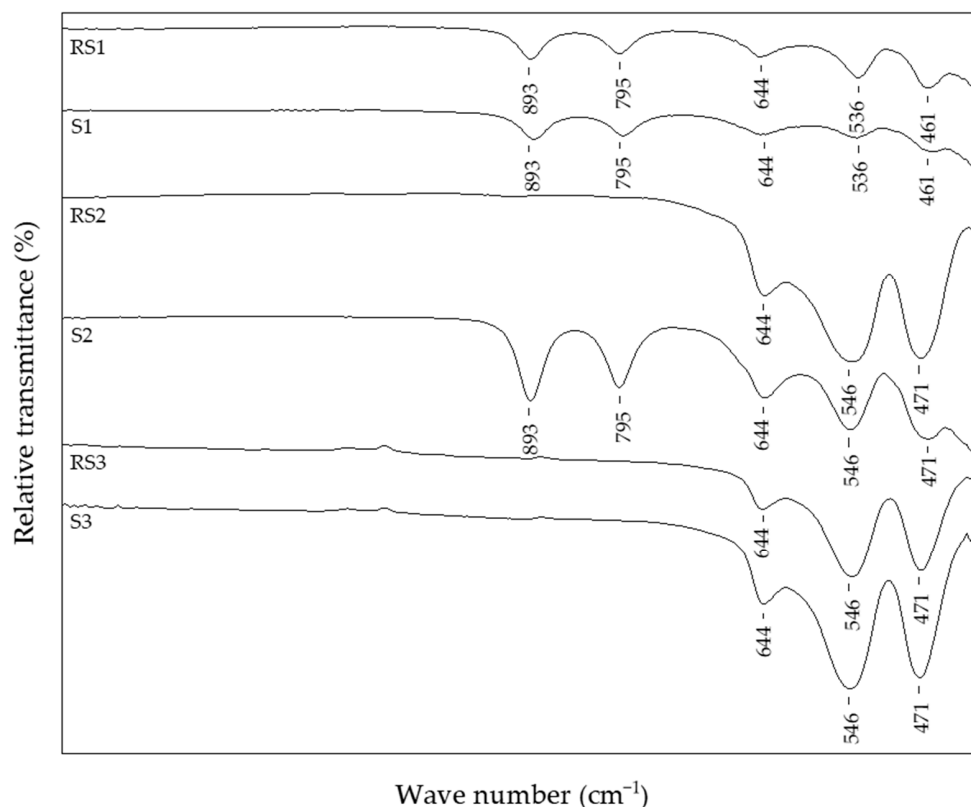

Figure 1. FT-IR spectra of reference samples and samples with 1% CTAB.

The reference sample RS1 and sample S1 with 1% CTAB, prepared at 150 °C, showed the same IR bands typical of goethite and hematite. The in-plane bending band (δOH), positioned at 893 cm^{-1}, and out-of-plane band (γOH), positioned at 795 cm^{-1}, are typically IR bands characteristic for α-FeOOH. The IR band recorded at 644 cm^{-1} presented the low-wave lattice mode of FeO$_6$ and its position was influenced by the particle shape [84] or could be related to the interaction of Fe-OH groups with Cl$^-$ ions [34]. On the other hand, the IR bands at 536 and 461 cm^{-1} indicated an α-Fe$_2$O$_3$ phase. As the IR active vibrations of hematite are dependent on optical parameters and geometric shape [85], the shift of the IR band at ~536 cm^{-1} might have been due to the different geometric shapes of hematite particles in these samples.

The results of the semi-quantitative phase analysis based on Hill and Howard formalism [86] along with the refined unit cell parameters are compiled in Table 2.

Table 2. Results of semi-quantitative phase analysis as obtained from Rietveld refinement against PXRD data at RT (λ = 1.5406 Å). R_{wp} is the discrepancy factor that characterizes the quality of the fit [87]. Standard deviations are given in parentheses.

Sample	Unit Cell Metrics					Phase Fraction (wt.%)	R_{wp} (%)
	α-Fe$_2$O$_3$ (s.g. *R*-3c)		α-FeOOH (s.g. *P*bnm)				
	a (Å)	*c* (Å)	*a* (Å)	*b* (Å)	*c* (Å)		
RS1	5.034 (2)	13.748 (1)	9.954 (6)	3.020 (4)	4.606 (5)	40.8 / 59.2	8.93
S1	5.0321 (3)	13.741 (1)	9.950 (1)	3.020 (4)	4.6049 (6)	20.6 / 79.4	7.47
RS2	5.025 (1)	13.725 (9)				100	8.97
S2	5.031 (2)	13.7397 (5)	9.949 (9)	3.0193 (2)	4.6016 (3)	41.1 / 58.9	7.35
S4	5.031 (1)	13.7397 (5)	9.956 (6)	3.018 (1)	4.598 (1)	89.7 / 10.3	8.26
S5	5.031 (3)	13.7388 (9)	9.950 (2)	3.0182 (5)	4.5994 (6)	52.2 / 47.8	7.24
S6	5.0325 (1)	13.749 (5)	9.957 (1)	3.0204 (3)	4.6040 (4)	39.5 / 60.5	6.89
S7	5.0416 (1)	13.766 (5)				100	9.33
RS3	5.0355 (1)	13.754 (4)				100	6.72
S3	5.0367 (4)	13.757 (1)				100	6.69

PXRD patterns of the samples RS1 and S1 indicated a presence of orthorhombic, goethite assembly (space group *P*bnm) and rhombohedral, hematite phase (space group *R*-3c) (Figure 2). However, the sample S2, with 1% CTAB addition, differed from sample RS2 prepared at the same temperature, 200 °C. Namely, the FT-IR spectra of sample RS2 (Figure 1) and PXRD patterns (Figure 3) indicated the formation of solely hematite phase. As opposed to that, the FT-IR spectra of sample S2 (Figure 1) showed IR bands that can be assigned to both goethite phase (IR bands at 893 and 795 cm^{-1}) and hematite phase (IR bands at 546 and 471 cm^{-1}). The mixture of both Fe phases in sample S2 was evidenced by the collected PXRD patterns (Figure 3). Reference sample RS3 and sample S3 prepared at 250 °C did not show IR bands at 893 cm^{-1} or 795 cm^{-1}, but very intense hematite bands were observed at 546 and 471 cm^{-1} (Figure 1). From the IR spectra and the PXRD pattern (Figure 4), the presence of hematite as a single phase was evident in the reference sample RS3 and sample with 1% CTAB addition, S3. The samples RS1 and S1, synthesized at 150 °C, differed in their composition ratio. Namely, the reference sample RS1 contained ~40 wt.% α-Fe$_2$O$_3$ and ~60 wt.% α-FeOOH, while sample S1, with 1% CTAB, contained ~20 wt.% α-Fe$_2$O$_3$ and ~80 wt.% α-FeOOH. Sample RS2, prepared at 200 °C, contained solely α-Fe$_2$O$_3$ and sample S2, made at the same experimental conditions as RS2 but with 1% of CTAB addition, contained ~40 wt.% of α-Fe$_2$O$_3$ and ~60 wt.% of α-FeOOH phase (Figure 3). Reference sample RS3 and sample S3, prepared at 250 °C, contained only the hematite phase (Figure 4). A similar trend was observed in sample S7, with 2.5% of CTAB. No impurities were detected in those samples. The values of crystallite sizes obtained from the line-broadening analysis during the crystal structure refinements were in the range between 24.6(1) and 81.0(1) for the α-Fe$_2$O$_3$ phase and 21.2(1) and 36.7(1) for the α-FeOOH (Table 3).
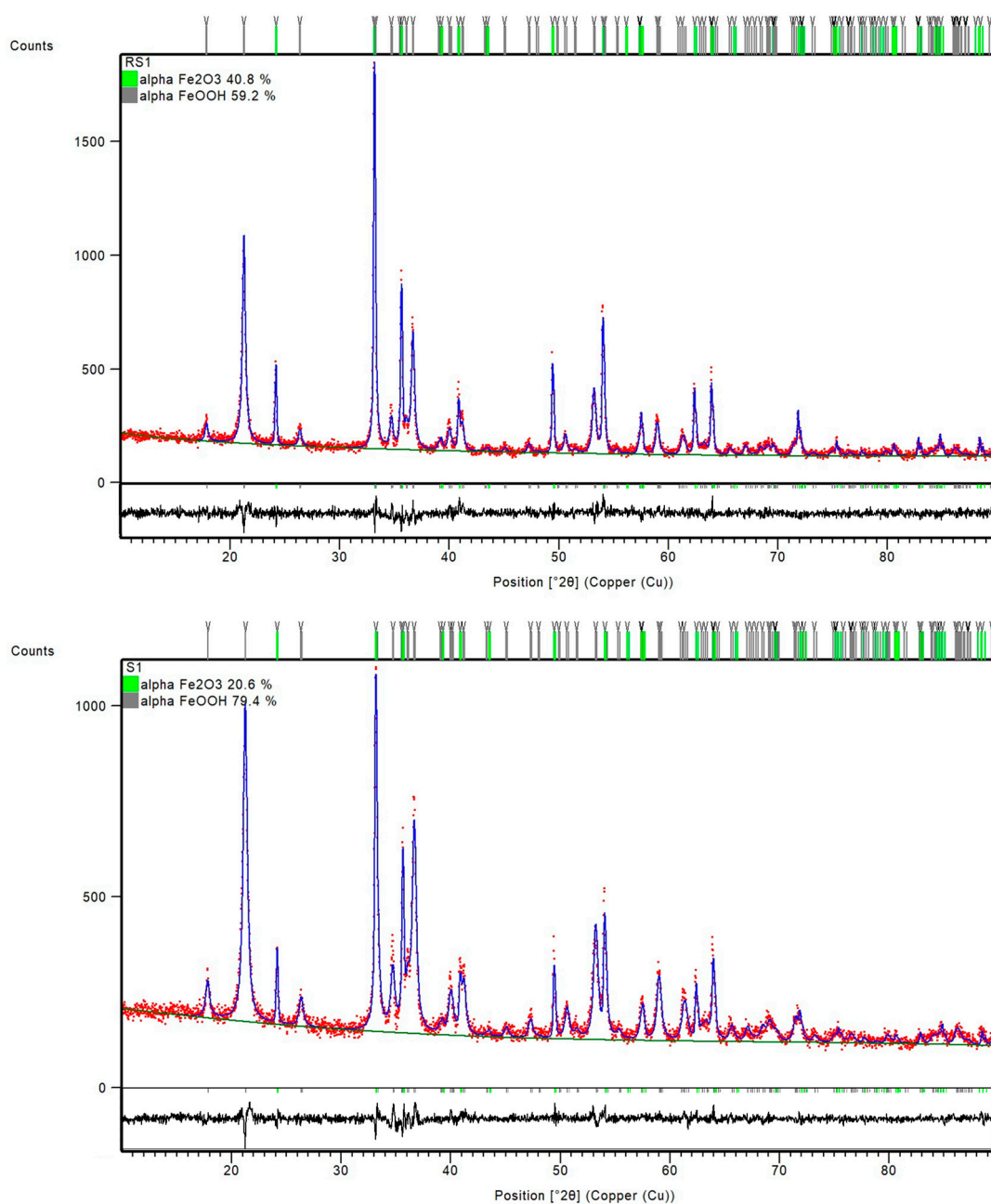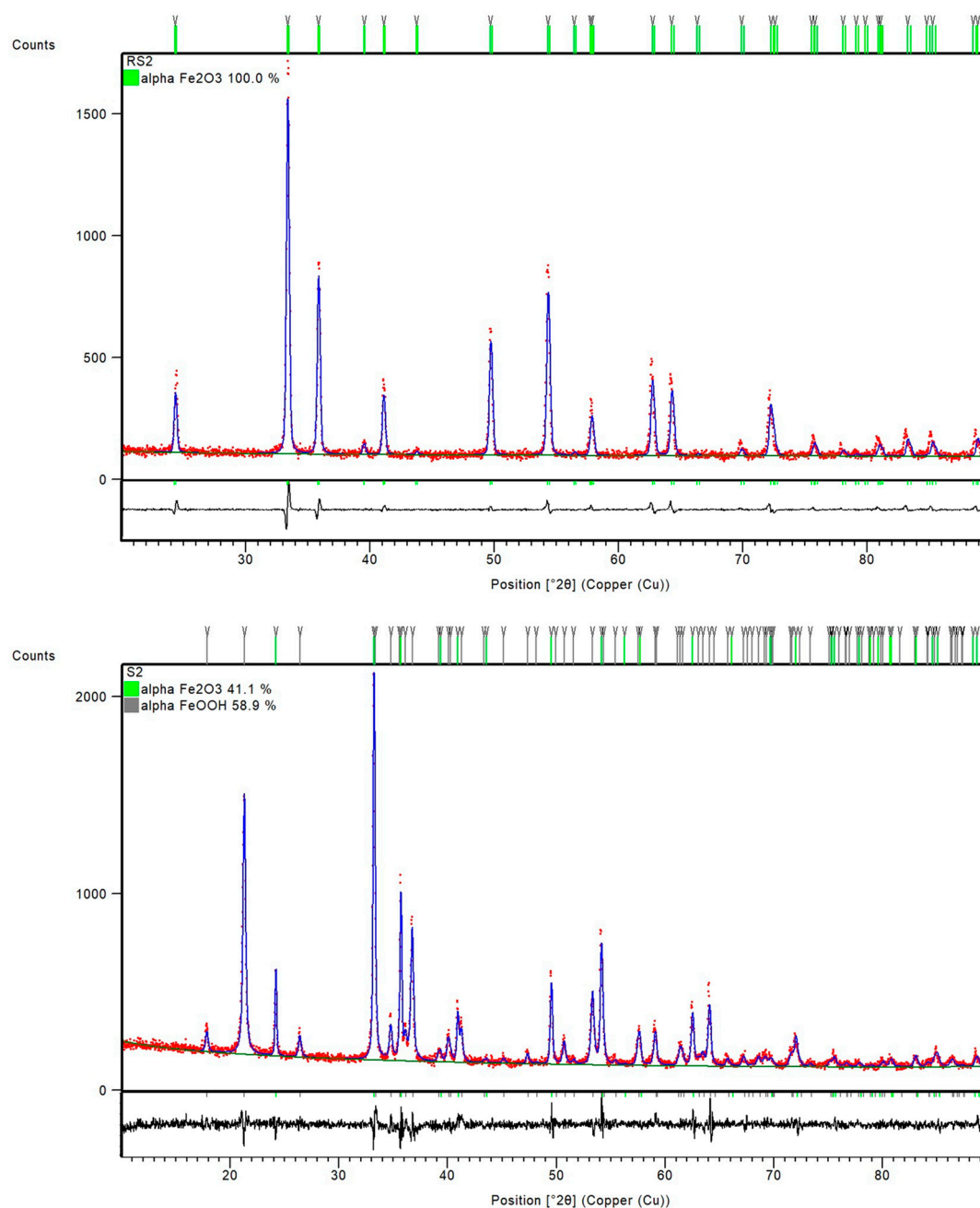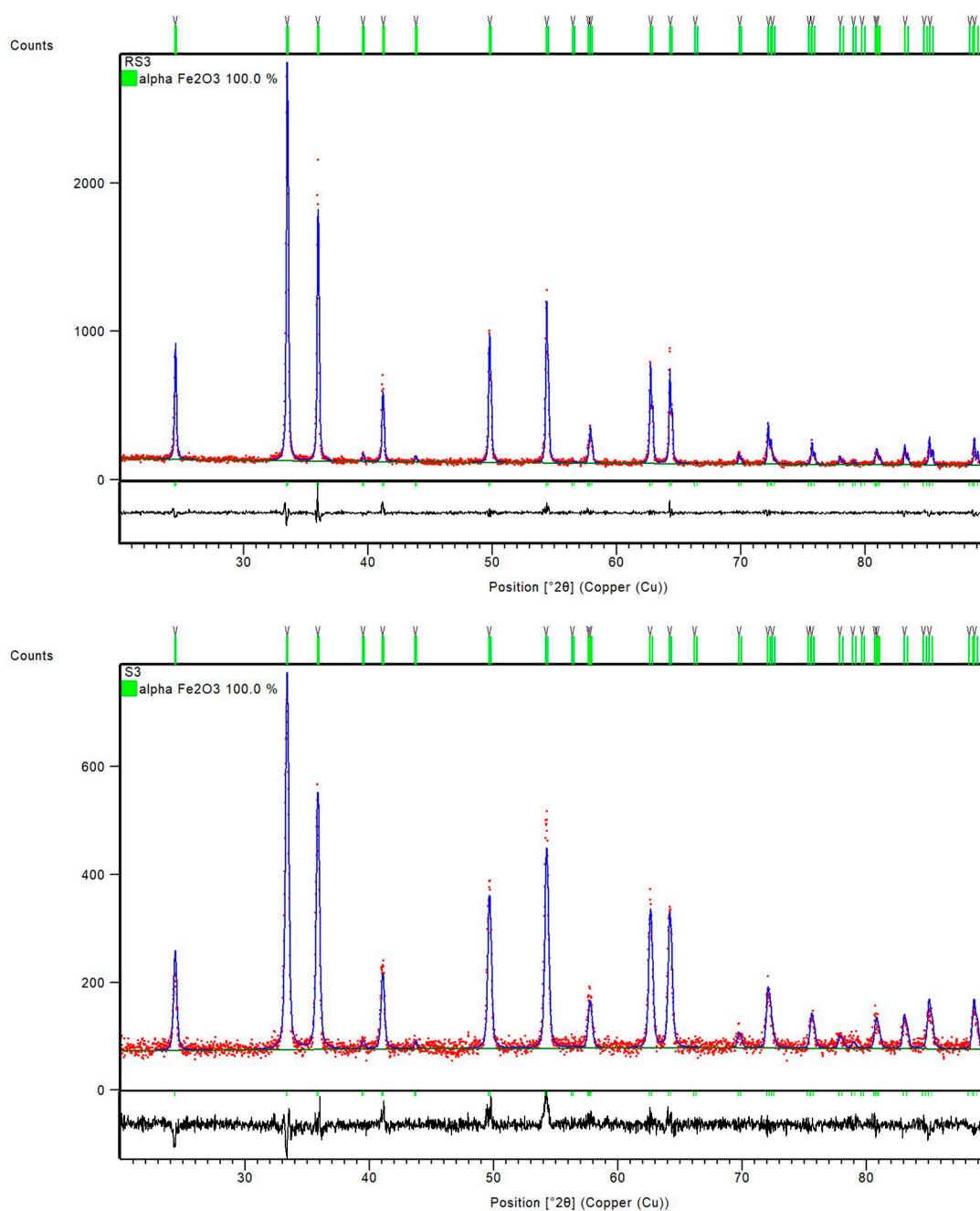
Figure 2. Final observed (red dots) and calculated (blue, solid lines) powder diffraction profiles for reference sample RS1 and sample S1 as obtained from the Rietveld refinement. The green and gray tick marks show the reflection positions of α-Fe_2O_3 and α-$FeOOH$, respectively. The lower, black, solid lines show the difference profiles.

Figure 3. Final observed (red dots) and calculated (blue, solid lines) powder diffraction profiles for reference sample RS2 and sample S2 as obtained from the Rietveld refinement. The green and gray tick marks show the reflection positions of α-Fe_2O_3 and α-FeOOH, respectively. The lower, black, solid lines show the difference profiles.

Figure 4. Final observed (red dots) and calculated (blue, solid lines) powder diffraction profiles for reference sample RS3 and sample S3 as obtained from the Rietveld refinement. The green and gray tick marks show the reflection positions of α-Fe$_2$O$_3$ and α-FeOOH, respectively. The lower, black, solid lines show the difference profiles.

Table 3. Results of crystallite size calculation as obtained from the phase refinements to PXRD data.

| Sample | Crystallite Size (nm) | | Phase Fraction (wt.%) |
	α-Fe$_2$O$_3$ (s.g. *R*-3c)	α-FeOOH (s.g. *P*bnm)	
RS1	66.2 (1)		40.8
		29.7 (1)	59.2
S1	63.7 (1)		20.6
		21.2 (1)	79.4
RS2	39.5 (1)		100
S2	65.7 (1)		41.1
		36.7 (1)	58.9
S4	42.3 (1)		89.7
		35.5 (1)	10.3
S5	38.7 (1)		52.2
		26.4 (1)	47.8
S6	38.8 (1)		39.5
		27.7 (1)	60.5
S7	24.6 (1)		100
RS3	81.0 (1)		100
S3	29.8 (1)		100

Figure 5 shows samples precipitated at 200 °C for 20 min, but with different additions of CTAB in the precipitation system: reference sample, RS2, without CTAB addition; sample S4 with 0.25% of CTAB addition; sample S6 with 2.5% of CTAB added in precipitation mixture. In these experimental conditions, without the CTAB addition, the final product comprised pure hematite phase, as evidenced from the IR spectra of reference sample RS2. Samples with the addition of CTAB (>0.5%) showed no difference according to FT-IR analysis and had the same IR bands positioned at 893 cm^{-1}, 795 cm^{-1}, 644 cm^{-1}, 546 cm^{-1}, 471 cm^{-1}, and 411 cm^{-1} of similar intensity, characteristic for the mixture of hematite and goethite phases. Sample S4, with the smallest amount of CTAB (0.25%), showed the same IR bands but reduced in intensity. Sample S4 contained the largest proportion of hematite, ~90 wt.%, of the final product. On the contrary, the sample S6, with the highest content of CTAB, comprised the smallest fraction of hematite, only 39.5 wt.%, of the final product (Table 2). Figure 6 shows a comparison of IR and the PXRD data of the reference sample RS3, synthesized at 250 °C, and the sample with 2.5% CTAB added to the precipitation mixture, S7, indicating the formation of pure hematite phases.

3.2. Surface Morphology Imaging

FE-SEM image of reference sample RS1 (Figure 7a) shows the presence of nanorods typical of goethite and irregular particles typical of hematite formed at high pH [22]. In the presence of CTAB (sample S1, Figure 7b), an increased fraction of goethite nanorods and smaller hematite irregular particles were visible. FE-SEM image of reference sample RS2 (Figure 7c) shows only the presence of irregular hematite particles, while in the FE-SEM image of sample S2 (Figure 7d) goethite nanorods are also visible.
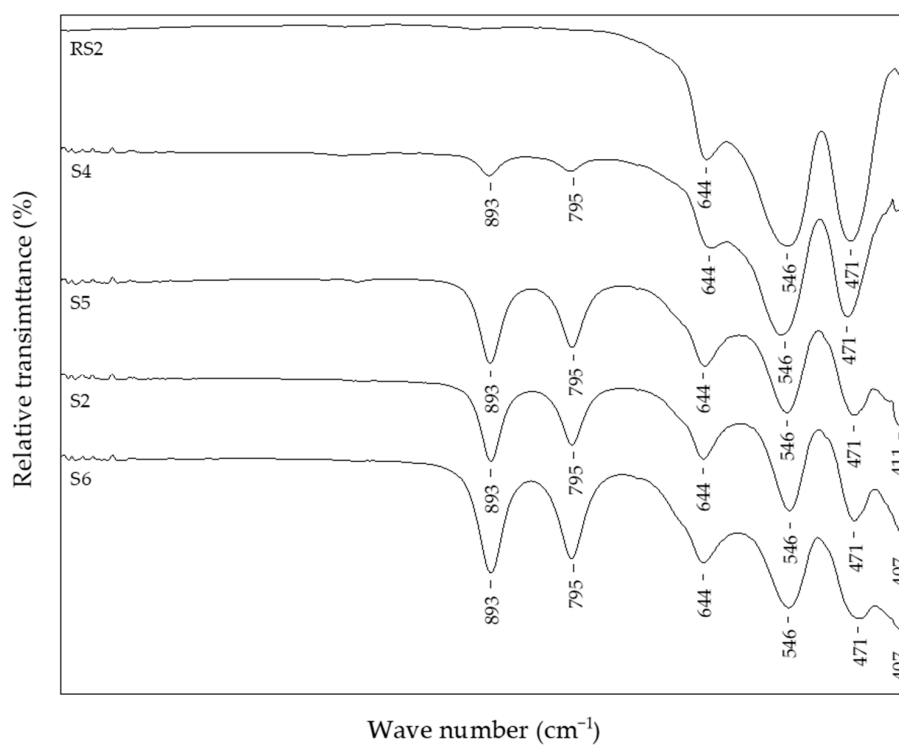
Figure 5. FT-IR spectra of samples with different percentages of CTAB in precipitation mixture.
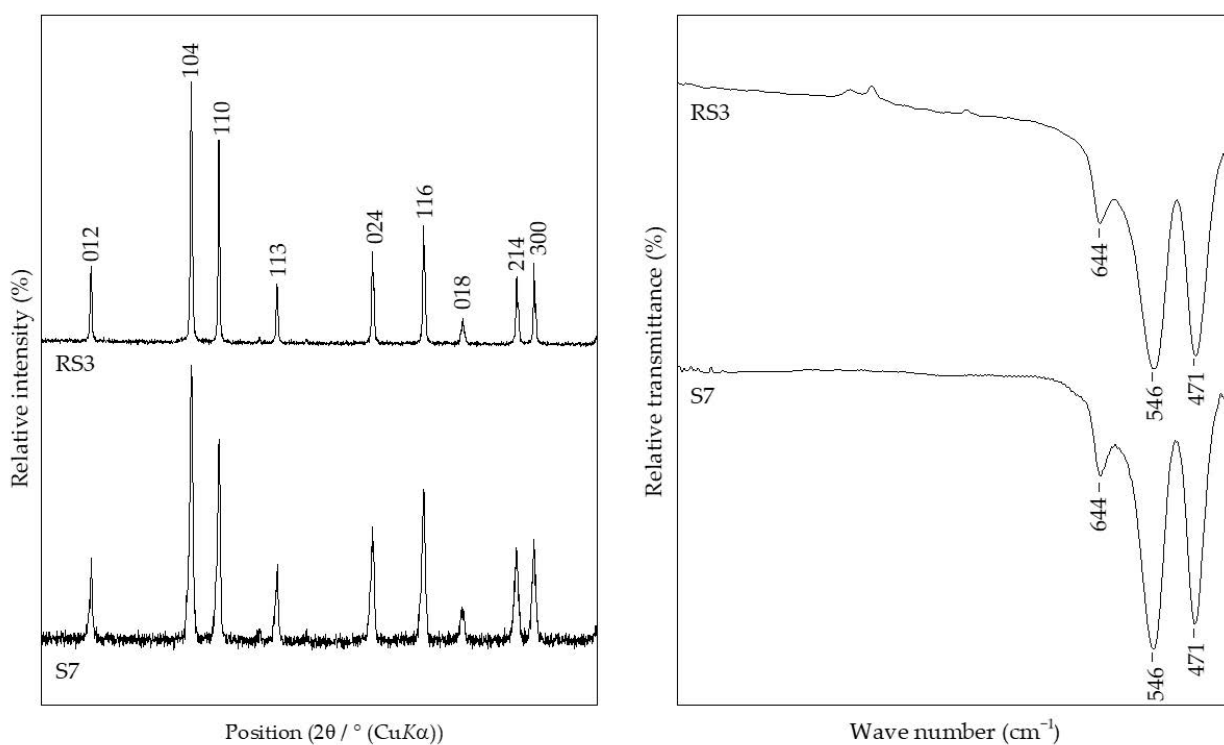

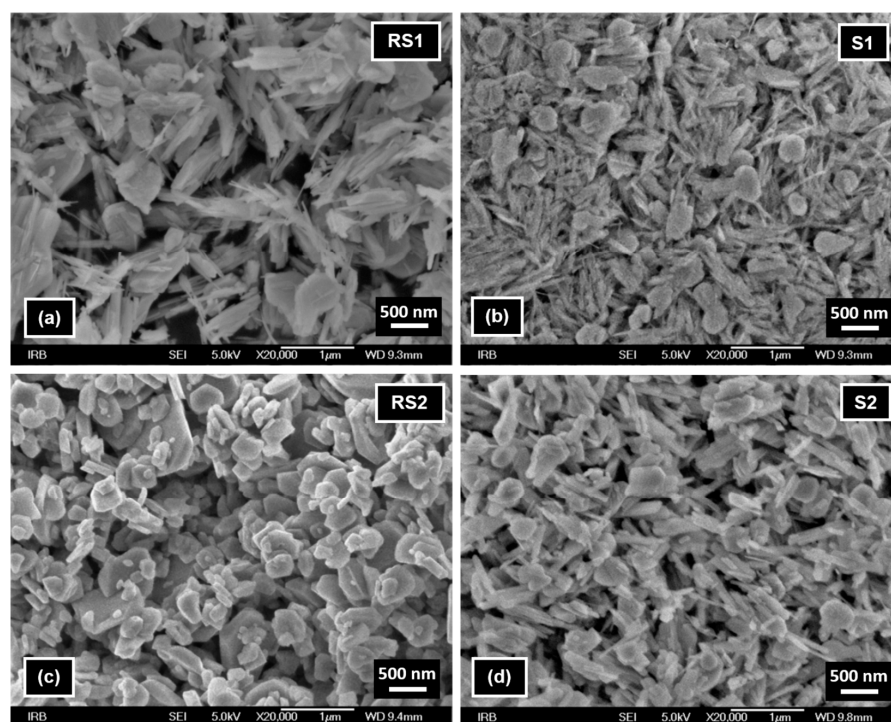**Figure 6.** Comparison of PXRD patterns and FT-IR spectra of samples RS3 and S7.

Figure 7. FE-SEM images of samples (**a**) RS1, (**b**) S1, (**c**) RS2, and (**d**) S2 recorded at magnification of 20,000×.

FE-SEM images of reference sample RS3 (Figure 8a) and samples S3 and S7 (Figure 8b–d) show the presence of similar irregular hematite particles of about several tens of nm to 1 μm in size. These images indicate an insignificant influence of the presence of CTAB during high-temperature (250 °C) synthesis on the size and shape of hematite particles.
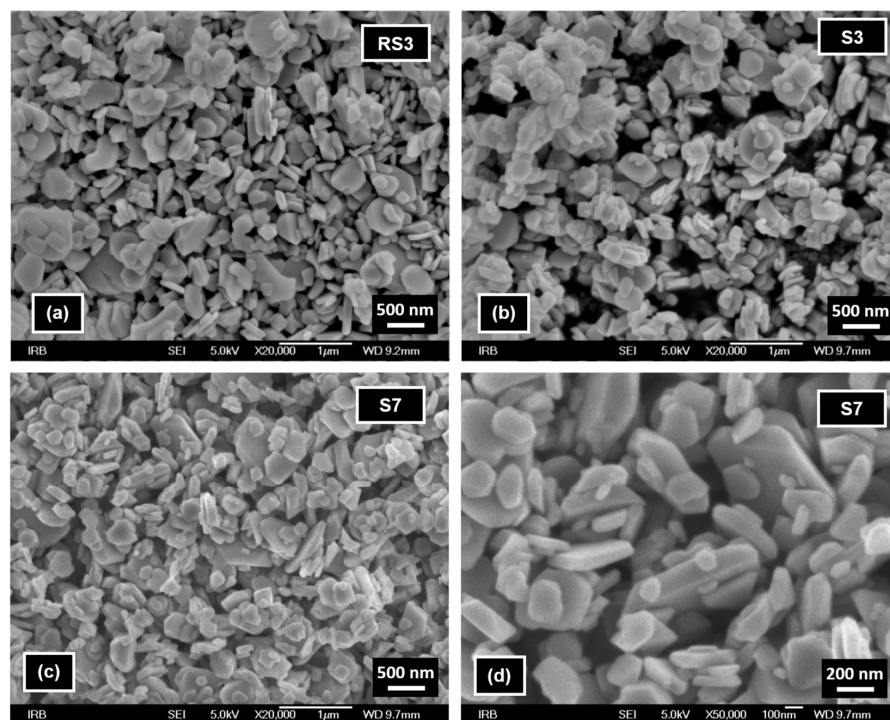
Figure 8. FE-SEM images of samples (**a**) RS3, (**b**) S3, and (**c**) S7 recorded at a magnification of 20,000×, and (**d**) sample S7 recorded at a magnification of 50,000×.

4. Discussion

The formation of α-Fe$_2$O$_3$ particles obtained by the precipitation from FeCl$_3$ solution by forced hydrolysis at elevated temperatures dissolved α-FeOOH particles and recrystallizes α-Fe$_2$O$_3$ particles, as reported in the literature [22,25,34]. The syntheses reported in these papers represent conventional hydrothermal routes in a gravity furnace under extended reaction time, hours or days. Foreign species in precipitation mixtures for iron oxide synthesis (i.e., anions, cations, or neutral molecules) can have two different effects: They can change either the composition ratio of the final product (goethite/hematite) or they can modify the properties of the final product [6]. The effect of the surfactant CTAB on particle morphology has been studied in previous work using conventional hydrothermal routes under extended reaction time [70].

In this work, we investigated a microwave-assisted hydrothermal accelerated synthesis of α-Fe$_2$O$_3$ and α-FeOOH particles from FeCl$_3$ solution in a highly alkaline medium at 150 °C, 200 °C, and 250 °C and 20-min reaction time. The effect of the percentage of a cationic surfactant, CTAB, on the composition, size, and shape of the final product was elaborated in detail.

Reference samples RS1–RS3 and samples S1–S3 were prepared as precipitated mixtures of 0.1 M FeCl$_3$ solution at pH values ~13 and heated at 150 °C, 200 °C, and 250 °C for 20 min in a microwave oven. Samples S1–S3 in the precipitated mixtures contained 1% CTAB. Reference sample RS1 and sample S1 prepared at 150 °C showed the same IR bands, assigned to the formation of goethite and hematite phases. The PXRD patterns in Figure 2 showed the mixture of α-Fe$_2$O$_3$ and α-FeOOH in both the reference sample RS1 and sample S1. According to the results of structure refinements, the reference sample RS1 and sample S1 differed in their composition ratio: The sample RS1 contained ~40 wt.% α-Fe$_2$O$_3$ and ~60 wt.% α-FeOOH, whereas the sample S1 comprised 20 wt.% α-Fe$_2$O$_3$ and 80 wt.% α-FeOOH. Therefore, it can be concluded that CTAB in sample S1 slowed down the rate of the goethite-to-hematite transformation process. A complete transformation of goethite to hematite phase was possible only at higher temperatures. In particular, under hydrothermal conditions, above 150 °C, the formation of the hematite phase was very fast [6]. The FT-IR spectra of the reference sample RS2 in Figure 1 and the PXRD patterns in Figure 3 showed the formation of single-phase α-Fe$_2$O$_3$ after 20 min at 200 °C. On the contrary, the sample S2, prepared with the same aging time and temperature as the reference sample RS2 but with 1% CTAB addition, comprised the mixture of both α-Fe$_2$O$_3$ and α-FeOOH phases. The mixture consisted of ~40 wt.% α-Fe$_2$O$_3$ and ~60 wt.% α-FeOOH. Indeed, slowing down the rate of the phase transformation from goethite to hematite induced by the CTAB addition followed a similar fashion as for the sample S1. Furthermore, the synthesis of samples RS3, S7, and S3 showed that the addition of CTAB did not affect the goethite-to-hematite transformation (see Figures 4 and 6). In these samples, single-phase α-Fe$_2$O$_3$ precipitated in the nanometer range, as unraveled from the PXRD line-broadening analysis.

Atyam et al. [88] described that the IR peaks at 536 and 468 cm^{-1} corresponded to Fe-O bonding of iron oxide for well-calcined particles appearing with the increase of temperature, which was in excellent agreement with our study, as we can see the shift of the IR band (Figure 1) compared to the samples prepared at 150 °C (sample S1) and those prepared at 200 or 250 °C (samples S2 and S3). The FE-SEM analysis revealed that the goethite particles in samples RS1, S1, and S2 were nanorods and the hematite particles in all samples had irregular shapes and sizes in the range from ~10 nm to 1 μm.

As mentioned in the Introduction, the microwave-assisted synthesis ensured a quick investigation of the influence of various additives and their addition amount in the synthesis mixture. In particular, the samples precipitated at 200 °C for 20 min, but with different addition levels of CTAB in the precipitated system, from 0.25% in sample S4 to 2.5% in sample S6 (Figure 5). The addition of less than 0.25% CTAB had no significant effect on the goethite-to-hematite transformation process. However, higher additions of CTAB, from 0.5% to 2.5%, according to Table 2, indicated that as the amount of CTAB in the precipitated

mixture of samples increased, the composition of goethite and hematite varied, resulting in a smaller mass fraction of hematite phase in the final product. According to FE-SEM images of samples RS3, S3, and S7 and results of PXRD line-broadening analysis, it was concluded that CTAB addition had an insignificant influence on the size and shape of hematite particles.

Based on this rapid and straightforward iron oxide preparation method, future studies will investigate the effects of other surfactants: anionic, cationic, or nonionic on the precipitated mixture, with a strong emphasis placed on the reproducibility of the synthesis data produced by microwave technology.

5. Conclusions

In this work, we reported the facile and fast microwave-assisted hydrothermal synthesis of α-Fe_2O_3 particles from $FeCl_3$ solution in highly alkaline media by heating at 200 °C and 250 °C for 20 min. In these synthesis routes for hematite particles, it was proven that 0.25% of added CTAB slows down the transformation of goethite-to-hematite at 200 °C, but any percentage of added CTAB had no effect on transformation at 250 °C. The shape of the synthesized particles, goethite nanorods, and irregular hematite was about a few tens of nm to 1 μm in size regardless of temperature or CTAB addition.

Author Contributions: Methodology, L.G. and A.P. (Andrea Paut); validation, I.M., Ž.S., and M.V.; formal analysis, I.M., Ž.S., and M.V.; investigation, I.M. and S.K.; resources, I.M.; data curation, I.M.; writing—original draft preparation, I.M.; writing—review and editing, I.M., L.G., A.P. (Andrea Paut), M.V., and S.K.; visualization, I.M. and M.V.; supervision, I.M.; project administration, A.P. (Ante Prkić) and S.K.; funding acquisition, I.M., A.P. (Ante Prkić), and S.K. All authors have read and agreed to the published version of the manuscript.

Data Availability Statement: Not applicable.

Conflicts of Interest: The authors declare no conflict of interest.

References

1. Bilecka, I.; Niederberger, M. Microwave chemistry for inorganic nanomaterials synthesis. *Nanoscale* **2010**, *2*, 1358–1374. [CrossRef]
2. Kappe, C.O. How to measure reaction temperature in microwave-heated transformations. *Chem. Soc. Rev.* **2013**, *42*, 4977–4990. [CrossRef] [PubMed]
3. Van der Eycken, E.V. Practical Microwave Synthesis for Organic Chemists.Strategies, Instruments, and Protocols. Edited by C. Oliver Kappe, Doris Dallinger and Shaun Murphree. *Angew. Chem. Int. Ed.* **2009**, *48*, 2828–2829. [CrossRef]
4. Schutz, M.B.; Xiao, L.S.; Lehnen, T.; Fischer, T.; Mathur, S. Microwave-assisted synthesis of nanocrystalline binary and ternary metal oxides. *Int. Mater. Rev.* **2018**, *63*, 341–374. [CrossRef]
5. Nüchter, M.; Ondruschka, B.; Bonrath, W.; Gum, A. Microwave assisted synthesis–a critical technology overview. *Green Chem.* **2004**, *6*, 128–141. [CrossRef]
6. Cornell, R.M.; Schwertmann, U. *The Iron Oxides: Structure, Properties, Reactions, Occurrence, and Uses*; VCH: New York, NY, USA, 2003.
7. Buxbaum, G. *Industrial Inorganic Pigments*, 1st ed.; VCH: New York, NY, USA, 1993; p. 281.
8. Li, P.; Miser, D.; Rabiei, S.; Yadav, R.; Hajaligol, M. The removal of carbon monoxide by iron oxide nanoparticles. *Appl. Catal. B* **2003**, *43*, 151–162. [CrossRef]
9. Zhang, W.; Singh, P.; Paling, E.; Delides, S. Arsenic removal from contaminated water by natural iron ores. *Miner. Eng.* **2004**, *17*, 517–524. [CrossRef]
10. Mohapatra, M.; Anand, S. Synthesis and applications of nano-structured iron oxides or hidroxides—A review. *Int. J. Eng. Sci. Technol.* **2010**, *2*, 127–146.
11. Lu, A.-H.; Salabas, E.L.; Schueth, F. Magnetic nanoparticles: Synthesis, protection, functionalization, and application. *Angew. Chem. Int. Ed.* **2007**, *46*, 1222–1244. [CrossRef] [PubMed]
12. Marinho, J.Z.; Montes, R.H.O.; de Moura, A.P.; Longo, E.; Varela, J.A.; Munoz, R.A.A.; Lima, R.C. Rapid preparation of alpha-FeOOH and alpha-Fe2O3 nanostructures by microwave heating and their application in electrochemical sensors. *Mater. Res. Bull.* **2014**, *49*, 572–576. [CrossRef]
13. Prkić, A.; Vukušić, T.; Mitar, I.; Giljanović, J.; Sokol, V.; Bošković, P.; Jakić, M.; Sedlar, A. New sensor based on AgCl containing Iron Oxide or Zinc Oxide Nanoparticles for Chloride Determination. *Int. J. Electrochem. Sci* **2019**, *14*, 861–874. [CrossRef]
14. Schwertmann, U.; Cornell, R.M. *Iron Oxides in the Laboratory: Preparation and Characterization*; VCH: New York, NY, USA, 2000; p. 204.

15. Wang, J.; Zhang, K.; Peng, Z.M.; Chen, Q.W. Magnetic properties improvement in Fe$_3$O$_4$ nanoparticles grown under magnetic fields. *J. Cryst. Growth* **2004**, *266*, 500–504. [CrossRef]

16. Akbarzadeh, A.; Samiei, M.; Davaran, S. Magnetic nanoparticles: Preparation, physical properties, and applications in biomedicine. *Nanoscale Res. Lett.* **2012**, *7*, 144–157. [CrossRef] [PubMed]

17. Laurent, S.; Forge, D.; Port, M.; Roch, A.; Robic, C.; Elst, L.; Muller, R. Magnetic iron oxide nanoparticles: Synthesis, stabilization, vectorization, physicochemical characterizations, and biological applications. *Chem. Rev.* **2008**, *108*, 2064–2110. [CrossRef] [PubMed]

18. Yue, J.; Jiang, X.; Kaneti, Y.V.; Yu, A. Experimental and theoretical study of low-dimensional iron oxide nanostructures. In *Smart Nanoparticles Technology*; InTech: London, UK, 2012; pp. 119–146.

19. Machala, L.; Tucek, J.; Zboril, R. Polymorphous transformations of nanometric iron(III) oxide—A review. *Chem. Mater.* **2011**, *23*, 3255–3272. [CrossRef]

20. Wu, W.; He, Q.; Jiang, C. Magnetic iron oxide nanoparticles: Synthesis and surface functionalization strategies. *Nanoscale Res. Lett.* **2008**, *3*, 397–415. [CrossRef] [PubMed]

21. Teja, A.S.; Koh, P.-Y. Synthesis, properties, and applications of magnetic iron oxide nanoparticles. *Prog. Cryst. Growth Charact. Mater.* **2009**, *55*, 22–45. [CrossRef]

22. Žic, M.; Ristić, M.; Musić, S. Fe^{57} Mössbauer, FT-IR and FE SEM investigation of the formation of hematite and goethite at high pH values. *J. Mol. Struct.* **2007**, *834*, 141–149. [CrossRef]

23. Gotić, M.; Popović, S.; Ljubešić, N.; Musić, S. Structural Properties of Precipitates Formed by Hydrolysis of Fe3+ Ions in Aqueous Solutions Containing NO3- and Cl- Ions. *J. Mater Sci.* **1994**, *29*, 2474–2480. [CrossRef]

24. Musić, S.; Vertes, A.; Simmons, G.W.; Czakonagy, I.; Leidheiser, H. Mössbauer spectroscopic study of the formation of Fe(III) oxyhydroxides and oxides by hydrolysis of aqueous Fe(III) salt-solutions. *J. Colloid Interface Sci.* **1982**, *85*, 256–266. [CrossRef]

25. Šarić, A.; Musić, S.; Nomura, K.; Popović, S. Microstructural properties of Fe-oxide powders obtained by precipitation from FeCl$_3$ solutions. *Mater. Sci. Eng. B* **1998**, *56*, 43–52. [CrossRef]

26. Musić, S.; Santana, G.P.; Smit, G.; Garg, V.K. Fe^{57} Mössbauer, FT-IR and TEM investigations of Fe-oxide powders obtained from concentrated FeCl$_3$ solutions. *J. Alloys Compd.* **1998**, *278*, 291–301. [CrossRef]

27. Musić, S.; Maljković, M.; Popović, S. Chemical and microstructural properties of iron oxide powders obtained from FeCl$_3$ solutions with decomposing urea. *ACH Models Chem.* **1999**, *136*, 299–316.

28. Musić, S.; Krehula, S.; Popović, S.; Skoko, Z. Some factors influencing forced hydrolysis of FeCl$_3$ solutions. *Mater. Lett.* **2003**, *57*, 1096–1102. [CrossRef]

29. Musić, S.; Krehula, S.; Popović, S. Effect of HCl additions on forced hydrolysis of FeCl$_3$ solutions. *Mater. Lett.* **2004**, *58*, 2640–2645. [CrossRef]

30. Krehula, S.; Music, S. Influence of ruthenium ions on the precipitation of α-FeOOH, α-Fe$_2$O$_3$ and Fe$_3$O$_4$ in highly alkaline media. *J. Alloys Compd.* **2006**, *416*, 284–290. [CrossRef]

31. Ristić, M.; Musić, S.; Godec, M. Properties of γ-FeOOH, α-FeOOH and α-Fe$_2$O$_3$ particles precipitated by hydrolysis of Fe^{3+} ions in perchlorate containing aqueous solutions. *J. Alloys Compd.* **2006**, *417*, 292–299. [CrossRef]

32. Gotić, M.; Musić, S. Mössbauer, FT-IR and FE SEM investigation of iron oxides precipitated from FeSO$_4$ solutions. *J. Mol. Struct.* **2007**, *834*, 445–453. [CrossRef]

33. Krehula, S.; Musić, S. Influence of aging in an alkaline medium on the microstructural properties of α-FeOOH. *J. Cryst. Growth* **2008**, *310*, 513–520. [CrossRef]

34. Žic, M.; Ristić, M.; Musić, S. Microstructural changes in particles detected during the transformation from β-FeOOH to α-Fe$_2$O$_3$ in dense aqueous suspensions. *J. Alloys Compd.* **2008**, *464*, 81–88. [CrossRef]

35. Gotić, M.; Musić, S.; Popović, S.; Sekovanić, L. Investigation of factors influencing the precipitation of iron oxides from Fe(II) containing solutions. *Croat. Chem. Acta* **2008**, *81*, 569–578.

36. Žic, M.; Ristić, M.; Musić, S. Precipitation of α-Fe$_2$O$_3$ from dense β-FeOOH suspensions with added ammonium amidosulfonate. *J. Mol. Struct.* **2009**, *924–926*, 235–242. [CrossRef]

37. Žic, M.; Ristić, M.; Musić, S. The effect of temperature on the crystallization of α-Fe$_2$O$_3$ particles from dense β-FeOOH suspensions. *Mater. Chem. Phys.* **2010**, *120*, 160–166. [CrossRef]

38. Opačak, I.; Ristić, M.; Musić, S. Preparation and characterization of hollow alpha-Fe2O3 irregular microspheres. *Mater. Lett.* **2010**, *64*, 2555–2558. [CrossRef]

39. Žic, M.; Ristić, M.; Musić, S. Monitoring the hydrothermal precipitation of α-Fe$_2$O$_3$ from concentrated Fe(NO$_3$)$_3$ solutions partially neutralized with NaOH. *J. Mol. Struct.* **2011**, *993*, 115–119. [CrossRef]

40. Ristić, M.; Opačak, I.; Musić, S. The synthesis and microstructure of goethite particles precipitated in highly alkaline media. *J. Alloys Compd.* **2013**, *559*, 49–56. [CrossRef]

41. Ristić, M.; Fujii, T.; Hashimoto, H.; Opačak, I.; Musić, S. A novel route in the synthesis of magnetite nanoparticles. *Mater. Lett.* **2013**, *100*, 93–97. [CrossRef]

42. Ristić, M.; Štajdohar, J.; Mitar, I.; Musić, S. Monitoring of the Forced Hydrolysis of FeCl3 Solutions in the Presence of Sodium Dodecyl Sulphate. *Croat. Chem. Acta* **2018**, *91*, 403–410. [CrossRef]

43. Ristić, M.; Mitar, I.; Musić, S. Forced hydrolysis of FeCl3 solutions in the presence of sodium dextran sulphate. *Colloid Polym. Sci.* **2019**, *297*, 177–182. [CrossRef]

44. Gupta, A.K.; Gupta, M. Synthesis and surface engineering of iron oxide nanoparticles for biomedical applications. *Biomaterials* **2005**, *26*, 3995–4021. [CrossRef]

45. Wu, W.; Jiang, C.Z.; Roy, V.A.L. Designed synthesis and surface engineering strategies of magnetic iron oxide nanoparticles for biomedical applications. *Nanoscale* **2016**, *8*, 19421–19474. [CrossRef] [PubMed]

46. Faraji, M.; Yamini, Y.; Rezaee, M. Magnetic nanoparticles: Synthesis, stabilization, functionalization, characterization, and applications. *J. Iran. Chem. Soc.* **2010**, *7*, 1–37. [CrossRef]

47. Wang, W.; Zhu, Y.; Ruan, M. Microwave assisted synthesis and magnetic property of magnetite and hematite nanoparticles. *J. Nanopart. Res.* **2007**, *9*, 419–426. [CrossRef]

48. Hu, L.; Percheron, A.; Chaumont, D.; Brachais, C.H. Microwave-assisted one-step hydrothermal synthesis of pure iron oxide nanoparticles: Magnetite, maghemite and hematite. *J. Sol Gel Sci. Technol.* **2011**, *60*, 198–205. [CrossRef]

49. Jiang, F.; Wang, C.; Fu, Y.; Liu, R. Synthesis of iron oxide nanocubes via microwave assisted solvolthermal method. *J. Alloys Compd.* **2010**, *503*, 31–33. [CrossRef]

50. Yin, S.; Luo, Z.; Xia, J.; Li, H. Microwave-assisted synthesis of Fe3O4 nanorods and nanowires in an ionic liquid. *J. Phys. Chem. Solids* **2010**, *71*, 1785–1788. [CrossRef]

51. Cao, S.-W.; Zhu, Y.-J. Iron oxide hollow spheres: Microwave–hydrothermal ionic liquid preparation, formation mechanism, crystal phase and morphology control and properties. *Acta Mater.* **2009**, *57*, 2154–2165. [CrossRef]

52. Xavier, C.S.; Paskocimas, C.A.; da Motta, F.V.; Araujo, V.D.; Aragon, M.J.; Tirado, J.L.; Lavela, P.; Longo, E.; Delmonte, M.R.B. Microwave-assisted Hydrothermal Synthesis of Magnetite Nanoparticles with Potential Use as Anode in Lithium Ion Batteries. *Mater. Res.* **2014**, *17*, 1065–1070. [CrossRef]

53. Osborne, E.A.; Atkins, T.M.; Gilbert, D.A.; Kauzlarich, S.M.; Liu, K.; Louie, A.Y. Rapid microwave assisted synthesis of dextran coated iron oxide nanoparticles for magnetic resonance imaging. *Nanotechnology* **2012**, *23*, 3461–3467. [CrossRef]

54. Komarneni, S.; D'Arrigo, M.C.; Leonelli, C.; Pellacani, G.C.; Katsuki, H. Microwave-hydrothermal synthesis of nanophase ferrites. *J. Am. Ceram. Soc.* **1998**, *81*, 3041–3043. [CrossRef]

55. Sreeja, V.; Joy, P. Microwave hydrothermal synthesis of γ-Fe2O3 nanoparticles and their magnetic properties. *Mater. Res. Bull.* **2007**, *42*, 1570–1576. [CrossRef]

56. Katsuki, H.; Komarneni, S. Microwave-Hydrothermal Synthesis of Monodispersed Nanophase α-Fe2O3. *J. Am. Ceram. Soc.* **2001**, *84*, 2313–2317. [CrossRef]

57. Ni, H.; Ni, Y.; Zhou, Y.; Hong, J. Microwave–hydrothermal synthesis, characterization and properties of rice-like α-Fe2O3 nanorods. *Mater. Lett.* **2012**, *73*, 206–208. [CrossRef]

58. Khollam, Y.B.; Dhage, S.R.; Potdar, H.S.; Deshpande, S.B.; Bakare, P.P.; Kulkarni, S.D.; Date, S.K. Microwave hydrothermal preparation of submicron-sized spherical magnetite (Fe3O4) powders. *Mater. Lett.* **2002**, *56*, 571–577. [CrossRef]

59. Bakare, P.P.; Date, S.K.; Khollam, Y.B.; Deshpande, S.B.; Potdar, H.S.; Salunke-Gawali, S.; Varret, F.; Pereira, E. Mössbauer effect studies on the formation of iron oxide phases synthesized via microwave–hydrothermal route. *Hyperfine Interact.* **2006**, *168*, 1127–1132. [CrossRef]

60. Dhage, S.R.; Khollam, Y.B.; Potdar, H.S.; Deshpande, S.B.; Bakare, P.P.; Sainkar, S.R.; Date, S.K. Effect of variation of molar ratio (pH) on the crystallization of iron oxide phases in microwave hydrothermal synthesis. *Mater. Lett.* **2002**, *57*, 457–462. [CrossRef]

61. Parsons, J.; Luna, C.; Botez, C.; Elizalde, J.; Gardea-Torresdey, J. Microwave assisted synthesis of iron(III) oxyhydroxides/oxides characterized using transmission electron microscopy, X-ray diffraction, and X-ray absorption spectroscopy. *J. Phys. Chem. Solids* **2009**, *70*, 555–560. [CrossRef] [PubMed]

62. Hu, X.L.; Yu, J.C.; Gong, J.M. Fast production of self-assembled hierarchical alpha-Fe2O3 nanoarchitectures. *J. Phys. Chem. C* **2007**, *111*, 11180–11185. [CrossRef]

63. Mahmoud, W.E.; Al-Hazmi, F.; Al-Noaiser, F.; Al-Ghamdi, A.A.; Bronstein, L.M. A facile method to syntheses monodisperse gamma-Fe2O3 nanocubes with high magnetic anisotropy density. *Superlattices Microstruct.* **2014**, *68*, 1–5. [CrossRef]

64. Deshmukh, R.G.; Badadhe, S.S.; Mulla, I.S. Microwave-assisted synthesis and humidity sensing of nanostructured alpha-Fe2O3. *Mater. Res. Bull.* **2009**, *44*, 1179–1182. [CrossRef]

65. Dias, A.M.G.C.; Hussain, A.; Marcos, A.S.; Roque, A.C.A. A biotechnological perspective on the application of iron oxide magnetic colloids modified with polysaccharides. *Biotechnol. Adv.* **2011**, *29*, 142–155. [CrossRef]

66. Ngenefeme, F.-T.J.; Eko, N.J.; Mbom, Y.D.; Tantoh, N.D.; Rui, K.W.M. A one pot green synthesis and characterisation of iron oxide pectin hybrid nanocomposite. *Open J. Compos. Mater.* **2013**, *3*, 30–37. [CrossRef]

67. Kim, D.K.; Zhang, Y.; Voit, W.; Rao, K.V.; Muhammed, M. Synthesis and characterization of surfactant-coated superparamagnetic monodispersed iron oxide nanoparticles. *J. Magn. Magn. Mater.* **2001**, *225*, 30–36. [CrossRef]

68. Shokuhfar, A.; Alibeigi, S.; Vaezi, M.R.; Sadrnezhaad, S.K. Synthesis of Fe3O4 Nanoparticles Prepared by Various Surfactants and Studying their Characterizations. *Defect Diffus. Forum.* **2008**, *273–276*, 22–27.

69. Ristić, M.; Kuzmann, E.; Homonnay, Z.; Mitar, I.; Musić, S. Hydrolysis of Fe(III) in the presence of mixed anions and promoters. *J. Radioanal. Nucl. Chem.* **2020**, *324*, 1293–1302. [CrossRef]

70. Ristić, M.; Opačak, I.; Stajdohar, J.; Musić, S. The influence of CTAB and gum arabic on the precipitation of alpha-FeOOH in a highly alkaline medium. *J. Mol. Struct.* **2015**, *1090*, 129–137. [CrossRef]

71. Ristić, M.; Štajdohar, J.; Opačak, I.; Musić, S. The Effect of Sodium Dodecyl Sulphate On The Forced Hydrolysis Of FeCl3 Solutions. *Contrib. Sect. Nat. Math. Biotech. Sci.* **2017**, *38*, 57–67. [CrossRef]

72. Yue, J.; Jiang, X.; Zeng, Q.; Yu, A. Experimental and numerical study of cetyltrimethylammonium bromide (CTAB)-directed synthesis of goethite nanorods. *Solid State Sci.* **2010**, *12*, 1152–1159. [CrossRef]

73. Karami, H.; Chidar, E. Pulsed-Electrochemical Synthesis and Characterizations of Magnetite Nanorods. *Int. J. Electrochem Sci.* **2012**, *7*, 2077–2090.

74. Williams, D.N.; Gold, K.A.; Holoman, T.R.P.; Ehrman, S.H.; Wilson, O.C., Jr. Surface modification of magnetic nanoparticles using gum arabic. *J. Nanopart. Res.* **2006**, *8*, 749–753. [CrossRef]

75. Wu, C.-C.; Chen, D.-H. Facile green synthesis of gold nanoparticles with gum arabic as a stabilizing agent and reducing agent. *Gold Bull.* **2010**, *43*, 234–240. [CrossRef]

76. Yang, C.-Y.; Cheng, M.-F.; Tsai, S.-S.; Hung, C.-F. Fluoride in Drinking Water and Cancer Mortality in Taiwan. *Environ. Res.* **2000**, *82*, 189–193. [CrossRef] [PubMed]

77. Cole, A.J.; David, A.E.; Wang, J.; Galban, C.J.; Hill, H.L.; Yang, V.C. Polyethylene glycol modified, cross-linked starch coated iron oxide nanoparticles for enhanced magnetic tumor targeting. *Biomaterials* **2011**, *32*, 2183–2193. [CrossRef] [PubMed]

78. Kumagai, M.; Imai, Y.; Nakamura, T.; Yamasaki, Y.; Sekino, M.; Ueno, S.; Hanaoka, K.; Kikuchi, K.; Nagano, T.; Kaneko, E.; et al. Iron hydroxide nanoparticles coated with poly(ethylene glycol)-poly(aspartic acid) block copolymer as novel magnetic resonance contrast agents for in vivo cancer imaging. *Colloids Surf. B* **2007**, *56*, 174–181. [CrossRef] [PubMed]

79. Yang, D.P.; Gao, F.; Cui, D.X.; Yang, M. Microwave Rapid Synthesis of Nanoporous Fe3O4 Magnetic Microspheres. *Curr. Nanosci.* **2009**, *5*, 485–488. [CrossRef]

80. *Origin 2020b*; OriginLab Corporation: Northampton, MA, USA, 2020.

81. Unlu, C.G.; Kaynar, M.B.; Simsek, T.; Tekgul, A.; Kalkan, B.; Ozcan, S. Structure and magnetic properties of (La1-xFex)FeO3(x = 0, 0.25, 0.50) perovskite. *J. Alloy. Compd.* **2019**, *784*, 1198–1204. [CrossRef]

82. Rietveld, H. A profile refinement method for nuclear and magnetic structures. *J. Appl. Crystallogr.* **1969**, *2*, 65–71. [CrossRef]

83. *HighScore Plus Program, Version 4.1*; PANalytical: Almelo, The Netherlands, 2014.

84. Cambier, P. Infrared study of goethites of varying crystallinity and particle size 1: Interpretation of OH and lattice vibration frequencies. *Clay Miner.* **1986**, *21*, 191–200. [CrossRef]

85. Wang, Y.S.; Muramatsu, A.; Sugimoto, T. FTIR analysis of well defined α-Fe$_2$O$_3$ particles. *Colloids Surf. A* **1998**, *134*, 281–297. [CrossRef]

86. Hill, R.J.; Howard, C.J. Quantitative phase analysis from neutron powder diffraction data using the Rietveld method. *J. Appl. Crystallogr.* **1987**, *20*, 467–474. [CrossRef]

87. Young, R.A.; Prince, E.; Sparks, R.A. Suggested guidelines for the publication of Rietveld analyses and pattern decomposition studies. *J. Appl. Crystallogr.* **1982**, *15*, 357–359. [CrossRef]

88. Atyam, K.K.; Ghosh, A.; Mukherjee, K.; Majumder, S.B. Hematite iron oxide nano-particles: Facile synthesis and their chemi-resistive response towards hydrogen. *Mater. Res. Express* **2015**, *2*, 7. [CrossRef]

Article 3

A. Paut, A. Prkić, I. Mitar, L. Guć, M. Marciuš, M. Vrankić, S. Krehula, L. Tomaško, The New Ion-Selective Electrodes Developed for Ferric Cations Determination, Modified with Synthesized Al and Fe−Based Nanoparticles, Sensors, 22 (2022), 1; 297, 17.

Author Contributions:

Conceptualization; Ante Prkić and Ivana Mitar

Methodology; Ante Prkić, Ivana Mitar, Marijan Marciuš, Stjepko Krehula, and Martina Vrankić

Software; Andrea Paut, Marijan Marciuš, Lucija Guć, and Martina Vrankić

Validation; Andrea Paut

Formal analysis; Andrea Paut and Lara Tomaško

Investigation; Ante Prkić, Ivana Mitar, Andrea Paut, Lucija Guć, and Lara Tomaško

Resources; Ante Prkić

 Data curation; Andrea Paut, Marijan Marciuš and Martina Vrankić

Writing-original draft preparation; Andrea Paut

Writing-review and editing; Ante Prkić, Andrea Paut, Ivana Mitar, Lucija Guć, Marijan Marciuš, Stjepko Krehula, and Martina Vrankić

Visualization; Andrea Paut, Lucija Guć, Marijan Marciuš, and Martina Vrankić

Supervision; Ante Prkić and Ivana Mitar

Project administration; Ante Prkić and Stjepko Krehula

Funding acquisition; Ante Prkić and Stjepko Krehula

Article

The New Ion-Selective Electrodes Developed for Ferric Cations Determination, Modified with Synthesized Al and Fe−Based Nanoparticles

Andrea Paut [1], Ante Prkić [1,*], Ivana Mitar [2], Lucija Guć [1], Marijan Marciuš [3], Martina Vrankić [4] and Stjepko Krehula [3] and Lara Tomaško [1]

1   Faculty of Chemistry and Technology, University of Split, Ruđera Boškovića 35, 21000 Split, Croatia; andrea.paut@ktf-split.hr (A.P.); lguc@pmfst.hr (L.G.); laratomasko6@gmail.com (L.T.)
2   Faculty of Science, University of Split, Ruđera Boškovića 33, 21000 Split, Croatia; imitar@pmfst.hr
3   Division of Materials Chemistry, Ruđer Bošković Institute, Bijenička cesta 54, 10000 Zagreb, Croatia; marijan.marcius@irb.hr (M.M.); krehul@irb.hr (S.K.)
4   Division of Materials Physics and Center of Excellence for Advanced Materials and Sensing Devices, Ruđer Bošković Institute, Bijenička cesta 54, 10000 Zagreb, Croatia; martina.vrankic@irb.hr
*   Correspondence: prkic@ktf-split.hr; Tel.: +385-21-329-462

Abstract: The solid-state ion-selective electrodes presented here are based on the $FePO_4$:Ag_2S:poly-tetrafluoroethylene (PTFE) = 1:1:2 with an addition of (0.25–1)% microwave-synthesized hematite (α-Fe_2O_3), magnetite (Fe_3O_4), boehmite [γ-AlO(OH)], and alumina (Al_2O_3) nanoparticles (NPs) in order to establish ideal membrane composition for iron(III) cations determination. Synthesized NPs are characterized with Fourier-Transform Infrared (FTIR) spectroscopy, Powder X-Ray Diffraction (PXRD), and Scanning Electron Microscopy (SEM) with Energy Dispersive Spectroscopy (EDS). The iron oxides NPs, more specifically, magnetite and hematite, showed a more positive effect on the sensing properties than boehmite and alumina NPs. The hematite NPs had the most significant effect on the linear range for the determination of ferric cations. The membrane containing 0.25% hematite NPs showed a slope of -19.75 mV per decade in the linear range from $1.2 \cdot 10^{-6}$ to 10^{-2} mol L^{-1}, with a correlation factor of 0.9925. The recoveries for the determination of ferric cations in standard solutions were 99.4, 106.7, 93.6, and 101.1% for different concentrations.

Keywords: potentiometry; nanoparticles; microwave synthesis; iron(III) cations

1. Introduction

The electroanalytical methods, with emphasis on ion-selective electrodes, are one of the most rapidly developing detection methods due to the wide range of applications and meet the requirements of sensitivity, selectivity, small size, ease of use, portability, timeliness, and low cost. Ion-selective electrodes can determine the exact concentration of the analyte over a wide concentration range, allowing the use of a single method to determine the analyte in a variety range of samples without pretreatment of the sample matrix [1,2]. Nanotechnology, i.e., the synthesis and usage of nanomaterials such as nanotubes, nanowires, nanofibers, nanorods, NPs, nanocomposites, and other nanostructures, has recently emerged as one of the most exciting and rapidly developing areas of analytical and electroanalytical chemistry. Various nanomaterials, especially NPs with different properties, have found a wide application in many types of electrochemical sensors [3,4]. An application of nanomaterials in chemosensors and biosensors is based on their specific properties, especially the large surface-to-volume ratio, which favors stronger interaction with analytes when nanostructures are part of the surface layer, as well as their good conductivity, electrocatalytic activity, and high mechanical strength [5]. The performance of sensor modification with NPs includes: (i) nanomaterials as solid contacts in solid-state ion-selective electrodes, (ii) nanomaterials (or ionophore-modified nanomaterials) dispersed

in ion-selective electrodes, and (iii) nanomaterial-based biosensors [4]. The metal oxide NPs are widely used as sensor and biosensor modifications thanks to their catalytic and conductive properties and their ability to roughen the conductive sensor interface. This particular area of scientific research is constantly evolving [6,7]. Some of the properties of these NPs depend mainly on their size, which can be controlled by different synthesis methods, at the physical or chemical level [8]. Namely, numerous metal oxide NPs, i.e., manganese [9,10], titanium [11], zinc [12–14], cobalt [15], nickel [16], and iron oxides [13] have been used in electrode modification processes.

Due to their biocompatibility and non-toxicity, the iron oxide NPs occupy a special place in improving the properties of electrochemical sensors. Moreover, these NPs are easy to produce and offer a wide range of biomedical applications, especially hematite and magnetite [1,6]. The iron oxide NPs are used as sensor modifiers for the determination of various analytes, such as hydrogen peroxide [17], glucose [18], Pb, Zn, Cd [19], Cl [13], F [20], nitrites [21] and some organic compounds [22–24]. The technology of iron oxide NPs synthesis has been highly developed and brought to a level where it is possible to obtain the desired phase and size of NPs by defining the synthesis process [25].

Although boehmite and alumina NPs are not so commonly used as electrochemical modifiers, the nanoporous electrochemical sensors based on alumina membranes have been recently used as biosensors. These types of modified sensors are used to detect viruses, proteins, and pathogens with exceptional sensitivity [26].

Iron is recognized as an essential nutritional element for all life forms. It is found as a cofactor in various enzymes and is very important for oxygen transport and electron transfer in the human body. Although the daily requirement of iron for humans is set at 8–18 mg, iron has been found to be toxic in an excessive concentration due to its pro-oxidant activity. Accordingly, it can be concluded that iron can be both essential and toxic to human health depending on the concentration [27]. Due to these facts, it is extremely important to develop a new, simple, relatively fast, inexpensive, and reliable method for the determination of iron content in food products, beverages, and food supplements.

Among different types of potentiometric sensors used for ferric cations determination, most of them are based on conductive polymers [28–35], carbon materials electrodes [36,37], and to a small extent with those based on iron salts [38]. Silver sulfide was used as a conductor in Ref. [38], where ferric cations were incorporated in membrane composition, unlike the Ref. [39] where Ag_2S-CuS mixture was used.

In this work, we investigate which type of NPs is the best suited to improve the detection properties of the ion-selective electrode for iron(III) cations. The miniaturized electrode based on the ferric phosphate ($FePO_4$), Ag_2S, and PTFE described in previous work [40] was modified with the hematite, magnetite, boehmite, and alumina oxide NPs, and their influence on the detection limit and sensitivity of the electrode was studied. Ferric-selective electrodes constructed from sparingly soluble salts that had been reported before showed linearity ($1 \cdot 10^{-5}$–$1 \cdot 10^{-2}$) mol L^{-1} [38,39] with a limit of detection of $5.1 \cdot 10^{-6}$ mol L^{-1} [38]. The synthesis process of hematite NPs used for electrode modification is described in detail in [25], while the synthesis of magnetite, boehmite, and alumina NPs is presented below. This work, with a detailed description of synthesized NPs as modifications for the ion-selective electrodes, is a great step forward compared to previous research.

Ion-selective electrodes are often modified with different types of metal nanomaterials, which is a combination of the simplicity of the potentiometric technique with the improvement of the sensor properties by their modernization with nanostructured materials, thus combining the advantages of these two scientific fields, which is the object of our research and thus, this paper.

2. Materials and Methods

2.1. Al and Fe-Based NPs Synthesis

All solutions used for the NPs synthesis were prepared by dissolving a precisely weighed mass of a required solid chemical in ultrapure water that was prepared using

the Millipore Simplicity 185 purification system (Millipore, Burlington, MA, USA) with a resistivity of 18.2 MΩ cm^{-1} at 25 °C. Mixtures of the corresponding chemicals were prepared at room temperature (RT) in plastic cuvettes and, after mixing, transferred to a non-stirred Milestone Teflon-lined pressure vessel (vessel volume up to 100 mL; maximum pressure of 100 bar and temperature of 300 °C). The samples were heated in a microwave oven (Milestone flexiWave SK15, Milestone, S.r.l., Sorisole, Italy) equipped with the ATC 400 sensor. The ATC sensor allows direct temperature control via microwave transparent fiber optic sensor up to 300 °C; magnetron frequency 2450 MHz; magnetron power 2 × 950 Watt; power supply 230 V, 50–60 Hz,) at the prevailing temperature according to a microwave oven program with the rotor turned on and continuous microwave emission at 800 W. After the reaction time, the obtained precipitates were centrifuged (Beckman Avanti J-25, Indianapolis, IN, USA) and washed several times with ultrapure water and ethanol. After the first centrifugation cycle, the mother liquor was isolated, and the pH of the solution was measured using a pH meter (MP220 Basic Mettler Toledo, Columbus, OH, USA). All precipitates were dried in a vacuum dryer (Thermo Scientific, 3608–1CE, Waltham, MA, USA) at temperatures that are listed in Table 1. In the case of alumina NPs, the precipitates obtained after the microwave synthesis and vacuum drying were calcined in a furnace (Vulcan A−550).

Table 1. Experimental conditions for boehmite and alumina NPs preparation.

Sample	0.1 M Al$_2$(SO$_4$)$_3$·18H$_2$O (mL)	25% NH$_3$ (mL)	Temperature (°C)	Time (min)	Drying Temperature (°C)	Calcination Temperature (°C)	pH
boehmite	24	~3.7	200	30	100	−	9
alumina	24	~3.7	200	30	100	800	9

Boehmite and alumina NPs were synthesized using the apparatus previously described under the conditions summarized in Table 1. The boehmite NPs were prepared using Al$_2$(SO$_4$)$_3$·18H$_2$O, p.a. (VWR chemicals, Radnor, PA, USA), dissolved in ultrapure water. The 24 mL of the prepared solution was placed in a plastic cuvette and mixed with ammonia (NH$_3$, 25%, p.a., Gram mol, Zagreb, Croatia) was to tune the pH to 9. After mixing the reactants, white milky precipitates were obtained. The reaction mixture was placed in the microwave Teflon vessel and exposed to 200 °C for 30 min. The precipitates were centrifuged and washed with ultrapure water and ethanol and dried in a vacuum at 100 °C for 20 h. On the other hand, the alumina NPs were prepared by calcination at 800 °C for 4 h.

The synthesis of hematite NPs incorporated in different proportions into the MN1, MN2, and MN3 ion-selective membranes is described in detail in Ref. [25]. The magnetite NPs are synthesized by mixing iron(II) chloride tetrahydrate (FeCl$_2$·4H$_2$O, p.a., 0.7952 g, VWR chemicals, Radnor, PA, USA), anhydrous iron(III) chloride (FeCl$_3$, p.a., 8 mL, 1 mol L^{-1}, Fluka, Charlotte, NC, USA), and ammonia (NH$_3$, 25%, p.a., 5.4 mL, Gram mol, Zagreb, Croatia). The mixed solution was then transferred to a Teflon vessel and heated up to 200 °C for 10 min. After cooling, the precipitates were centrifuged and washed with ultrapure water and ethanol. The synthesis conditions are summarized in Table 2.

Table 2. Experimental conditions for magnetite NPs preparation.

Sample	1 M FeCl$_3$ (mL)	25% NH$_3$ (mL)	FeCl$_2$·4H$_2$O (g)	Temperature (°C)	Time (min)	Drying Temperature (°C)	pH
magnetite	8	~5.4	0.792	200	10	60	8.7

2.2. Ion-Selective Membranes

The main components of the ion-selective electrode presented in this work, i.e., ferric phosphate ($FePO_4$), silver sulfide (Ag_2S) and 4 different types of NPs, were preproduced or synthesized in our laboratory. The procedure for the preparation of $FePO_4$, and Ag_2S was described in detail in previous work [40]. The $FePO_4$, Ag_2S, Al, and Fe-based NPs, polytetrafluoroethylene (PTFE, p.a.) (Alfa Aesar, Haverhill, MA, USA) were weighted and pressed under 625 MPa for 2 h to form membranes weighing 500 mg with a 10 mm in diameter. Once the membrane was prepared, it was inserted into the electrode body and ultimately tested. The electrode body used in this work and represented in [40] was made of an epoxy plate with the cooper layer responsible for charge transfer between the membrane and cable connected to the millivoltmeter. Contact between the membrane and the copper layer was ensured with a conductive graphite adhesive. The copper layer was protected with a non-conductive varnish to avoid the influence of the testing solution. The composition of 12 different membranes, with indicated percentages for every component regarding total membrane mass, is shown in Table 3.

Table 3. Composition of the membranes for the determination of the ferric cation.

Membrane	Membrane Mixture Composition (%)						
	FePO$_4$	Ag$_2$S	PTFE	NP Type			
				Hematite	Magnetite	Alumina	Boehmite
MN1	25	25	50	0.25			
MN2	25	25	50	0.5			
MN3	25	25	50	1			
MN4	25	25	50		0.25		
MN5	25	25	50		0.5		
MN6	25	25	50		1		
MN7	25	25	50			0.25	
MN8	25	25	50			0.5	
MN9	25	25	50			1	
MN10	25	25	50				0.25
MN11	25	25	50				0.5
MN12	25	25	50				1

Membranes presented in Table 3 were tested in ferric nitrate nonahydrate [$Fe(NO_3)_3 \cdot 9H_2O$, p.a.), (VWR chemicals, Radnor, PA, USA), solution at pH of 1 and 5. The pH value 1 was adjusted with nitric acid (HNO_3, p.a. Merck, KGaA, Darmstadt, Germany), while pH value 5 with acetic buffer prepared by mixing sodium acetate (CH_3COONa, p.a., Kemika, Zagreb, Croatia) and acetic acid (CH_3COOH, p.a., VWR chemicals, Radnor, PA, USA). As it was reported before, membranes with $FePO_4$, Ag_2S, and PTFE composition showed the best response at pH = 1 [40], and ferric selective electrodes modified with nanoparticles of iron oxides showed the best response at pH = 5 [20]. The tests were carried out at RT. Additionally, the possibility of quantitative application for some sensors was tested in standard solution (BDH chemicals, VWR 455532A iron standard solution for ICP, p.a., Radnor, PA, USA). The reference electrode used in potentiometric measurements was a double junction silver/silver chloride (Ag/AgCl) electrode (Reference plus, Mettler Toledo, Columbus, OH, USA). Both electrodes were immersed in the testing solution, which was positioned on a magnetic stirrer (Heildoph MR 300, Schwabach, Germany). The potential change was recorded by a millivoltmeter (SevenExcellence, Mettler Toledo, Columbus, OH, USA).

2.3. Characterization

The Al and Fe-based NPs were characterized by FTIR spectroscopy (Shimadzu IR Prestige−21, FTIR-8400S spectrophotometer, Kyoto, Japan) and PXRD measurements (Empyrean X-ray diffractometer with Cu Kα1 radiation, λ = 1.5406 Å, Malvern Panalytical

Ltd. Malvern, Worcestershire, UK). Samples were scanned over a 2θ range between 10° and 75° with a scan step of 0.013°. Crystallite size information was extracted from the phase fitting method based on the change in profile widths compared to a standard sample. For insight into nanoparticles morphology, thermal field-emission scanning electron microscope ((FE-SEM), model JSM-7000F, manufactured by Jeol Ltd., Tokyo, Japan) was used, while the composition of the samples was checked with an energy dispersive spectrometer (EDS, model Oxford Inca 350, manufactured by Oxford Instruments, Abingdon, UK)

3. Results and Discussion

3.1. Bohemite NPs

The FTIR spectra of boehmite NPs is shown in Figure 1. The intense peaks located at 3308 and 3088 cm^{-1} originate from the O−H stretching, while the peak positioned at 1630 cm^{-1} indicates the presence of adsorbed water [41]. Peaks at 1067 cm^{-1} and 1159 cm^{-1} were characteristic for the symmetric and asymmetric Al−O−H bending, respectively, while the Al−O vibrations were located at 737, 610, and 476 cm^{-1} [42].
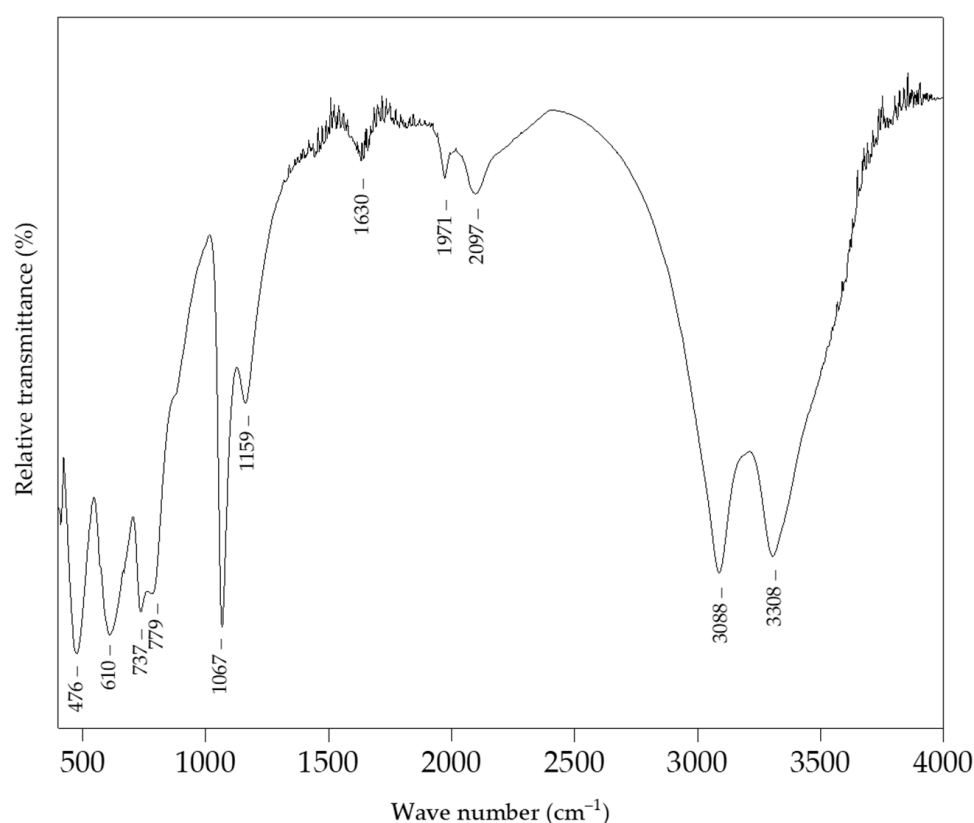
Figure 1. The FTIR spectrum of boehmite NPs.

A single-phase PXRD pattern of boehmite preserves the crystal structure of orthorhombic γ-AlO(OH) exclusively with *Cmcm* space group [43] symmetry (a = 2.8612(6) Å, b = 12.244(7) Å, c = 3.6841(8) Å, and V = 129.06(8) Å^3, R_{wp} = 7.31%) as indicated from the FTIR analysis and Rietveld refinement (see Figure 2). The value of the crystallite size obtained from the line-broadening analysis performed during the Rietveld structure refinements at RT was 11.7(1) nm.

Figure 3a,b shows SEM images of boehmite NPs. Magnifications from 20,000× up to 33000× are represented and nanosized, (<20 nm in diameter), needle-shaped particles are visible under higher magnifications [44,45].
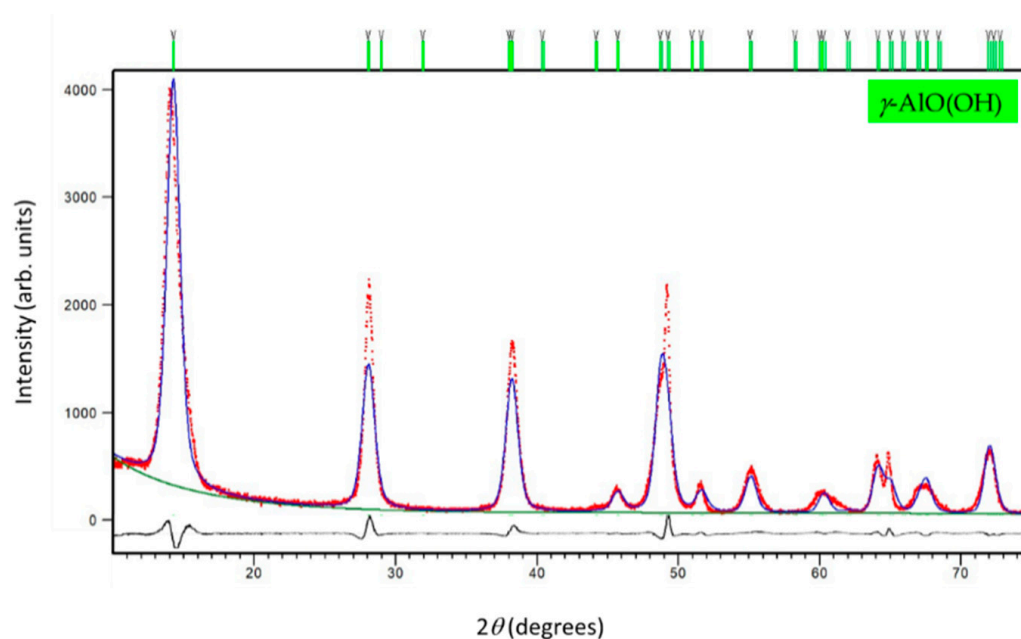
Figure 2. The final observed (red dots), calculated (blue solid line), and difference (black solid line) PXRD profiles of boehmite NPs at RT. The fitted background contribution is represented by the lower green solid line. The upper green tick marks show the reflection positions of the orthorhombic γ-AlO(OH) phase.
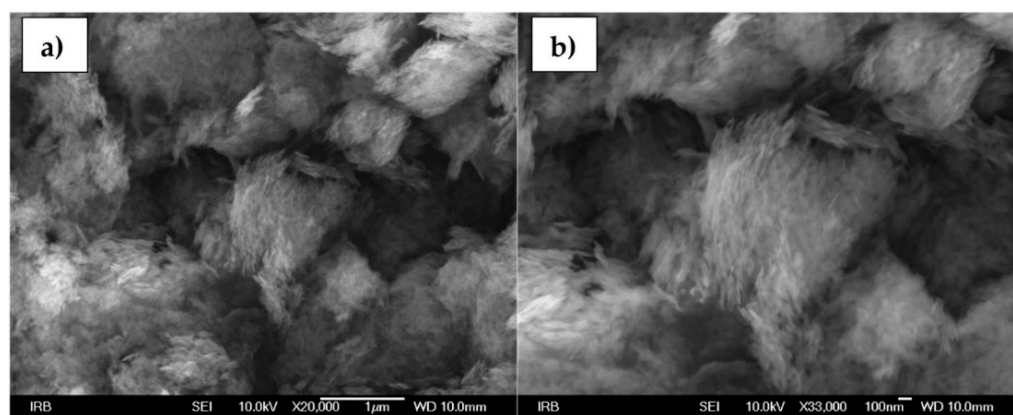

Figure 3. SEM images of boehmite NPs at (**a**) 20,000× and (**b**) 33,000× magnification.

Figure 4 represents EDS data of boehmite NPs. The atomic ratio of 32% Al and 68% O matches for γ-AlO(OH) particles.

3.2. Alumina NPs.

The FTIR spectra of the alumina NPs (Figure 5) show the presence of adsorbed water, as indicated by peaks located at 3451 cm^{-1} and 1630 cm^{-1}. The characteristic peak at 1115 cm^{-1} can be attributed to the Al−O bond stretching. The peaks at 745 cm^{-1} and 554 cm^{-1} were attributed to the symmetric stretching and bending vibrations of the Al−O−Al bond, respectively [46].

The PXRD pattern (Figure 6) of the alumina sample shows an indication of the hexagonal Al_2O_3 formation. Undoubtedly, X-ray diffraction indicates the appearance of an amorphous phase and a rather poor crystallinity of this sample.
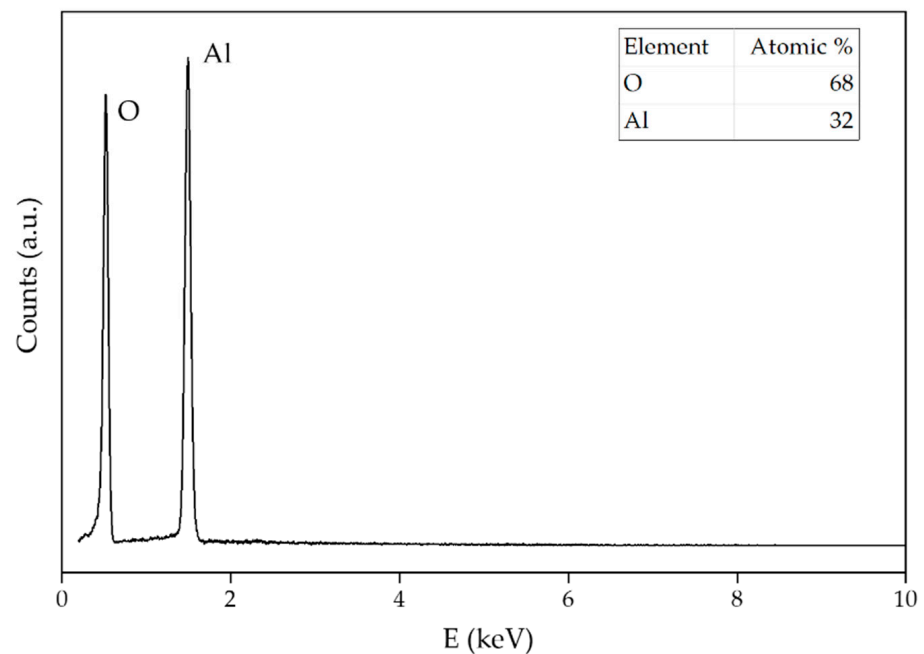
Figure 4. The EDS pattern of boehmite NPs. The results of the element analysis are shown in the inset.
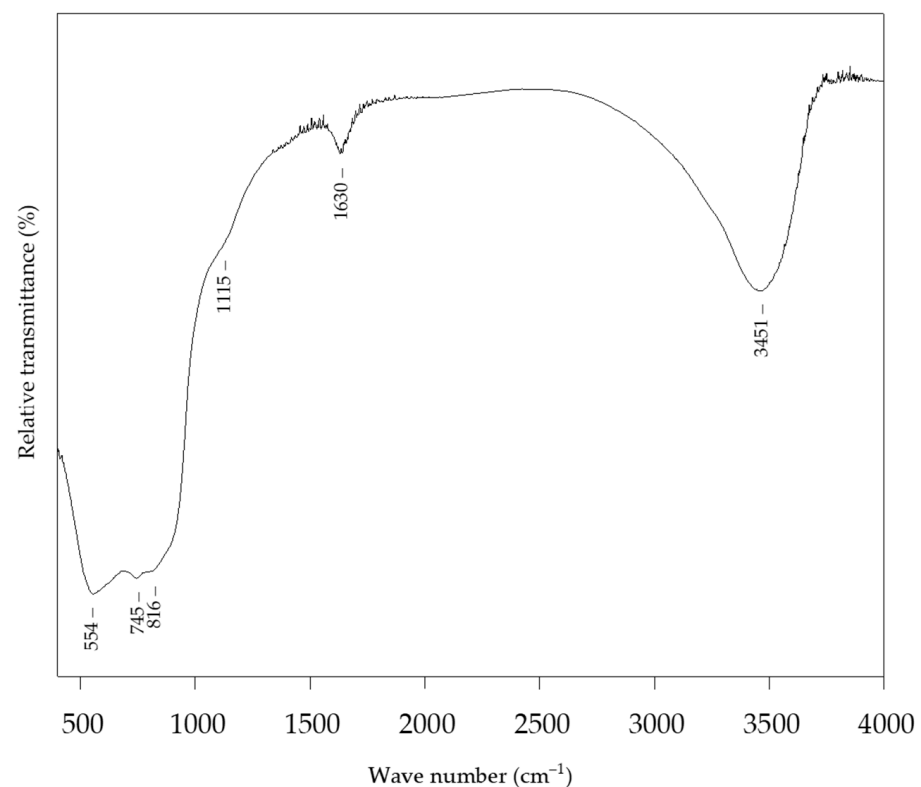
Figure 5. FTIR spectrum of alumina NPs.

The morphology of alumina NPs is shown in Figure 7a,b. Under a high magnification of 50,000×, as with the boehmite NPs, a needle-like structure is visible for the alumina NPs as well.

The EDS spectrum of alumina NPs (Figure 8) shows a stoichiometric Al/O ratio almost ideal for alumina. The absence of any other element besides aluminum and oxygen proves sample purity.
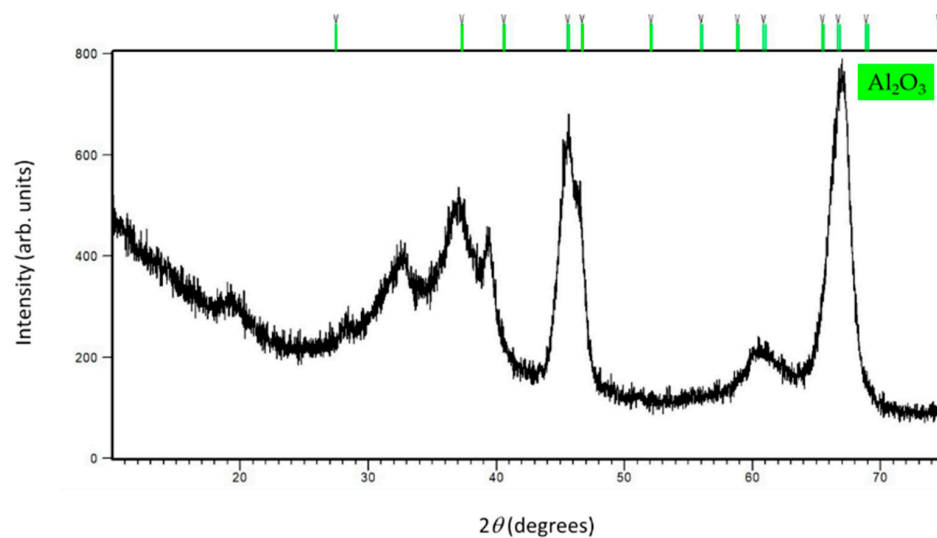
Figure 6. The final observed PXRD profile of alumina NPs at RT. The upper green tick marks show the reflection positions of the hexagonal Al_2O_3 phase formation.
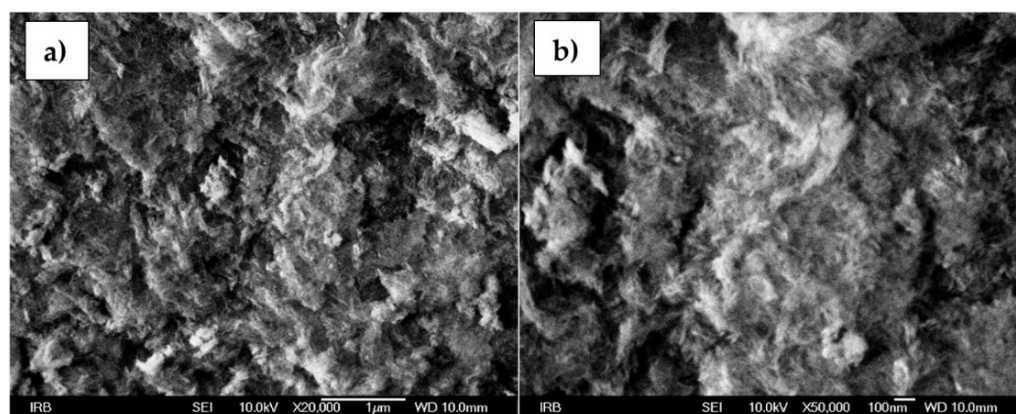
Figure 7. SEM images of alumina NPs at (**a**) 20,000× and (**b**) 50,000× magnification.
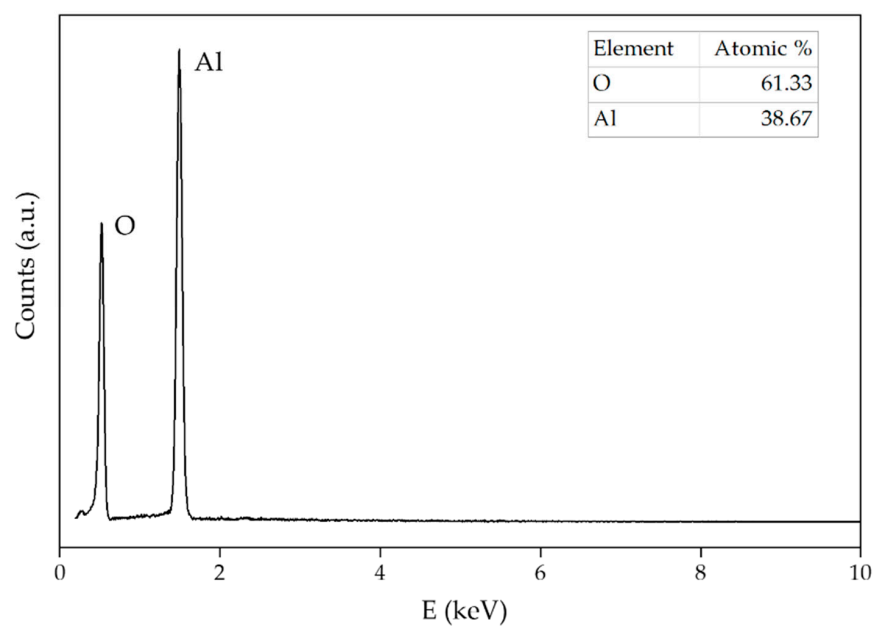
Figure 8. EDS pattern of alumina NPs. The results of the element analysis are shown in the inset.

3.3. Magnetite NPs

The FTIR spectrum of magnetite NPs is shown in Figure 9, indicating a characteristic Fe−O stretching vibration located at 571 cm^{-1} [47].
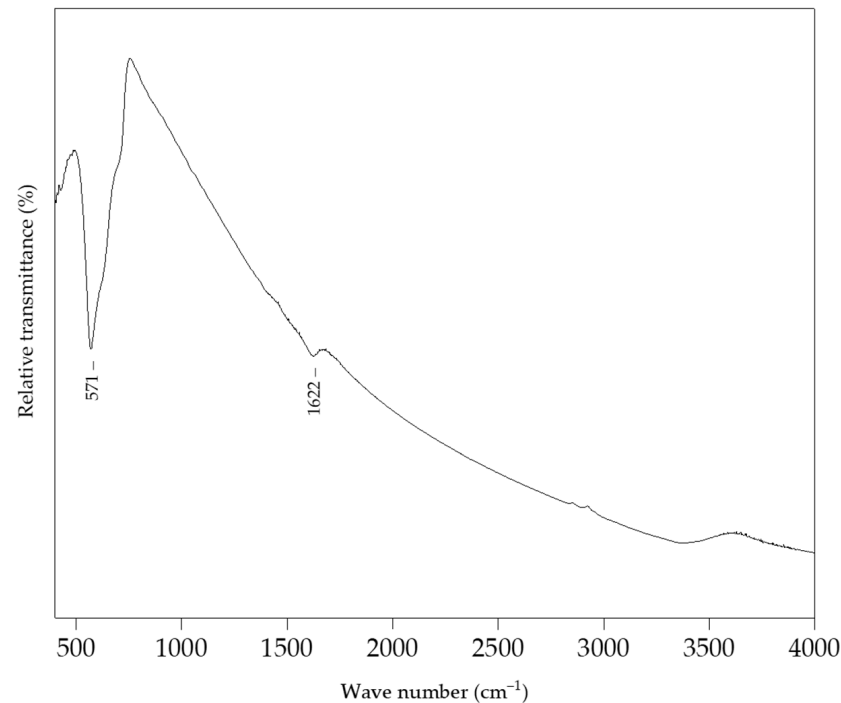
Figure 9. FTIR spectrum of magnetite NPs.

The PXRD pattern of magnetite NPs confirmed a formation of the phase pure sample. As obtained from the Rietveld structure refinement at RT (see Figure 10), the unit cell metrics was assigned to cubic Fe$_3$O$_4$ symmetry [48] (s. g. *Fd-3m*, a = 8.357(1) Å, V = 583.56 Å3, R_{wp} = 5.32%). The crystallites of 14.2(1) nm were calculated to form the line-broadening analysis.
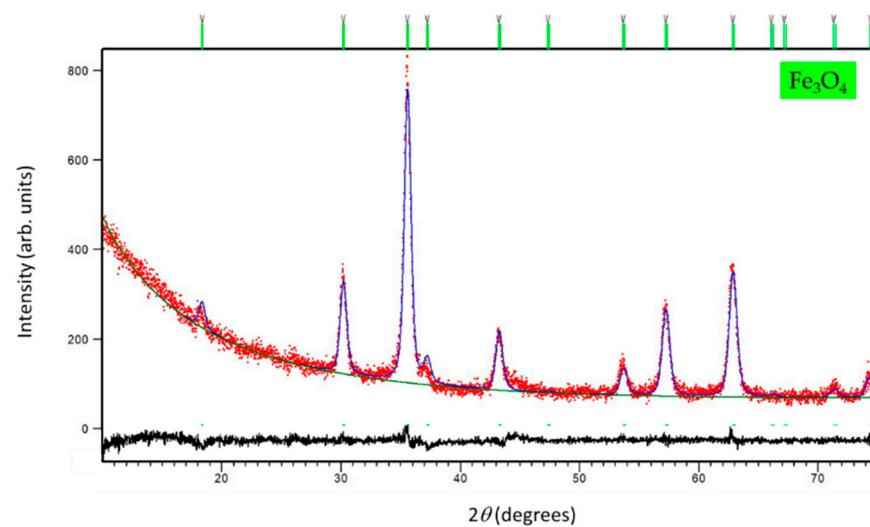
Figure 10. The final observed (red dots), calculated (blue solid line) and difference (black solid line) PXRD profiles of magnetite NPs at RT. The fitted background contribution is represented by the lower green solid line. The upper green tick marks show the reflection positions of the cubic Fe$_3$O$_4$ phase.

Figure 11a,b shows SEM images of magnetite NPs. Irregularly shaped aggregates are visible on SEM micrographs of magnetite. The individual magnetite nanoparticles within the aggregates are smaller than 20 nm.
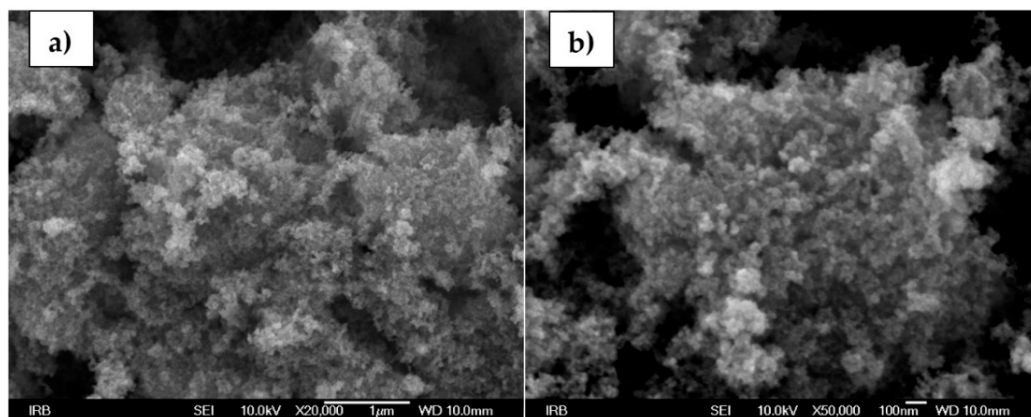

Figure 11. SEM images of magnetite NPs at a (**a**) 20,000× and (**b**) 50,000× magnification.

The EDS spectra of magnetite NPs (Figure 12), apart from the ideal ratio of iron and oxygen for this type of NPs, do not show the presence of any impurities. The atomic ratio for magnetite NPs was 54.82% of oxygen and 45.18% of iron.
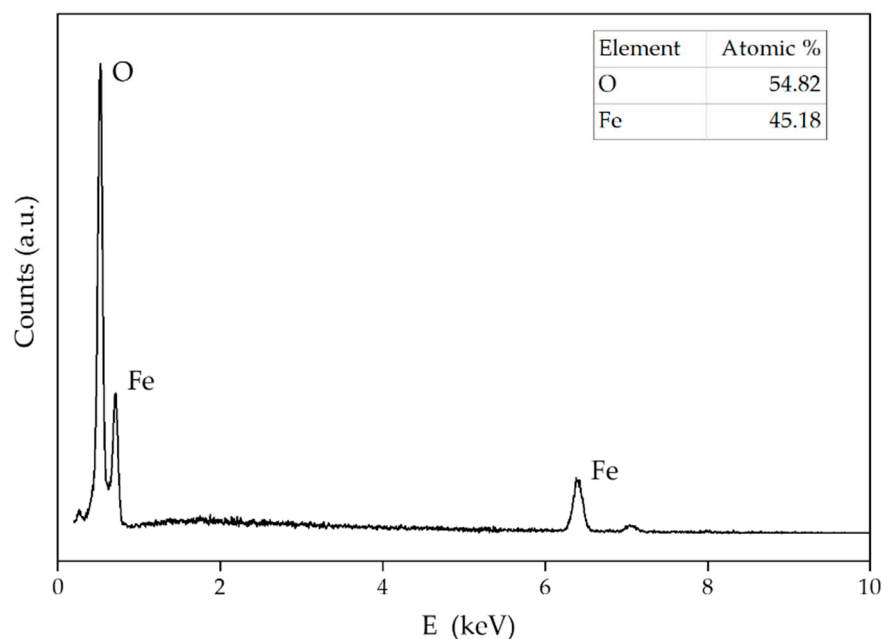

Figure 12. EDS pattern of magnetite NPs. The results of the element analysis are shown in the inset.

Hematite NPs complete characterization is reported in Ref. [25].

3.4. Membranes with Alumina, Boehmite, Magnetite and Hematite NPs

The response of a solid-state ion-selective electrodes is generally based on ion exchange processes occurred between the solution phase and the solid phase of the sensor. Since the membranes presented in this paper contain iron(III) phosphate, the reaction that takes place on the surface of the membrane is:

$$Fe^{3+}{}_{(aq)(solution)} + PO_4{}^{3-}{}_{(aq)(membrane)} \rightleftarrows Fe(PO_4)_{(s)} \tag{1}$$
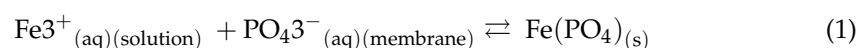
Table 4 summarizes the most important features of membranes with the addition of aluminum oxide and boehmite NPs in different percentages according to total membrane mass. Results obtained for MN7 and MN8 membranes are from tests under strongly acidic conditions (pH = 1), while results for MN10 were obtained under weakly acidic conditions (pH = 5). The calibration curves for MN7, MN8, and MN10 membranes are represented in Figure 13.

Table 4. Test results using membranes modified with boehmite and alumina NPs.

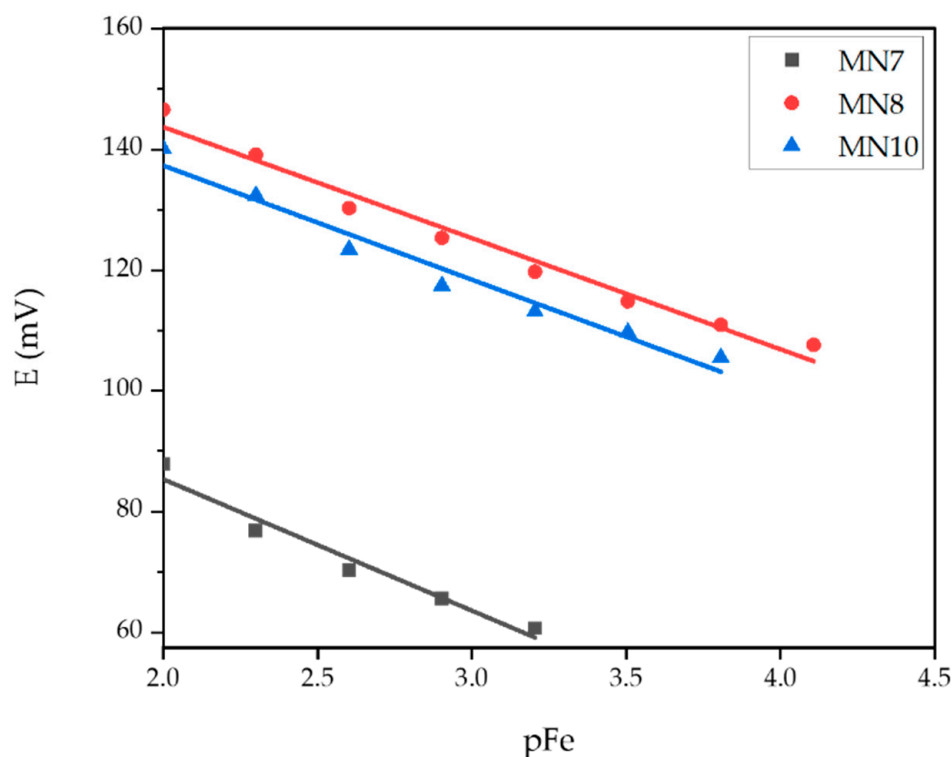| Membrane	Slope (mV dec^{-1})	Linear Range (mol L^{-1})	LOD (mol L^{-1})	R^2
MN7	−21.73	$6.25 \cdot 10^{-4}$–$1 \cdot 10^{-2}$	$2.66 \cdot 10^{-4}$	0.9635
MN8	−18.37	$7.81 \cdot 10^{-5}$–$1 \cdot 10^{-2}$	$4.87 \cdot 10^{-5}$	0.9774
MN10	−18.86	$1.56 \cdot 10^{-4}$–$1 \cdot 10^{-2}$	$8.38 \cdot 10^{-5}$	0.9674

Figure 13. Potential change dependence of pFe evaluated for MN7, MN8, and MN10 membranes.

The MN7 membrane with an addition of 0.25% alumina NPs showed a linear response to ferric cations in Fe(NO$_3$)$_3$ solution at pH 1. The recorded slope was −21.73 mV per decade with a correlation factor of 0.9635. The addition of a larger amount of alumina NPs in the MN8 membrane (0.5%) had a positive effect on extending the linearity range of the membrane. Accordingly, the linearity of this membrane was measured in a concentration range from $7.81 \cdot 10^{-5}$ mol L^{-1} to $1 \cdot 10^{-2}$ mol L^{-1}. The slope obtained in the mentioned concentration range was −18.75 mV per decade with a correlation factor of 0.9774. Therefore, it is obvious that the increased content of alumina NPs had a positive effect on the membrane properties, considering the increase of the linear dynamic range for the whole decade as well as the sensitivity. The membranes MN7 and MN8 did not show significant results at pH 5. On the other hand, the MN10 membrane with an addition of 0.25% boehmite NPs showed linearity in the determination of ferric cations in the concentration range of $1.56 \cdot 10^{-4}$–$1 \cdot 10^{-2}$ mol L^{-1} with a slope of −18.86 mV per decade and a correlation factor of 0.9674, while tested in acetic buffer at pH 5. The detection limit for this membrane

was $8.38 \cdot 10^{-5}$ mol L^{-1}. Since the ideal slope for the determination of trivalent cations according to the Nernst equation was -19.73 mV per decade, the slopes obtained with the membranes MN7, MN8, and MN10 agreed quite well with the theoretical requirements.

A summary of test results for membranes containing iron oxide NPs is given in Table 5. The membranes were tested in a precisely prepared Fe(NO$_3$)$_3$ $\cdot$9H$_2$O solution at pH 1 and 5. The calibration curves for MN1, MN2 (pH = 5), and MN4 (pH = 1) membranes are shown in Figure 14.

Table 5. Test results using membranes modified with magnetite and hematite NPs.

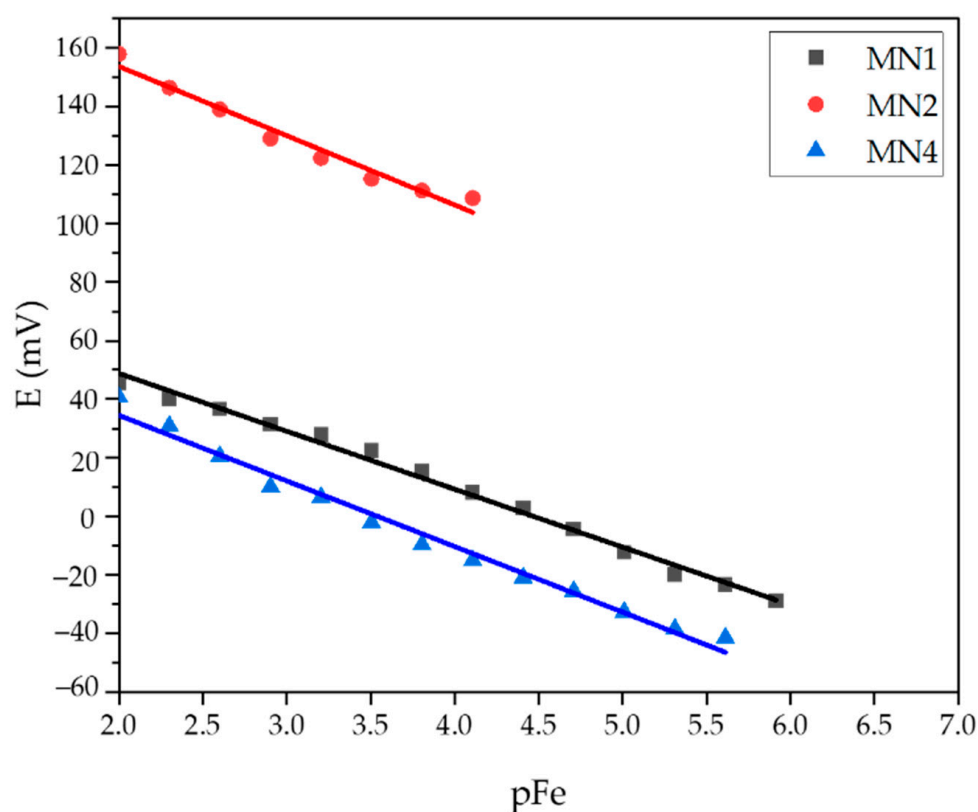| Membrane	Slope (mV dec^{-1})	Linear Range (mol L^{-1})	LOD (mol L^{-1})	R^2
MN4	-22.38	$2.44 \cdot 10^{-6}$–$1 \cdot 10^{-2}$	$1.85 \cdot 10^{-6}$	0.9853
MN1	-19.75	$1.22 \cdot 10^{-6}$–$1 \cdot 10^{-2}$	$1.01 \cdot 10^{-6}$	0.9925
MN2	$-23,64$	$7.81 \cdot 10^{-5}$–$1 \cdot 10^{-2}$	$4.49 \cdot 10^{-5}$	0.9691

Figure 14. Potential change dependence of pFe evaluated for MN1, MN2, and MN4 membranes.

The MN4 membrane with 0.25% magnetite NPs showed linearity in the determination of iron cations in the concentration range of $2.44 \cdot 10^{-6}$ to 10^{-2} mol L^{-1} with a slope of -22.38 mV per concentration decade and a correlation factor of 0.9853. The detection limit for this membrane was $1.85 \cdot 10^{-6}$ mol L^{-1}. The MN1 and MN2 membranes contained 0.25% and 0.50% hematite NPs, respectively. The MN2 membrane, with 0.50% hematite showed -23.64 mV per decade slope in the range from 7.81×10^{-5} to 10^{-2} mol L^{-1} of ferric cations concentration.

To obtain a better insight into the differences in the values of the limit of determination and the sensitivity between the presented membranes, the results from the tables above are also presented in the comparative bar graph (Figure 15).
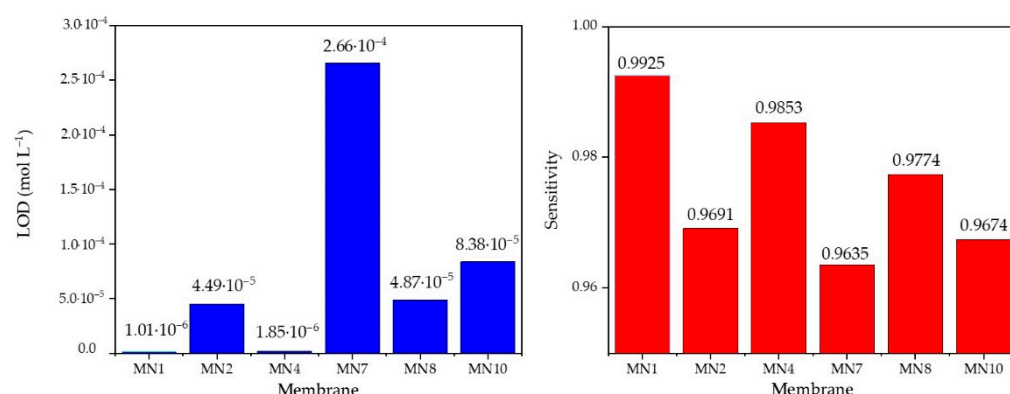
Figure 15. A comparative bar graph for LOD and sesnsitivity values fo MN1, MN2, MN4, MN7, MN8, and MN10 membranes.

When analyzing the data from Table 5, the addition of 0.25% hematite had the greatest effect on the extension of the linear dynamic range of the membrane as well as on the detection limit, which plays an important role in this measurement method. As mentioned before, an ideal theoretical slope for trivalent cations determination was established using the Nernst equation and was −19.3 mV per one concentration decade. Since MN1 membrane has a slope of −19,75 mV per decade, it is obvious that it is an ideal one. The correlation factor was also very close to ideal value (~1) as R^2 = 0.9925. The detection limit of $1.01 \cdot 10^{-6}$ was approximately the lower limit of the potentiometry method. Since the MN1 sensor responded best to the determination of ferric cations, this membrane was verified by the control experiments for the quantitative determination of ferric cations. Table 6 shows the results of the test of MN1 membrane in iron standard (VWR 455532A, BDH chemicals, plasma emission standard) at pH 5 with the calculated values using the calibration curve $E = -19.753pFe + 88.334$ mV obtained just before the test in the standard solution.

Table 6. Test results for MN1 in standard solution for $m(Fe^{3+})$ = 1.1169 mg.

	$m(Fe^{3+})$ = 1.1169 mg; $E_{calc.}$ = 23.1 mV			
	1st Cycle	2nd Cycle	3rd Cycle	Average
$E_{(measured)}$ (mV)	23.3	23.1	22.8	23.07
$m(Fe^{3+})_{measured}$ (mg)	1.1394	1.1169	1.0749	1.1104
recovery (%)	102.01	100	96.2	99.4

The measurements for the same concentration of ferric cations are repeated three times intraday, and the arithmetic middle of these measurements showed a rather high recovery value of 99.4%

After testing in a laboratory prepared $Fe(NO_3)_3$ solution, the MN1 membrane was tested in an iron standard solution using sequential dilution method and obtained calibration curve (Figure 16) was used to verify the possibility of a quantitative application of the proposed membrane (Table 7).

The slope recorded during MN1 testing in iron standard solution was −14.405 mV per decade with 0.9931 correlation factor. The linear range was $2.44 \times 10^{-6} - 10^{-2}$ mol L^{-1} ferric cations concentration.

The high arithmetic recovery values listed in Table 7 confirm the possibility of using the MN1 sensor for the quantitative determination of ferric cations. The lowest recovery value (among arithmetic values of three measurements), obtained for 1.1169 mg of analyte in solution was 93.6%. However, it is also important to consider the reproducibility values in the context of the agreement of the potential of the calculated and measured values. Evidently, the difference of only 0.4 mV between calculated and measured potential change causes 6.4% uncertainty if analyte masses are compared in solution. Thus, there is a big

difference in results interpretation according to ion charge number, and this must be taken into account when considering the effectiveness of a particular sensor. This sensor showed a limited lifetime of approximately one month. During testing processes, the changes in potential as a function of the changing concentration of ferric cations and reading times of potential were recorded. The approximate time for reading was 30 s.
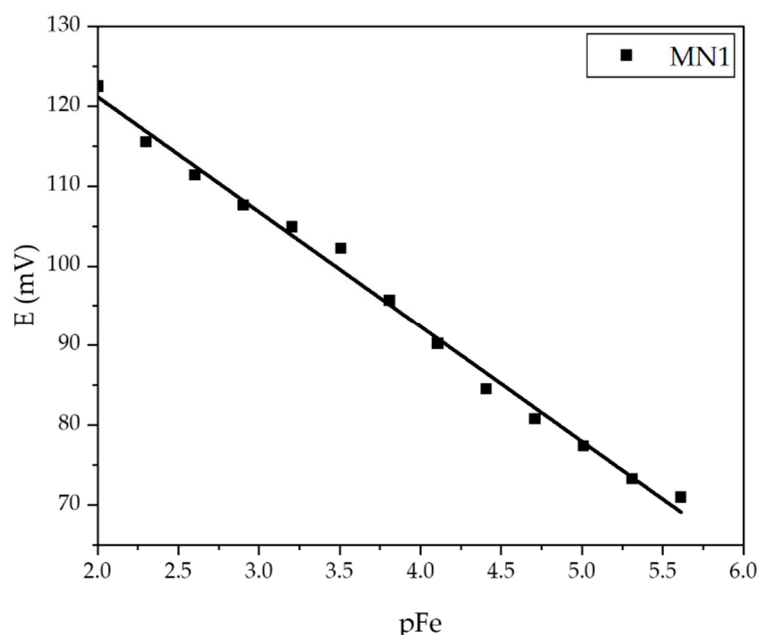

Figure 16. Potential change dependence of pFe evaluated for MN1 membrane in standard solution.

Table 7. Test results for MN1 in standard solution for $m(Fe^{3+})$ = 2.238 mg, $m(Fe^{3+})$ = 1.1169 mg and $m(Fe^{3+})$ = 0.2234 mg.

	$m(Fe^{3+})$ = 2.2338 mg; E_{calc} = 106.8 mV			
	1st Cycle	2nd Cyle	3rd Cycle	Average
$E_{measured}$ (mV)	108	107	106.4	107.1
$m(Fe^{3+})_{measured}$ (mg)	2.7213	2.3193	2.1072	2.3826
recovery (%)	121.8	103.8	94.3	106.7
	$m(Fe^{3+})$ = 1.1169 mg; $E_{calc.}$ = 102.4 mV			
	1st cycle	2nd cycle	3rd cycle	average
$E_{measured}$ (mV)	102.5	102	101.5	102
$m(Fe^{3+})_{measured}$ (mg)	1.1297	1.0429	0.9628	1.0451
recovery (%)	101.1	93.4	86.2	93.6
	$m(Fe^{3+})$ = 0.2234 mg; $E_{calc.}$ = 92.4 mV			
	1st cycle	2nd cycle	3rd cycle	average
$E_{measured}$ (mV)	92.9	92	92.4	92.4
$m(Fe^{3+})_{measured}$ (mg)	0.2435	0.2109	0.2234	0.2259
recovery (%)	109.0	94.4	100	101.1

3.5. Surface of an Ion-Selective Membrane

Figure 17a,b represents the morphology of the tested MN1 sensor. At 500× magnification, a very heterogeneous surface is noticeable, unlike one that could be seen by an eye. Lines visible under 500× magnification are the result of membrane polishing. In addition, the PTFE, since it is an insulator, interfered with the resolution quality when recording large magnifications. Different sizes and particle agglomerations are noticeable at 10,000× magnification.
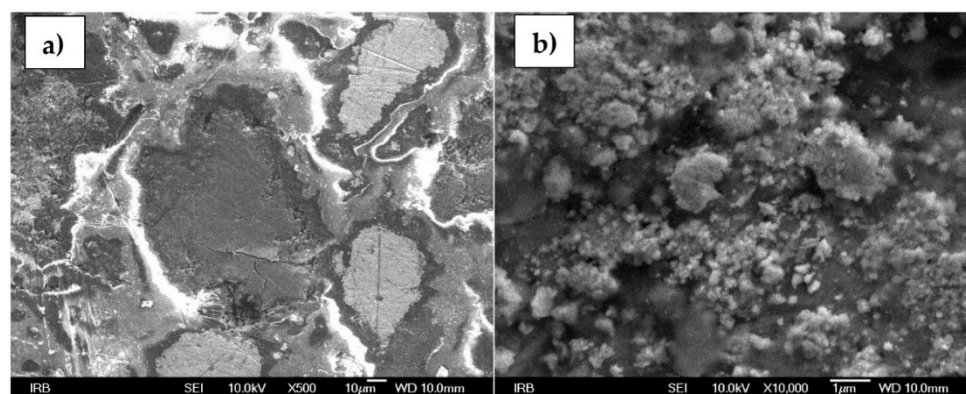
Figure 17. SEM images of MN1 membrane surface at a (**a**) 500× and (**b**) 10,000× magnification.

4. Conclusions

Boehmite and alumina NPs as well as magnetite and hematite, were synthesized under very precise conditions and characterized by FTIR and PXRD followed by Rietveld analysis to determine the structural and microstructural features. Additionally, the samples were characterized by FE-SEM and EDS to determine the shape of the particles. Not only detailed synthesis and characterization of NPs was represented but also the possibility of their application in the modification of the ion-selective electrode. As reported in previous work, membranes with only three main components; $FePO_4$, Ag_2S, and PTFE showed a smaller linear range for ferric cations determination in regard to membranes enriched with specific NPs types. Electrodes with an addition of alumina and boehmite NPs showed less desirable results in comparison to the results obtained when testing sensors were modified with hematite and magnetite NPs. The results of testing the MN1 membrane having composition $FePO_4$:Ag_2S:PTFE = 1:1:2 with the addition of 0.25% hematite NPs, particularly stand out. The slope of -19.75 mV per decade and 0.9925 correlation factor are in almost ideal agreement with the requirements of the Nernstian equation for the ion-selective electrodes for trivalent cations. The detection limit of $1.01 \cdot 10^{-6}$ mol L^{-1} is very close to the lower detection limit of ion-selective electrodes. Recovery values for ferric cations determination were 99.4% for the membrane when calibration curve was performed in $Fe(NO_3)$ $9H_2O$ solution and 106.7%, 93.6%, and 101.1% when calibration curve was performed in standard iron solution. Such high values prove the possibility of quantitative determination of analytes in a wide range of concentrations. The lifetime of sensors was approximately one month with only 30 s of detection time. This way, a new homemade membrane for an ion-selective electrode was constructed and presented.

Author Contributions: Conceptualization, A.P. (Ante Prkić) and I.M.; methodology, A.P. (Ante Prkić), I.M., M.M., S.K. and M.V.; software, A.P. (Andrea Paut), M.M., L.G. and M.V.; validation, A.P. (Andrea Paut); formal analysis, A.P. (Andrea Paut) and L.T.; investigation, A.P. (Ante Prkić), I.M., A.P. (Andrea Paut), L.G. and L.T.; resources, A.P. (Ante Prkić); data curation, A.P. (Andrea Paut), M.M. and M.V.; writing—original draft preparation, A.P. (Andrea Paut).; writing—review and editing, A.P. (Ante Prkić), A.P. (Andrea Paut), I.M., L.G., M.M., S.K. and M.V.; visualization, A.P. (Andrea Paut), L.G., M.M. and M.V.; supervision, A.P. (Ante Prkić) and I.M.; project administration, A.P. (Ante Prkić) and S.K.; funding acquisition, A.P. (Ante Prkić) and S.K. All authors have read and agreed to the published version of the manuscript.

Institutional Review Board Statement: Not applicable.

Informed Consent Statement: Not applicable.

Data Availability Statement: Not applicable.

References

1. Urbanova, V.; Magro, M.; Gedanken, A.; Baratella, D.; Vianello, F.; Zboril, R. Nanocrystalline iron oxides, composites, and related materials as a platform for electrochemical, magnetic, and chemical biosensors. *Chem. Mater.* **2014**, *26*, 6653–6673. [CrossRef]
2. Shao, Y.Z.; Ying, Y.B.; Ping, J.F. Recent advances in solid-contact ion-selective electrodes: Functional materials, transduction mechanisms, and development trends. *Chem. Soc. Rev.* **2020**, *49*, 4405–4465. [CrossRef] [PubMed]
3. Kakhki, R.M. Application of nanoparticles in the potentiometric ion selective electrodes. *Russ. J. Electrochem.* **2013**, *49*, 458–465. [CrossRef]
4. Yin, T.; Qin, W. Applications of nanomaterials in potentiometric sensors. *TrAC Trends Anal. Chem.* **2013**, *51*, 79–86. [CrossRef]
5. Asefa, T.; Duncan, C.T.; Sharma, K.K. Recent advances in nanostructured chemosensors and biosensors. *Analyst* **2009**, *134*, 1980. [CrossRef]
6. George, J.M.; Antony, A.; Mathew, B. Metal oxide nanoparticles in electrochemical sensing and biosensing: A review. *Microchim. Acta* **2018**, *185*, 358. [CrossRef] [PubMed]
7. Katz, E.; Willner, I.; Wang, J. Electroanalytical and Bioelectroanalytical Systems Based on Metal and Semiconductor Nanoparticles. *Electroanalysis* **2004**, *16*, 19–44. [CrossRef]
8. Wang, F.; Hu, S. Electrochemical sensors based on metal and semiconductor nanoparticles. *Microchim. Acta* **2009**, *165*, 1–22. [CrossRef]
9. Li, Y.; Zhang, J.; Zhu, H.; Yang, F.; Yang, X. Gold nanoparticles mediate the assembly of manganese dioxide nanoparticles for H2O2 amperometric sensing. *Electrochim. Acta* **2010**, *55*, 5123–5128. [CrossRef]
10. Zhang, S.; Zheng, J. Synthesis of single-crystal α-MnO2 nanotubes-loaded Ag@C core–shell matrix and their application for electrochemical sensing of nonenzymatic hydrogen peroxide. *Talanta* **2016**, *159*, 231–237. [CrossRef]
11. Fan, Y.; Huang, K.-J.; Niu, D.-J.; Yang, C.-P.; Jing, Q.-S. TiO2-graphene nanocomposite for electrochemical sensing of adenine and guanine. *Electrochim. Acta* **2011**, *56*, 4685–4690. [CrossRef]
12. Prkic, A.; Vukusic, T.; Giljanovic, J.; Sokol, V.; Boskovic, P.; Lavcevic, M.L.; Mitar, I.; Jakic, M. Development of a New Potentiometric Sensor based on home made Iodide ISE Enriched with ZnO Nanoparticles and its Application for Determination of Penicillamine. *Int. J. Electrochem. Sc.* **2018**, *13*, 10894–10903. [CrossRef]
13. Prkic, A.; Vukusic, T.; Mitar, I.; Giljanovic, J.; Sokol, V.; Boskovic, P.; Jakic, M.; Sedlar, A. New sensor based on AgCl containing Iron Oxide or Zinc Oxide Nanoparticles for Chloride Determination. *Int. J. Electrochem. Sc.* **2019**, *14*, 861–874. [CrossRef]
14. Chekin, F.; Yazdaninia, M. A sensor based on incorporating Ni2+ into ZnO nanoparticles-multi wall carbon nanotubes-poly methyl metacrylat nanocomposite film modified carbon paste electrode for determination of carbohydrates. *Russ. J. Electrochem.* **2014**, *50*, 967–973. [CrossRef]
15. Li, S.-J.; Du, J.-M.; Zhang, J.-P.; Zhang, M.-J.; Chen, J. A glassy carbon electrode modified with a film composed of cobalt oxide nanoparticles and graphene for electrochemical sensing of H2O2. *Microchim. Acta* **2014**, *181*, 631–638. [CrossRef]
16. Yao, S.S.; Zhi, L.F.; Guo, J.; Yan, S.J.; Zhang, M.G. Hierarchical Porous NiCo2O4 array grown on Ni foam for the Simultaneous Electrochemical Detection of Copper(II) and Mercury(II). *Int. J. Electrochem. Sc.* **2018**, *13*, 542–550. [CrossRef]
17. Yuan, M.; Li, J.; Yu, Y.; Fu, Y.; Fong, A.; Hu, J. Fabrication of a Fe2O3Nanoparticles Implantation-modified Electrode and its Applications in Electrochemical Sensing. *Electroanalysis* **2015**, *28*, 954–961. [CrossRef]
18. G. Uc-Cayetano, E. Enhancement of Electrochemical Glucose Sensing by Using Multiwall Carbon Nanotubes decorated with Iron Oxide Nanoparticles. *Int. J. Electrochem. Sci.* **2016**, *11*, 6356–6369. [CrossRef]
19. Lee, S.; Oh, J.; Kim, D.; Piao, Y. A sensitive electrochemical sensor using an iron oxide/graphene composite for the simultaneous detection of heavy metal ions. *Talanta* **2016**, *160*, 528–536. [CrossRef]
20. Radić, J.; Bralić, M.; Kolar, M.; Genorio, B.; Prkić, A.; Mitar, I. Development of the New Fluoride Ion-Selective Electrode Modified with Fe(x)O(y) Nanoparticles. *Molecules* **2020**, *25*, 5213. [CrossRef]
21. Absalan, G.; Akhond, M.; Bananejad, A.; Ershadifar, H. Highly sensitive determination of nitrite using a carbon ionic liquid electrode modified with Fe3O4 magnetic nanoparticle. *J Iran Chem Soc* **2015**, *12*, 1293–1301. [CrossRef]
22. Kaushik, A.; Solanki, P.R.; Ansari, A.A.; Sumana, G.; Ahmad, S.; Malhotra, B.D. Iron oxide-chitosan nanobiocomposite for urea sensor. *Sens. Actuators B* **2009**, *138*, 572–580. [CrossRef]
23. Adekunle, A.S.; Agboola, B.O.; Pillay, J.; Ozoemena, K.I. Electrocatalytic detection of dopamine at single-walled carbon nanotubes–iron (III) oxide nanoparticles platform. *Sens. Actuators B* **2010**, *148*, 93–102. [CrossRef]
24. Zhang, Y.; Cheng, Y.; Zhou, Y.; Li, B.; Gu, W.; Shi, X.; Xian, Y. Electrochemical sensor for bisphenol A based on magnetic nanoparticles decorated reduced graphene oxide. *Talanta* **2013**, *107*, 211–218. [CrossRef] [PubMed]
25. Mitar, I.; Guć, L.; Soldin, Ž.; Vrankić, M.; Paut, A.; Prkić, A.; Krehula, S. Rapid Microwave Method for Synthesis of Iron Oxide Particles under Specific Conditions. *Crystals* **2021**, *11*, 383. [CrossRef]
26. Baig, N.; Sajid, M.; Saleh, T.A. Recent trends in nanomaterial-modified electrodes for electroanalytical applications. *TrAC Trends Anal. Chem.* **2019**, *111*, 47–61. [CrossRef]
27. Goldhaber, S.B. Trace element risk assessment: Essentiality vs. toxicity. *Regul. Toxicol. Pharmacol.* **2003**, *38*, 232–242. [CrossRef]
28. Isildak, I.; Attar, A.; Demir, E.; Kemer, B.; Aboul-Enein, H.Y. A Novel all Solid-State Contact PVC-Membrane Beryllium-Selective Electrode Based on 4-Hydroxybenzo-15-Crown-5 Ether Ionophore. *Curr. Anal. Chem.* **2018**, *14*, 43–48. [CrossRef]
29. Mizani, F.; Ganjali, M.R.; Faridbod, F.; Esmaeilnia, S. A Novel Iron(III) Selective Potentiometric Sensor Based on 9-Ethylacenaphtho [1, 2-B]Quinoxaline. *Int. J. Electrochem. Sc.* **2013**, *8*, 10473–10486.

30. Bita, S.; Sadati, S.O.; Soleymanpour, A.; Amouzad, F. Highly Selective Solid Contact Sensor for Low Level Concentration Measurements of Iron(III) in Pharmaceutical and Biological Media. *J. Anal. Chem.* **2018**, *73*, 1202–1208. [CrossRef]

31. Yari, A.; Bagheri, M.; Ghazizadeh, M. A Novel Iron(III) Potentiometric Sensor Based on (E)-N′-((2-hydroxynaphthalen-3-yl)methylene)benzohydrazide. *Int. J. Electrochem. Sc.* **2016**, *11*, 6597–6608. [CrossRef]

32. Fakhari, A.R.; Alaghemand, M.; Shamsipur, M. Iron(III)-selective membrane potentiometric sensor based on 5,10,15,20-tetrakis(pentafluorophenyl)-21H, 23H-porphyrin. *Anal. Lett.* **2001**, *34*, 1097–1106. [CrossRef]

33. Ekmekci, G.; Uzun, D.; Somer, G.; Kalayci, S. A novel iron(III) selective membrane electrode based on benzo-18-crown-6 crown ether and its applications. *J. Membr. Sci.* **2007**, *288*, 36–40. [CrossRef]

34. Vlascici, D.; Fagadar-Cosma, E.; Popa, I.; Chiriac, V.; Gil-Agusti, M. A Novel Sensor for Monitoring of Iron(III) Ions Based on Porphyrins. *Sensors* **2012**, *12*, 8193–8203. [CrossRef] [PubMed]

35. Gupta, V.K.; Sethi, B.; Upadhyay, N.; Kumar, S.; Singh, R.; Singh, L.P. Iron (III) Selective Electrode Based on S-Methyl N-(Methylcarbamoyloxy) Thioacetimidate as a Sensing Material. *Int. J. Electrochem. Sc.* **2011**, *6*, 650–663.

36. Ali, T.A.; Mahmoud, W.H.; Mohamed, G.G. Construction and characterization of nano iron complex ionophore for electrochemical determination of Fe(III) in pure and various real water samples. *Appl. Organomet. Chem.* **2019**, *33*, e5206. [CrossRef]

37. Ali, T.A.; Mohamed, G.G.; El-Dessouky, M.M.I.; Abou El Ella, S.M.; Mohamed, R.T.F. Modified Carbon Paste Ion Selective Electrodes for the Determination of Iron (III) in Water, Soil and Fish Tissue Samples. *Int. J. Electrochem. Sci.* **2013**, *8*, 1469–1486.

38. Duzgun, E.; Tastekin, M.; Atakol, O. A new modified Fe(III)-selective solid membrane electrode. *Rev Anal Chem* **2008**, *27*, 83–90. [CrossRef]

39. Fung, Y.; Fung, K. Determination of iron (III) with a copper selective electrode. *Anal. Chem.* **1977**, *49*, 497–499. [CrossRef]

40. Paut, A.; Prkić, A.; Mitar, I.; Bošković, P.; Jozić, D.; Jakić, M.; Vukušić, T. Potentiometric Response of Solid-State Sensors Based on Ferric Phosphate for Iron(III) Determination. *Sensors* **2021**, *21*, 1612. [CrossRef]

41. Lewis, D.G.; Farmer, V.C. Infrared absorption of surface hydroxyl groups and lattice vibrations in lepidocrocite (γ-FeOOH) and boehmite (γ-AlOOH). *Clay Miner.* **1986**, *21*, 93–100. [CrossRef]

42. Hou, H.; Xie, Y.; Yang, Q.; Guo, Q.; Tan, C. Preparation and characterization of γ-AlOOH nanotubes and nanorods. *Nanotechnology* **2005**, *16*, 741. [CrossRef]

43. Milligan, W.O.; McAtee, J.L. Crystal Structure of γ-AlOOH and γ-ScOOH. *J. Phys. Chem.* **1956**, *60*, 273–277. [CrossRef]

44. Buining, P.A.; Pathmamanoharan, C.; Jansen, J.B.H.; Lekkerkerker, H.N.W. Preparation of Colloidal Boehmite Needles by Hydrothermal Treatment of Aluminum Alkoxide Precursors. *J. Am. Ceram. Soc.* **1991**, *74*, 1303–1307. [CrossRef]

45. Štefanić, G.; Musić, S. Microstructural analysis of boehmite nanoparticles prepared by rapid hydrolysis of aluminum sec-butoxide. *Croat. Chem. Acta* **2011**, *84*, 481–485. [CrossRef]

46. Prabhakar, R.; Samadder, S.R. Low cost and easy synthesis of aluminium oxide nanoparticles for arsenite removal from groundwater: A complete batch study. *J. Mol. Liq.* **2018**, *250*, 192–201. [CrossRef]

47. Stoia, M.; Istratie, R.; Păcurariu, C. Investigation of magnetite nanoparticles stability in air by thermal analysis and FTIR spectroscopy. *J. Therm. Anal. Calorim.* **2016**, *125*, 1185–1198. [CrossRef]

48. Fleet, M.E. The structure of magnetite. *Acta Crystallogr. Sect. B Struct. Crystallogr. Cryst. Chem* **1981**, *37*, 917–920. [CrossRef]

BIOGRAPHY

Andrea Paut (born as Sedlar) ███████████ █ ████████████ After finishing natural sciences-mathematical high school, she enrolled at Faculty of Chemistry and Technology in University of Split. In 2015, she completed her undergraduate study and with defending her bachelor thesis entitled Determination of bromides in nucleophylic substitution with 1-phenylethanol in acidic media earned univ. bacc. chem title. In 2017, she graduated at Faculty of Chemistry and Technology with defending her diploma thesis entitled Isolation and identification of volatile sulphur compounds from selected *Brassicaceae* family plants. In 2018, she supplemented her education with Pedagogical, Psychological, Didactic and Teaching Methodology Training at Faculty of Humanities and Social Sciences in Josip Juraj Strossmayer University of Osijek. Her first employment was in 2017 at Institute for Adriatic Crops and Karst Reclamation where she worked in accredited analytical laboratory for wine analysis. Next year, she started working as an assistant on a project of the Croatian Science Foundation at Faculty of Chemistry and Technology in University of Split. A project entitled *Development of new membranes for ion-selective electrodes enriched with nanoparticles of metals and metal oxides* is under the supervision of PhD Ante Prkić, Associate Professor. In the same year she enrolled in the postgraduate doctoral course Chemical Engineering and Applied Chemistry at Faculty of Chemical Engineering and Technology in University of Zagreb. Under the supervision of her mentors, Associate Professor Ante Pkić, Associate Professor Stjepan Milardović† and Assistant Professor Petar Kassal, she started working on development of membranes for ion-selective electrodes and their modification with metal oxides nanoparticles. The doctoral research resulted in the publication of three articles in scientific journals which are cited in Current Contents Connect database and ranked in two top quartiles of their respective subject categories. Other than papers from doctoral research, she is co-author in one more scientific journal article. She presented her doctoral research at two international conferences and was co-author in two poster presentations on international conferences where part of her diploma thesis research was presented. Other than mentioned conferences, she was co-author of poster presentation but also one of the conference moderators, at the 4th International Webinar on Materials Chemistry held in 2021 and participated at 26th Young Investigators' Seminar on Analytical Chemistry with an oral statement.

List of published papers:

1) A. Prkić, T. Vukušić, I. Mitar, J. Giljanović, V. Sokol, P. Bošković, M. Jakić, A. Sedlar, New sensor based on AgCl containing Iron Oxide or Zinc Oxide Nanoparticles for Chloride Determination, International Journal of Electrochemical Science, 14 (2019), 1; 861-874.

2) A. Paut, A. Prkić, I. Mitar, P. Bošković, D. Jozić, M. Jakić, T. Vukušić, Potentiometric Response of Solid-State Sensors Based on Ferric Phosphate for Iron(III) Determination, Sensors, 21 (2021), 5.

3) I. Mitar, L. Guć, Ž. Soldin, M. Vrankić, A. Paut, A. Prkić, S. Krehula, Stjepko Rapid Microwave Method for Synthesis of Iron Oxide Particles under Specific Conditions, Crystals, 11 (2021), 4.

4) A. Paut, A. Prkić, I. Mitar, L. Guć, M. Marciuš, M. Vrankić, S. Krehula, L. Tomaško, The New Ion-Selective Electrodes Developed for Ferric Cations Determination, Modified with Synthesized Al and Fe−Based Nanoparticles, Sensors, 22 (2022), 1; 297, 17.

List of conferences:

1) M. N. Mužek, A. Đulović, M. Buljac, D. Omanović, T. Kozina, A. Sedlar, L. Radaš, S. Svilović, I. Blažević, Distribution of volatile sulfur compounds and heavy metals in kohlrabi and leek, 28th International Scientific-Expert Conference of Agriculture and Food Industry – Book of Abstracts, Drkenda, Pakeza; Dučić, Belma (ur.), Sarajevo: TMP d.o.o., 2017. str. 56 (poster, međunarodna recenzija, sažetak, znanstveni)

2) A. Đulović, A. Sedlar, V. Čikeš-Čulić, I. Generalić Mekinić, F. Burčul, I. Blažević, *Bunias erucago* L. Chemistry and biological activity, 10th CMAPSEEC: Book of abstracts, Carović-Stanko, Klaudija; Grdiša, Martina (ur.), Zagreb: Novi Val d.o.o., 2018. str. 185 (poster, međunarodna recenzija, sažetak, znanstveni)

3) A. Sedlar, A. Prkić, I. Mitar, J. Giljanović, V. Sokol, P. Bošković, PREPARATION OF A NOVEL MEMBRANES FOR ION-SELECTIVE ELECTRODES FOR IRON DETERMINATION BASED ON IRON(II) SULFIDE AND SILVER SULFIDE, 26th Young Investigators' Seminar on Analytical Chemistry, Pardubice, Češka, 2019. str. 13 (predavanje, međunarodna recenzija, sažetak, ostalo)

4) A. Paut, A. Prkić, I. Mitar, J. Giljanović, L. Guć, Ionsko-selektivne elektrode za određivanje željezovih(III) kationa, 18. Ružičkini dani "Danas znanost-sutra industrija", Vukovar, Hrvatska, 2020. str. 44 (poster, međunarodna recenzija, sažetak, znanstveni)

5) A. Prkić, A. Paut, I. Mitar, J. Giljanović, P. Bošković, Determination of Ferric Cations by Potentiometric Sensors Modified with Different Metal Oxides and Oxyhydroxides Nanoparticles, 3rd International Conference on Analytical and Bioanalytical Methods, virtualno, 2021. (poster, međunarodna recenzija, neobjavljeni rad, znanstveni)

6) I. Mitar, M. Vrankić, S. Krehula, A. Prkić, A. Paut, Influence of the addition of surfactants in iron oxide microwave synthesis, Journal of Materials Engineering and Applications, vol. 5, (4th International Webinar on Materials Chemistry), virtualno, 2021. str. 26 (poster, međunarodna recenzija, sažetak, znanstveni)